HUMBOLDT-UNIVERSITÄT ZU BERLIN

Characterization of mitochondrial isocitrate dehydrogenase in cellular reprogramming in *C. elegans*

DISSERTATION

zur Erlangung des akademischen Grades

Doctor of Philosophy

(Ph.D.)

eingereicht an der

Lebenswissenschaftlichen Fakultät der Humboldt-Universität zu Berlin

von

Nida ul Fatima, Master of Science (Industrial Biotechnology)

Präsidentin der Humboldt-Universität zu Berlin

Prof. Dr.-Ing. Dr. Sabine Kunst

Dekan der Lebenswissenschaftlichen Fakultät der Humboldt-Universität zu Berlin

Prof. Dr. Bernhard Grimm

Date of defence: April 12, 2021

Vorsitzender:

Prof. Dr. Andrew Plested

Gutachterinnen/Gutachter:

Prof. Dr. Thomas Sommer
Dr. Baris Tursun
Prof. Dr. Janine Kirstein

Weitere/s Mitglied/er:
Prof. Dr. Andreas Herrmann

Conducted in

Max-Delbrueck-Center for Molecular Medicine Berlin Buch
Berlin Institute of Medical Systems Biology (BIMSB)
Research Group: Gene regulation and Cell Fate Decision in *C. elegans*
September 2015 – December 2020

Affidavit

Hiermit erkläre ich, Nida ul Fatima, Matrikel-Nr: 602866, dass ich die vorliegende Dissertation selbstständig und ohne Benutzung anderer als der angegebenen Hilfsmittel angefertigt habe.

Die aus fremden Quellen direkt oder indirekt übernommenen Gedanken sind als solche kenntlich gemacht.

Ich habe mich anderweitig nicht um einen Doktorgrad beworben und besitze keinen entsprechenden Doktorgrad. Die Dissertation wurde bisher in gleicher oder ähnlicher Form keiner anderen Prüfungsbehörde vorgelegt oder veröffentlicht.

Berlin, am 22.04.2021

Publications

Ul Fatima, N. &Tursun, B., 2020. Conversion of germ cells to somatic cell types in C. elegans. *Journal of Developmental Biology*, *8*(4), p.24.

Hajduskova, M., Baytek, G., Kolundzic, E., Gosdschan, A., Kazmierczak, M., Ofenbauer, A., del Rosal, M.L.B., Herzog, S., **Ul Fatima, N.,** Mertins, P. and Seelk-Müthel, S., 2019. MRG-1/MRG15 is a barrier for germ cell to neuron reprogramming in Caenorhabditis elegans. *Genetics*, *211*(1), pp.121-139.

ABSTRACT

Direct reprogramming makes use of transcription factors (TFs) that induce the identity of specific cell types. These TFs often are restricted in most cell types by inhibitory mechanisms. In order to identify these barriers in *C. elegans,* we used the previously described zinc-finger TF CHE-1 that is required to induce the glutamatergic ASE neuron fate. Upon ectopic expression of CHE-1 and removal of barrier genes by RNAi, induction of the ASE neuronal fate marker can be seen in a variety of cell types. In this study, we identified and characterized a candidate barrier for reprogramming germ cells into neurons, the NAD+ dependent mitochondrial isocitrate dehydrogenase 3 (IDH3). RNAi knockdown of alpha (IDHA-1) or gamma (IDHG-1) subunit of this complex gave a consistent and reliable phenotype of the expression of ASE reporter in the germ line upon ectopic expression of CHE-1. Furthermore, we assessed pan-neuronal and neuron-type specific gene/protein expression, and morphological changes to determine the neuron like identity of the converted germ cells.

This study shows that *idha-1* depletion-mediated reprogramming of germ cells to neurons is partially repressed in animals that lack the hypoxia-induced factor, TF HIF-1. HIF-1 has been implicated in regulating induced pluripotent stem cell (iPSC) reprogramming, a process that is triggered by changes in the level of the metabolite produced by IDH3- alpha-ketoglutarate (a-KG).

It has been shown that mitochondrial dynamics change during differentiation. This suggests that disturbing mitochondrial function may feed-back to chromatin thus altering gene expression and allowing reprogramming. We were able to identify that knock down of *idha-1* leads to global histone modification changes; and by performing a genetic screen we identified members of the Jumonji proteins, the a-KG dependent histone demethylases, involved in this conversion phenotype. However, transcriptome analysis in IDH3 depleted worms showed minor differences compared to the control suggesting that although chromatin becomes more accessible, no appreciable transcriptional changes occur by IDH3 depletion alone.

By performing Mass Spectrometry and genetic screens, we have identified that cells utilize glutamine anaplerosis to replenish a-KG levels and display a partially active citric acid cycle upon IDH3 depletion; and these processes are required for the TF- mediated reprogramming to occur. Furthermore, the IDH3 depletion mediated germ cell reprogramming

is not tissue autonomous. We identified that signals from the somatic gonad enable the reprogramming process.

Overall, this study identifies the role of the conserved Isocitrate Dehydrogenase 3 in cell fate safeguarding and thus as a barrier to reprogramming. In a broader context, these findings highlight the role of mitochondria and metabolism in the maintenance of cell fate.

Keywords: Cellular reprogramming, *C. elegans,* Mitochondria, Metabolism

ZUSAMMENFASSUNG

Direkte Zellreprogrammierung basiert auf Transkriptionsfaktoren (TFs), die die Identität bestimmter Zelltypen induzieren. Diese TF vermittelte Zellreprogrammierung ist in den meisten Zelltypen häufig durch hemmende Mechanismen limitiert. Um solche Barrieren in *C. elegans* zu identifizieren, verwendeten wir den zuvor charakterisierten Zinkfinger-TF CHE-1, der erforderlich ist, um glutamaterge ASE-Neuronen zu induzieren. Nach ektopischer Expression von CHE-1 und Entfernung von bestimmten Barrieregenen durch RNAi, kann die Induktion des neuronalen ASE Markers in einer Vielzahl von Zelltypen beobachtet werden. In dieser Studie haben wir eine mögliche Barriere für die Reprogrammierung von Keimzellen zu Neuronen identifiziert und charakterisiert: die NAD+ abhängige mitochondriale Isocitratdehydrogenase 3 (IDH3). Der RNAi-Knockdown der Alpha (IDHA-1) - oder Gamma (IDHG-1) -Untereinheit dieses Komplexes ergab in Kombination mit ektopischer Expression von CHE-1 einen konsistenten Phänotyp hinsichtlich der Expression des neuronalen ASE-Reporters in der Keimbahn. Darüber hinaus untersuchten wir die pan-neuronale und neuronentypspezifische Gen- bzw. Proteinexpression sowie morphologische Veränderungen, um die neuronale Identität der konvertierten Keimzellen zu bestimmen.

Diese Studie zeigt, dass die durch IDH3-Entfernung vermittelte Reprogrammierung von Keimzellen zu Neuronen bei Tieren, denen der Hypoxie-induzierte Faktor HIF-1 fehlt, teilweise unterdrückt wird. HIF-1 ist an der Regulierung der Reprogrammierung induzierter pluripotenter Stammzellen (iPSC) beteiligt, ein Prozess, der durch Änderungen des IDH3-alpha-Ketoglutarat (a-KG) abhängigen Metabolitenspiegels ausgelöst wird.

Es konnte des Weiteren gezeigt werden, dass sich die metabolische Dynamik während der Zelldifferenzierung ändert. Dies deutet darauf hin, dass eine Störung der Mitochondrienfunktion sich auf den Chromatinstatus auswirken kann, wodurch die Genexpression verändert und eine Reprogrammierung ermöglicht wird. Wir konnten feststellen, dass IDH3-Knockdowns zu globalen Veränderungen der repressiven Histonmodifikationen führen. Mittels genetischer Untersuchungen identifizierten wir Mitglieder der Jumonji-Proteine sowie die a-KG-abhängigen Histon-Demethylasen, die an diesem Reprogammierungsphänotyp beteiligt sind. Die Transkriptomanalyse bei Tieren mit IDH3-Depletion zeigte jedoch nur geringfügige Beeinträchtigungen der Genexpression, was

darauf hindeutet, dass Chromatin zwar leichter zugänglich wird, jedoch keine nennenswerten Transkriptionsänderungen allein durch IDH3-Mangel auftreten.

Durch Massenspektrometrie und weiterführenden genetische Untersuchungen haben wir festgestellt, dass Zellen bei IDH3-Mangel eine sogenannte Glutamin-Anaplerose verwenden, um den a-KG-Spiegel wieder aufzufüllen und somit einen teilweise aktiven Zitronensäurezyklus beizubehalten. Des Weiteren sind diese Prozesse erforderlich, damit die TF vermittelte Zellreprogrammierung stattfinden kann. Wir haben außerdem festgestellt, dass Signale von Zellen der somatischen Gonade diesen durch IDH3-Mangel vermittelten Zellreprogrammierungsprozess von Keimzellen ermöglichen. Daher ist anzunehmen, dass der Reprogrammierungsphänotyp in der Keimbahn nicht gewebsautonom ist.

Zusammengefasst identifiziert diese Studie die Rolle der evolutionär konservierten Isocitrat-Dehydrogenase 3 (IDH3) bei der Aufrechterhaltung der Zellidentität und damit auch als Barriere für die Zellreprogrammierung. Im erweiterten Kontext unterstreichen die Ergebnisse die allgemeine Rolle von Mitochondrien sowie des Stoffwechsels hinsichtlich epigenetischer Kontrolle der Genexpression und Schutz von Zellidentitäten.

Schlüsselwörter: Zellreprogrammierung, *C. elegans*, Mitochondrien, Stoffwechsel

Table of Contents

1. INTRODUCTION

1.1 Cellular reprogramming

1.1.1 Reprogramming to pluripotency

The development of a multicellular organism begins after the fertilization of the oocyte with a sperm to form a zygote. The zygote is totipotent in nature and hence has the potential to form all lineages of the organism (Smith et al., 2016; Yamanaka and Blau, 2010). Diverse tissues with specific cell types are formed by the uncommitted cells in the zygote by undergoing differentiation. This process of differentiation is tightly regulated by complex exogenous and endogenous mechanisms that ensure the precise timing and generation of the required cell types (Ladewig et al., 2013; Smith et al., 2016). These diverse cells generated during development have distinctive fates both in terms of function and morphology; and are marked by cell type-specific gene expression profile. Once established, the states of these cells are remarkably stable and such differentiated cells do not switch fates under normal circumstances (Yamanaka and Blau, 2010).

Based on the 'apparent' fixed committed state of the differentiated cells, it was widely accepted that terminally differentiated cells lose chromosomes or permanently inactivate genes that are not required. However, this idea was challenged by the experiments of Gurdon and later by Wilmut & colleagues which suggested that cell fates can be plastic in a different environment (Gurdon et al., 1958; Campbell et al., 1996). By transplantation of the nucleus from fully differentiated frog somatic cells into unfertilized oocytes, Gurdon successfully obtained tadpoles and adult frogs (Gurdon et al., 1958). This use of somatic cell nuclear transfer (SCNT) or cloning was eventually employed by Campbell to clone Dolly the sheep (Campbell et al., 1996). Since then, more than 20 mammalian species including monkeys have been cloned using SCNT (Figure 1.1) (Matoba & Zhang, 2018). However, SCNT is limited due to its inefficiency and abnormalities observed in extraembryonic tissues and cloned animals including obesity, immunodeficiency and early death (Loi et al., 2016; Ogura et al., 2013).

An alternative method employed to achieve nuclear reprogramming involves the fusion of two or more cell types to form a single entity. This can result in fusion of nuclei to create hybrids, or non-proliferating heterokaryons that retain multiple nuclei (Figure 1.1) (Yamanaka and Blau, 2010; Vierbuchen and Wernig, 2012). Hybrids created by the fusion of somatic and embryonic cells exhibit properties of the parental embryonic cells due to the activation of silent

pluripotency genes and reactivation of the inactive X chromosome (Foshay et al., 2012; Jaenisch and Young, 2008; Yamanaka and Blau, 2010). Although this method is not dependent on nuclear transfer to create pluripotent cells, generation of polyploids can lead to aberrant chromosome segregation and aneuploidy (Alvarez-Dolado, 2007). In order to be used for transplant therapy, selective elimination of chromosomes has been attempted from the hybrid to generate diploid customized cells (Matsumura et al., 2007). However, this poses a risk of large-scale genomic instability and thus limits the applications of this technique for research and therapy (Hochedlinger & Jaenisch, 2006; Jaenisch and Young, 2008).

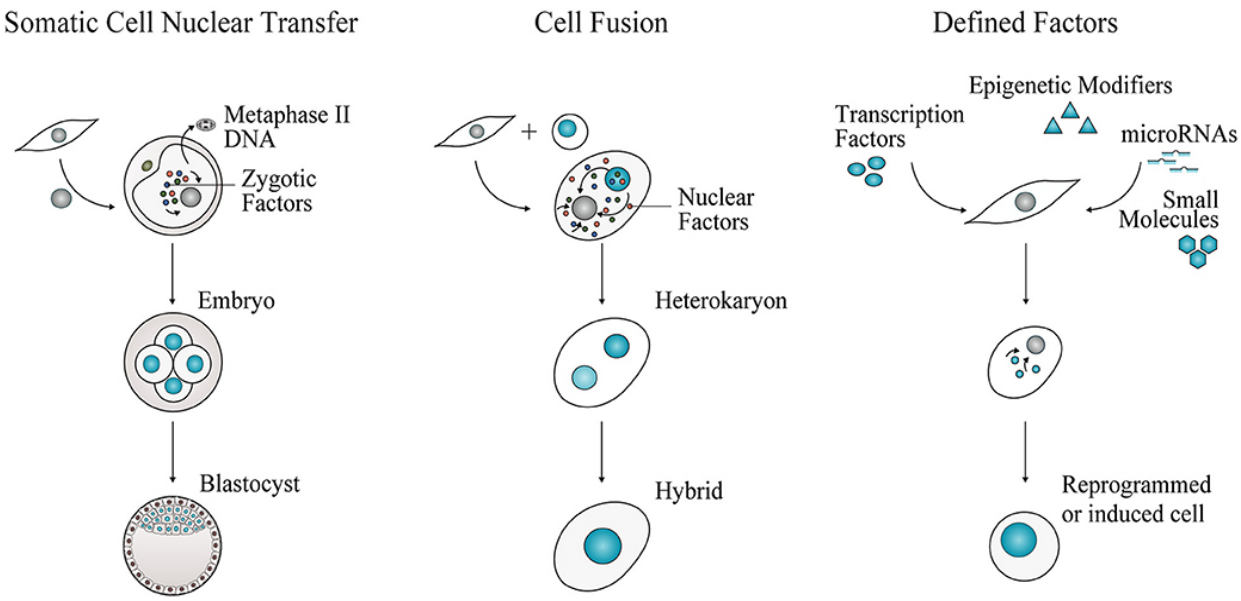

Figure 1.1: Experimental approaches for cell fate reprogramming. In SCNT, a nucleus of an adult cell is transferred into an enucleated oocyte. The somatic cell nucleus is reprogrammed to totipotency by the action of zygotic factors. An alternative approach is by cell fusion. In this method, two cells are fused to generate a multinucleated heterokaryon. Nuclear fusion gives rise to a tetraploid hybrid cell that is able to proliferate. Cell fate conversion can also be achieved by defined factors, including cell type specific transcription factors, epigenetic modifiers, microRNAs and small molecules acting together to induce pluripotency or a different somatic identity (Adopted from Pires et al., 2019).

The discovery in 2006 by Takahashi and Yamanaka that cell fates can be reversed to pluripotency completely changed the field of cellular reprogramming. Takahashi and Yamanaka showed that expression of transcription factors (TFs) OCT4 (octamer- binding TF, also known as POU5F1), SRY-box 2 (SOX2), Krüppel-like factor 4 (KLF4) and c-MYC proto-oncogene protein (collectively referred to as OSKM) converted mouse fibroblasts to embryonic stem cell (ESC)-like pluripotent cells (Takahashi and Yamanaka, 2006). These generated cells, termed induced pluripotent stem cells (iPSCs), displayed similar morphology, gene expression profiles and other characteristics of ESCs. Notably, the transgene expression of these OSKM

TFs is needed only during the generation of iPSCs (Wernig et al, 2007; Takahashi et al., 2007). Once the cells have established pluripotency, their self-renewal abilities and maintenance of their pluripotent state is self-regulated by the endogenous gene expression suggesting that these iPSCs have undergone robust reprogramming (Yamanaka & Blau, 2010). Subsequently, human iPSCs have been generated using the same, different, or overlapping set of TFs in fibroblasts, keratinocytes, hepatocytes as well as pancreatic ß cell for example (Wernig et al, 2007; Okita et al., 2007). However, the reprogramming efficiency of differentiated cells into pluripotent cells is variable and depends on the cell type, age, physiological state and its tissue of origin; thereby highlighting the context dependency of the ability to reprogram differentiated cells (Yamanaka and Blau, 2010).

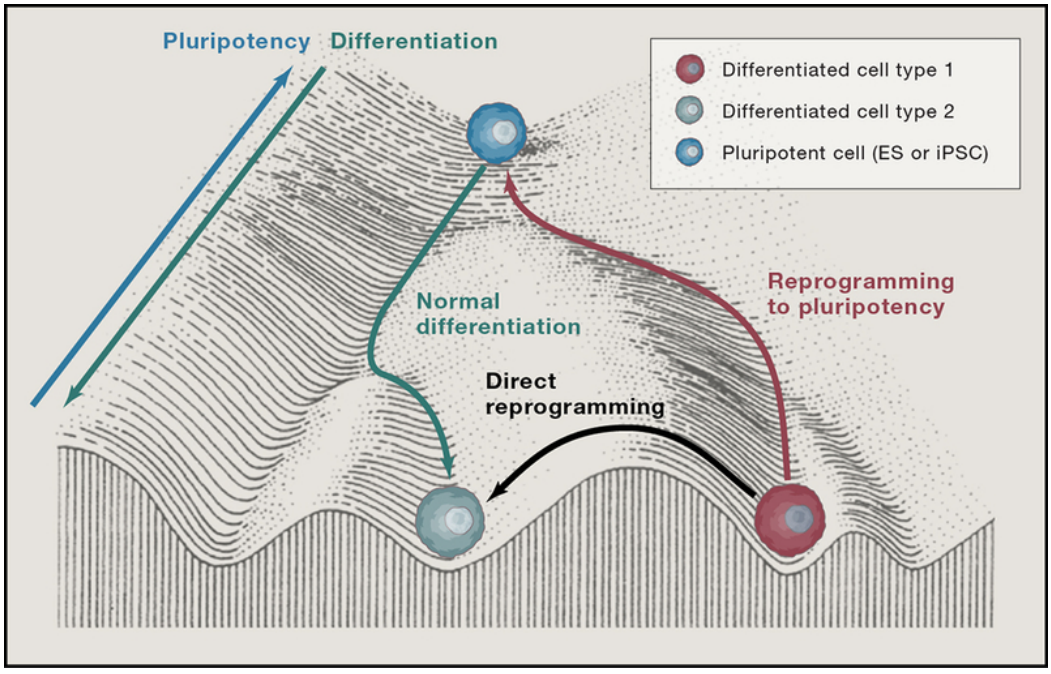

Figure 1.2 Waddington's model for cellular reprogramming. Waddington described cell fate using the model in which a pluripotent cell is depicted as a marble rolling downhill into one of several grooves that represent the fully differentiated cell type. In this model, cellular reprogramming can be represented as a cell can rolling back up the hill to achieve a pluripotent state, or jumping from one groove to another by direct reprogramming (Reprinted from Srivastava and DeWitt, 2016).

These studies involving the generation of iPSCs relied on the classical concept that a cell fate hierarchy exists, where the pluripotent cells lie above the differentiated or committed cells on the developmental landscape in the Waddington model and that lineage commitment and differentiation of cells is unidirectional. This concept of lineage specification was described by Conrad Hal Waddington in an epigenetic landscape model (Figure 1.2) (Waddington, 1957). This model by Wallington proposes that the cells are progressively

restricted in terms of differentiation potential during the course of development. This is illustrated by a marble rolling down a landscape, segregating into different groves on the slope and in doing so, determining its final fate (Ladewig et al., 2013). The model implies that in order to convert a differentiated cell into a distinct, differentiated cell, it is necessary to first bring it back to a pluripotent state. Nevertheless, cell fates are also interchangeable outside the context of pluripotency and dedifferentiation.

1.1.2 Direct reprogramming

Early clues of direct reprogramming or transdifferentiation were provided by the experiments performed by Hadorn and Schläpfer in *Drosophila melanogaster (D. melanogaster*) who demonstrated for the first time that the fully committed cells are plastic and their fate can be changed upon exposure to a different microenvironment (Hadorn, 1963; Schläpfer, 1963). Notably, it was shown that when cells from the imaginal discs of the fly pupae were serially transplanted into the abdomen of an adult, cells that were originally destined to form genital structures instead gave rise to leg or antennae and eventually to wings (Hadorn, 1963; Schläpfer, 1963; Gehring, 1966). Although this 'transdetermination' was triggered by surgical manipulation, the resulting fate change was an entirely endogenous phenomenon (Gehring, 1966). This demonstration of 'trans determination' thus paved the way for the idea that trans differentiation or direct reprogramming could also be possible.

An example of naturally occurring transdifferentiation was later discovered in *Caenorhabditis elegans* (*C. elegans*), where a specialized rectal epithelial cell converts to neuron during larval development. This occurs after the first larval stage L1, during which the rectal epithelial cell Y retracts from the rectum and converts to PDA neuron without dividing (Jarriault et al., 2008; Richard et al., 2011). Members of the NODE-like (Nanog and Oct4-associated deacetylase) complex, *sox-2* gene as well as histone modification enzymes were shown to be involved during this conversion event (Kagias et al., 2012; Zuryn et al., 2014).

In the reprogramming field, a major development was made following experiments in *D. melanogaster*, in which Gehring et al. showed that overexpression of a single transcription factor in somatic cells activated gene programs that were normally expressed in other somatic cells (Gehring et al., 1966). This study showed for the first time that a given cell type can be converted directly into another. This was followed by similar observations in mammals where forced expression of a transcription factor resulted in changes of the cell fate. Davis et al.

demonstrated that expression of the muscle helix–loop–helix transcription factor MyoD resulted in phenotypic conversion of fibroblasts into contracting myoblasts (Davis et al., 1987) (Figure 1.3). MyoD was later shown to be able to induce conversion of other cell types including fat and liver cells into muscle-like cells. However, this occurred at a very low frequency and the resulting muscle cells looked aberrant (Weintraub et al., 1989). Studies by Graf and colleagues showed conversion between different cell types of the haemopoietic system (Graf et al., 1995) (Figure 1.3). Their studies demonstrated the conversion of fully differentiated B and T cell progenitors into functional macrophages upon ectopic expression of basic leucine zipper transcription factor C/EBPα or β (CCAAT/enhancer binding proteinα or β) (Xie et al., 2004).

A significant advancement in therapeutic applications of direct reprogramming was made when a cocktail of TFs (Ngn3, Pdx1, and Mafa) was shown to convert exocrine cells of the pancreas into insulin-producing β-islet cells *in vivo* (Zhou et al., 2008). Zhou and colleagues demonstrated that the newly reprogrammed β-islet cells were functional and could alleviate the hyperglycemia caused by insulin deficiency in a type 1 diabetes mouse model *(*Zhou et al., 2008) (Figure 1.3). Later studies also showed the conversion of liver and intestinal cells into insulin-secreting cells (Banga et al., 2012; Ariyachet et al., 2016).

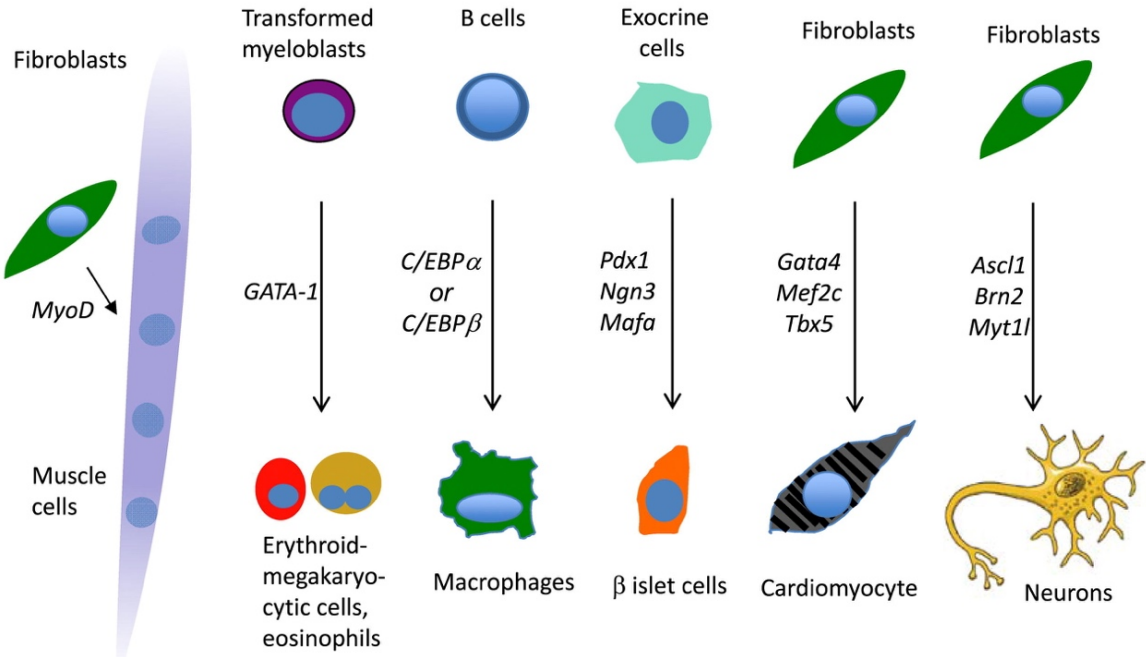

Figure 1.3: Examples of TF-induced trans differentiation. Davis et al demonstrated conversion of fibroblasts into muscle cells using TF MyoD (Davis et al., 1987); TF GATA-1 can be used to convert

myeloblasts to megakaryocytes (Kulessa et al., 1995); Overexpression of C/EBPα or β leads to conversion of B and T cell progenitors into macrophages (Xie et al., 2004); Exocrine cells of the pancreas can be converted to insulin-producing β-islet cells by using a cocktail of Ngn3, Pdx1, and Mafa (Zhou et al., 2008); Cocktail of TF Gata4, Mef2c and Tbx5-based conversion of mouse fibroblasts into cardiomyocytes (Ieda et al., 2010); Mouse and human fibroblast conversion into functional neurons by cocktail of Brn2, Ascl1 and Myt1l (Vierbuchen et al., 2010). (Reprinted from Graf, 2011).

Similarly, cardiac and dermal fibroblasts have been shown to be converted to beating cardiomyocytes upon the expression of Gata4, Mef2c and Tbx5 (Figure 1.3) (Ieda et al., 2010). Interestingly, *in vivo* delivery of this cocktail of TFs directly into the heart converted endogenous mouse fibroblasts into functional cardiomyocytes with even greater quality than *in vitro* (Inagawa et al., 2012; Qian et al., 2012; Srivastava and DeWitt, 2016).

Studies carried out by Vierbuchen et al. and Pang et al. demonstrated the conversion of mouse and human fibroblasts into functional neurons by the expression of Brn2, Ascl1 and Myt1l, as well as NeuroD1 (Vierbuchen et al. 2010; Pang et al. 2012) (Figure 1.3). Recently, direct *in vivo* reprogramming to neurons in rodent models of brain injury have also been attempted (Guo et al., 2014; Pereira et al., 2017). Recently Ascl1 alone was shown to be sufficient for *in vivo* reprogramming of astrocytes into induced neurons (Liu et al., 2015). In addition, NeuroD1 has also been demonstrated to reprogram cortical glial cells to glutamatergic and GABAergic neurons after brain injury and in Alzheimer's disease model (Guo et al., 2014).

Despite great progresses in the reprogramming field, the efficacy and context dependency of the conversion remain major challenges. Studies focusing on the mechanisms that safeguard cell fate and counteract reprogramming can help us to understand how cell fate is maintained and thereby, help us to overcome these limitations in reprogramming.

1.1.3 Cell fate safeguarding mechanisms

The field of reprogramming has challenged the concept of terminal differentiation. This concept is useful but biologically inaccurate. Instead, the differentiated cells can be viewed as stable cellular states that are maintained by mechanisms that safeguard their identity and pose a barrier to conversion by reprogramming factors (Blau and Baltimore, 1991; Sánchez Alvarado and Yamanaka, 2014). These safeguarding mechanisms are employed during the course of development and prevent changes to cell type-specific transcription programs. Interestingly, a balance of repressors and activators of this cell memory maintains the cellular identity by sustaining identity-specific gene expression, but also allowing the possibility of

switching to a different fate. The context dependency that is observed for a transcription factor to convert a given cell type underscores these cell fate safeguarding mechanisms and the ability of the transcription factor to overcome them. The presence of these safeguard mechanisms thus underlies the overall low efficacy in reprogramming as well as the slow kinetics of the process (Wang et al., 2011; Polo et al., 2010).

Studies have demonstrated that this memory of cellular identity operates during its establishment and maintenance by employing chromatin modifications, non-coding RNAs, as well as blocking the activity of RNA polymerase II (Brumbaugh et al., 2019). Furthermore, cellular metabolism also plays a role in the regulation of cell fate (Chang & Ng, 2017). Collectively, these cell fate mechanisms silence the expression of a specific set of genes when and where it must be repressed. Recent studies have demonstrated the role of chromatin modifiers including members of the conserved Polycomb group (PcG) as well as trithorax group (trxG) in maintaining the transcription patterns and thus cellular identity. The PcG and trxG comprise of multi-protein complexes which have been shown to modify chromatin to repress and activate transcription across genes involved in various processes including development and cell cycle regulation (Kuzmichev et al., 2002; Milne et al., 2002, Nakamura et al., 2002; Müller et al., 2002). Moreover, they have been shown to operate in the early stages of embryonic life, development and in adulthood (Orlando et al., 2003). This modification and accessibility in chromatin structure form the molecular imprint of the cellular identity. Interestingly, components of the polycomb repressive complex LIN-53, CAF-1p48 (mammalian ortholog of LIN-53) and Bmi1, have been shown to be barriers in reprogramming in *C. elegans* and mice, respectively (Tursun et al. 2011; Cheloufi et al., 2015; Zhou et al., 2016). Similarly, members of the FACT (Facilitates Chromatin Transcription) complex of chromatin regulators comprising Spt16/SUPT16H and Pob3/SSRP1, have been shown to maintain cellular identities and prevent reprogramming to neurons in *C. elegans,* as well as to iPSCs in human fibroblasts. Furthermore, Onder et al described the role of a histone methyltransferase DOT1L, which upon knockdown, increases the reprogramming efficiency by modifying the DNA and histone methylation patterns (Onder et al., 2012). Recently, the role of chromodomain-containing chromatin regulator MRG-1 in preventing germ cell conversion to neurons has also been described in *C. elegans* reflecting a prevalence of epigenetic regulation in cell fate safeguarding (Hajduskova et al., 2019).

Various microRNAs (miRNAs) are highly expressed in specialized cells and post-transcriptionally regulate gene expression. A number of studies have identified the role of short hairpin RNAs (shRNAs) in enhancing as well as suppressing the process of reprogramming (Onder et al., 2012; Qin et al., 2014; Cheloufi et al., 2015; Miles et al., 2017). Knock down of members of the miR-34 family of miRNAs have been shown to result in enhanced reprogramming efficiency due to posttranscriptional derepression of pluripotency-associated genes, Nanog, Sox2 and N-Myc (Choi et al., 2011; Lee et al., 2012). Similarly, Melton et al. depleted the miRNA let-7 in Mouse Embryonic Fibroblasts (MEFs) which resulted in dramatically increased reprogramming efficiency (Melton et al., 2010). It also acts as a reprogramming barrier to human iPSC generation by stimulating the expression of pro-differentiation genes (Worringer et al., 2014). Another study used the model in which the human fibroblasts were converted to iPSCs. Using a whole genome knock-down screen by shRNAs, a number of reprogramming barriers were identified including genes involved in ubiquitination, as well as novel pathways like cell adhesion, motility and endocytosis (Buckley et al., 2012; Qin et al., 2014). In addition to ubiquitylation, another post-translational modification that involves the addition of SUMOs (small ubiquitin-like modifiers) termed Sumoylation has been implicated in cell fate maintenance. Borkent et al. showed the depletion of SUMO2 resulted in enhanced and accelerated reprogramming during iPSC generation (Borkent et al., 2016).

Furthermore, cellular signaling pathways including glycogen synthase kinase-3ß (GSK-3ß) and SMAD signaling have been implicated in conversion of neonatal human fibroblasts into functional neuron-like cells (Ladewig et al., 2012). Several studies have demonstrated the role of cell cycle inhibitors $p16^{Ink4a}$ and $p19^{Arf}$ in reprogramming to neurons as well as generation of iPSCs through control of cellular senescence (Banito et al., 2009; Li et al., 2009; Utikal et al., 2009). Furthermore, a similar inhibitory role of apoptosis during direct reprogramming to neurons has also been described. Gascon et al. demonstrated that upon overexpression of the anti-apoptotic protein Bcl2 together with TF Ascl1, the glial-to-neuron conversion efficiency is increased (Gascon et al., 2016). In addition, recent studies have also demonstrated the role of metabolism and the metabolic state of cells to be involved in maintaining cell identity (Tatapudy et al., 2017; Cliff et al., 2017).

However, significant gaps still exist to better understand how cellular processes such as metabolism maintain cell fates. Also, it is unclear whether they act as reprogramming barriers in a cell specific way and how well they are conserved across species.

1.2 Mitochondria, metabolism and reprogramming

1.2.1 Mitochondrial dynamics during development, cell differentiation and reprogramming

Since its initial discovery about a hundred years ago, mitochondria as an organelle and its functions have been extensively studied. Widely described as the power house of the cell, the function of mitochondria however is not limited to energy generation. In addition to its role of producing energy by oxidative phosphorylation and beta oxidation of lipids, mitochondria are involved in regulation of intracellular levels of calcium, iron-sulfur protein assemblage, apoptosis and innate immunity cell signaling pathways (Jacobson & Duchen, 2004; Stehling et al., 2014; Tait & Green, 2010; Cloonan & Choi, 2013). Unlike other organelles, mitochondria contain their own DNA content and are not formed by de novo synthesis. Mitochondrial content in the cell is balanced by fusion and fission of the pre-existing mitochondria and allows them to form different structures (Chan, 2012; Otera et al., 2013). The morphology of the mitochondria is influenced by both extracellular and intracellular signals, and can range from tubular and networked to fragmented and isolated depending on the rate of these fusion and fission processes; and differs in different cell types, cell division stages and through development (Smirnova et al., 2001; Taguchi et al., 2007).

During fertilization, the mitochondria are provided by the oocytes and are therefore of maternal origin. In the early developmental phases of the embryo, mitochondria do not undergo biogenesis and its number is reduced to one half upon each round of replication (Blerkom et al., 2009). In addition, these cells typically consist of mitochondria with a poorly developed cristae network and a low mitochondrial DNA (mtDNA) copy number. In contrast, the differentiated somatic cells comprise of mitochondria consisting of a complex, cristae-rich and tubular structure characterized by a dense matrix and a high mtDNA number (John et al., 2005; Suhr et al., 2010; Folmes & Nelson., 2011). This structural complexity arises during the process of cell differentiation during embryogenesis.

Lineage commitment and cell differentiation is characterized by a progressive increase in complexity, mass and size of the mitochondria (Chung et al., 2007) (Figure 1.4). This corresponds with an increase in the cellular dependence on energy driven by biochemical reactions occurring in the organelle in order to support its differentiation and specialized cellular functions. Since energy demands vary between different cell types depending on function, the adaptation of energy production based on the physiological requirement forms the basis of cell identity (Harvey, 2019). Specialized cell types including, for example, cardiomyocyte and adipocytes display an increase in matrix complexity and hence increased functionality of the mitochondria, reflecting the cellular needs to perform their respective function (Chung et al., 2007; Hom et al., 2011; Tormos et al., 2011). In addition, mitochondrial functions including energy generation, ROS signaling and Ca^{2+} storage play an important role during the development and maintenance of fully differentiated neurons (Flippo & Strack, 2017). A number of neurodegenerative diseases including Parkinson's and ataxias are characterized by genetic mutations coding for genes associated with mitochondrial function highlighting the role of mitochondria in maintaining neuronal homeostasis (Bertholet et al., 2016).

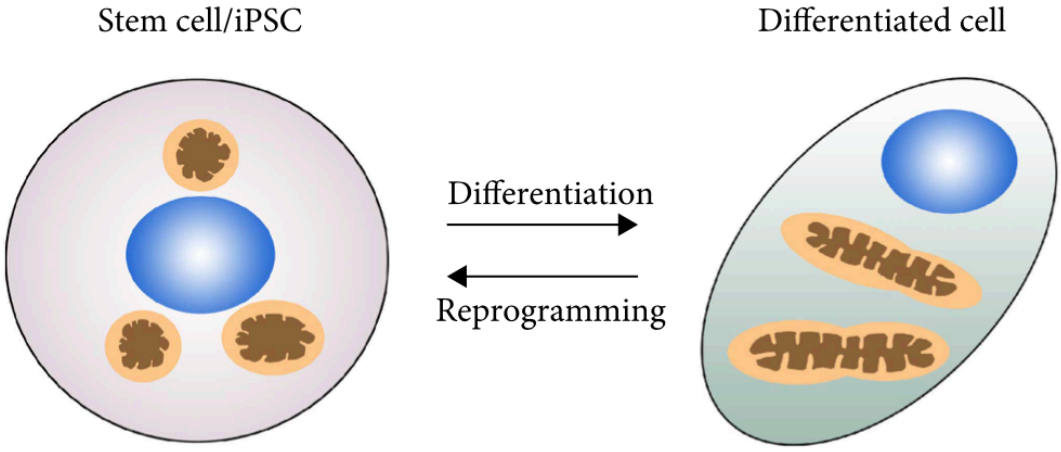

Figure 1.4: Schematic representation of mitochondrial dynamics in stem cells and differentiated cells. Stem cells and iPSCs are characterized by spherical shaped mitochondria, localized in the nuclear periphery and with poorly developed cristae. In differentiated cells, mitochondria are enlarged, with a dense matrix and complex cristae network. (Adapted from Fu et al., 2019).

Similar to embryonic development, the switch to differentiation in stem cells is characterized by increased mitochondrial content and complexity, and respiration by oxidative phosphorylation (OXPHOS), contrasting the poorly developed mitochondria and reliance on glycolysis as the main energy source in stem cells (Folmes et al., 2011). The reliance on

glycolysis instead of OXPHOS for energy generation (termed the Warburg effect) is also a characteristic of cancer cells which thereby retain their rather undifferentiated state and increased proliferation status. This is characterized by a poorly developed, isolated mitochondrial structure (Craene & Berx, 2013).

During somatic cell reprogramming of fibroblasts to pluripotent state by the Yamanaka factors, cells undergo a sequence of events eventually attaining plasticity (Stadtfelt et al., 2008) (Figure 1.4). It starts with the downregulation of somatic cell markers followed by cell proliferation and induction of metabolic switch from OXPHOS to glycolysis and eventually mesenchymal to epithelial transition (Mikkelsen et al., 2008; Folmes et al., 2011; Li et al., 2010; Tehrani et al., 2010). This results in the attainment of pluripotency and also actively erases the somatic epigenetic signature (Figure 1.5). During this process, mitochondrial dynamics follow the reverse path as compared to embryonic development; they become fragmented, show reduced mtDNA content and exhibit decreased functionality (Suhr et al., 2010; Prigione & Adjaye, 2010; Kelly et al., 2013; Folmes et al., 2011; Choi et al., 2015). The work of Preito et al. describes the role of proteins involved in mitochondrial fission and shows that they play an important role in this cell reprogramming process (Preito et al., 2016). They demonstrated a decreased reprogramming efficiency upon knock down of Mid51 and Gdap1, knockout of the latter being responsible for the phenotype due to the failure in mitochondrial fragmentation resulting in G2/M arrest (Preito et al., 2016; Qian et al., 2012).

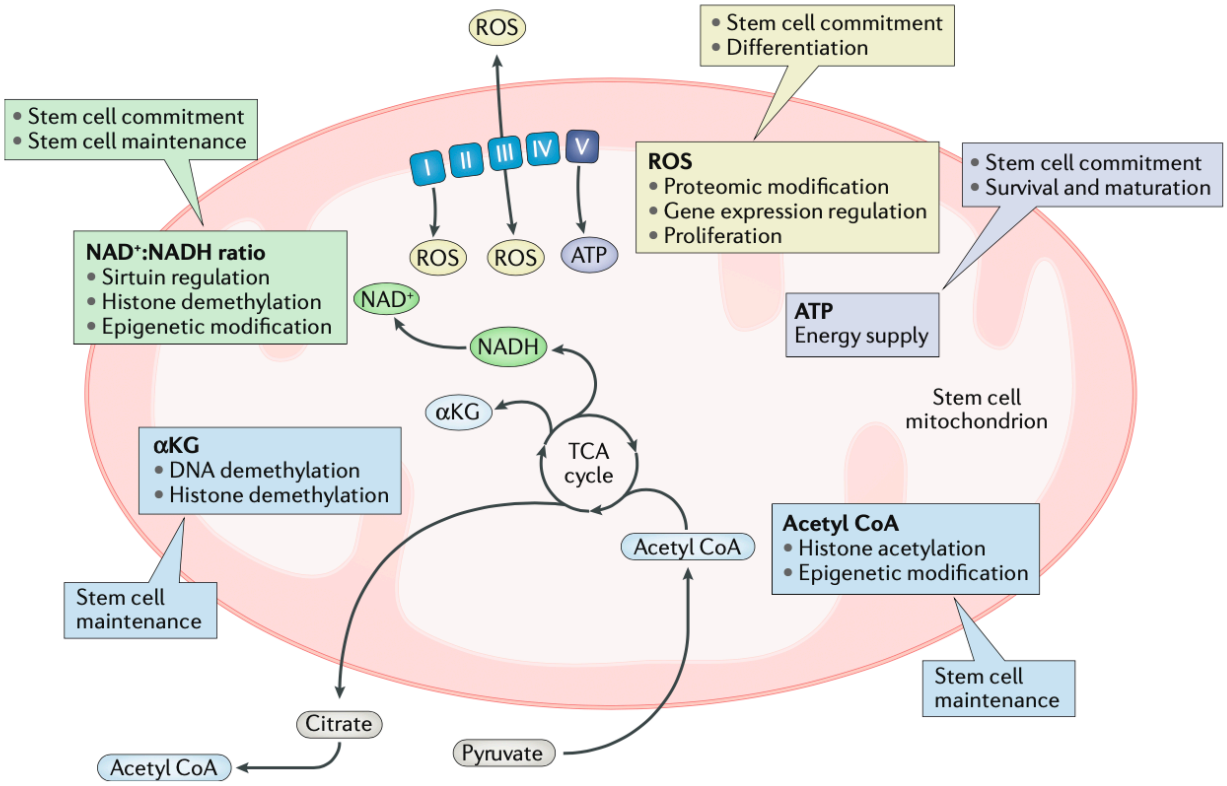

Figure 1.5: Mitochondrial metabolism and its regulation of cell functions. Schematic representation of the metabolites generated by the the tricarboxylic acid (TCA) cycle and the electron transport chain occurring in mitochondria act as signaling molecules to regulate several aspects of stem cell function. The different coloured boxes represent stem cell regulatory mechanisms mediated by mitochondrial ATP (purple), ROS (yellow), TCA cycle intermediates (blue) and NAD^+ (green). αKG, α-ketoglutarate. (Reprinted from Khacho et al., 2018).

Recent studies have also highlighted the role of mitochondrial function and its linked metabolism in specifying the cell fate and actively maintaining cellular identity (Chung et al., 2007). Studies by Mandel et al. and Preira et al. illustrate the failure of embryonic stem cells (ESCs) to differentiate upon inhibition of mitochondrial function by treatment with antimycin A or carbonyl cyanide m-chlorophenyl hydrazine (CCCP) (Mandal et al., 2011; Preira et al., 2013). This challenges the previous understanding whereby mitochondrial development dynamics were considered to be the result of commitment to cellular identity, and instead places mitochondrial functionality as one of the drivers that shape it (Chung et al., 2007). Recent studies show that various mitochondrial metabolites previously considered to be by-products of metabolic reactions, act as signaling molecules, and are co-factors to the enzymes that modify the epigenetics of the cell and thus alter gene expression. In addition, metabolites such as alpha ketogluterate (a-KG), acetyl coenzyme A (acetyl coA), citrate, $NADH/NAD^+$,

as well as other citric acid cycle intermediates are important substrates for these epigenetic modifications (Figure 1.5). The change in the global gene expression profile as a result of these modifications can have important implications in cell fate decisions (Shyh-Chang et al. 2013a; Folmes & Terzic 2014; Harvey et al. 2016).

1.2.2 Metabolic remodeling during cell fate specification

Metabolic reactions serve various purposes in the cell with the most well recognized being the generation of ATP that allows the cells to carry out energetically unfavorable anabolic reactions. In addition, metabolic reactions generate carbon precursors including phospholipids, amino acids and nucleotides that are needed for the generation of biomass required for the cell division to occur (Ly et al., 2020; Lunt and Vander Heiden, 2011).

A number of inputs influence and define the given metabolic state of a cell. These include nutrient and oxygen availability, cell signaling, as well as energetic and biomass demands of the cell. These inputs and demands collectively affect the energy generation through glycolysis in the cytoplasm, versus OXPHOS (occurring in the mitochondria), as well as the side reactions that produce anabolic intermediates. During the process of cell differentiation, changes occur in the inputs that influence metabolism and thus result in the change in the metabolic state of the cell. However, in addition to the changes in metabolic state (termed as metabolic reprogramming) as a result of differentiation, metabolic shifts in the cells can have permissive and sometimes instructive roles in promoting cellular differentiation (Shyh-Chang et al., 2013). An increasing number of recent studies including self-renewal in muscle stem cells and haemopoietic stem cells provided evidence in shaping the perspective on this role of metabolism as the driver and regulator of cell fate transitions (Theret et al., 2017; Ito et al., 2012) (Figure 1.6).

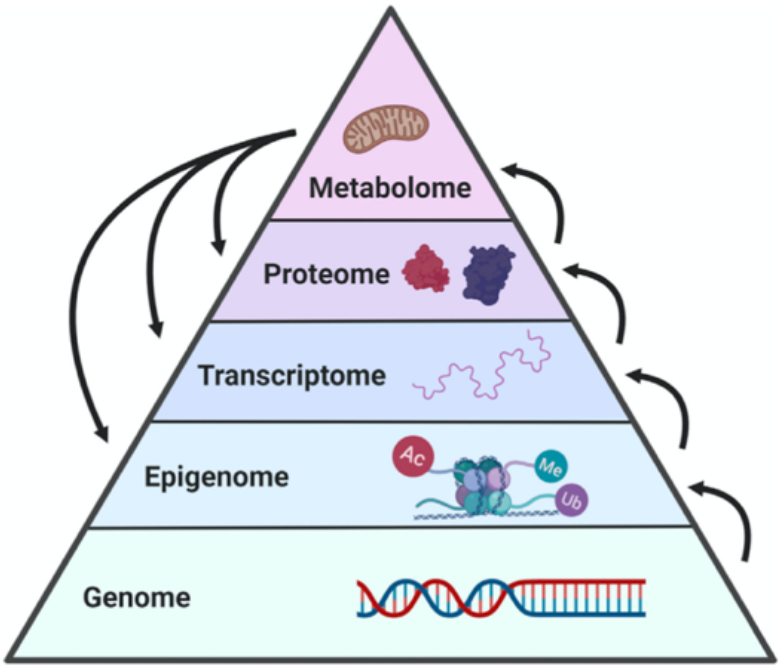

Figure 1.6: Factors affecting cell fate decisions. The conventional dogma of molecular biology describes a hierarchy from DNA to RNA to protein. However, understanding of this view has expanded to include the epigenome and the metabolome as important determinants of cellular fate and function. Recent works have not only included the above mentioned (and other) additional determinants, but also demonstrated the complex relationship between them: instead of the feed forward hierarchy, there are feedback mechanisms as well. Together, these form complex relationships that eventually regulate cell fate decisions. (Reprinted from Ly et al., 2020).

In the context of pluripotent cells, cellular reliance on metabolism is different based on cell type as well as differentiation status. In adult stem cell lineages, the less active long-term progenitors including the stem cells of skeletal muscle - the satellite cells as well as the quiescent pluripotent stem cells, predominantly employ glycolysis. However, stem cell populations that undergo active proliferation display bivalent metabolic state utilizing OXPHOS in addition to glycolysis (Simsek et al., 2010; Suda et al., 2011; Almada et al., 2016). ESCs exhibit transitions through several metabolic states during differentiation. In the naïve state, these ESCs show high levels of OXPHOS although these cells still consume high amounts of glucose and glutamine (Zhau et al., 2012; Carey et al., 2015). Differentiation of these ESCs towards a more primed state is characterized by an increased dependence on glycolysis for energy and biomass generation. As the process of differentiation proceeds beyond this primed state, cellular energy demands are again met predominantly by OXPHOS. Similarly, the reprogramming of somatic cells into induced pluripotent stem cells (iPSCs) necessitates the shift from reliance of the bivalent metabolic program of glycolysis and

OXPHOS towards predominantly glycolytic state resembling the metabolism of ESCs (Folmes et al., 2012; Folmes et al., 2011). Interestingly, recent studies have demonstrated that this metabolic shift precedes the changes in gene expression, highlighting the metabolic reprogramming as the driver rather than the consequence of this cell fate change (Hansson et al., 2012) (Figure 1.6).

In most cases, however, changes in cellular metabolism are the result of cell signaling molecules including 5' AMP-activated protein kinase (AMPK), Hypoxia Inducible Factor alpha (HIF1a), Serine Thionine protein kinase (AKT) and V-Myc Avian Myelocytomatosis Viral Oncogene Homolog (Myc). A cellular stress response program is activated by AMPK upon high [Adenosine monophosphate (AMP)]/[Adenosine triphosphate (ATP)] ratios resulting from low nutrient availability and metabolic stress. Upon activation, AMPK increases cellular energy generation through glycolysis, induces the expression of antioxidants as well as cellular growth restriction though mammalian target of Rapamycin (mTOR) (Mihaylova et al., 2011; Ito et al., 2014). This stress response program operates in cell self-renewal as well as differentiation owing to its important role in regulating cellular homeostasis. Under conditions of low oxygen concentration, the transcription factor HIF-1a is active and steers cellular energy generation towards glycolysis over OXPHOS during periods of low activity in quiescent and slow dividing adult stem cells including HSCs, MSCs as well as satellite cells (Takubo et al., 2010). This HIF-1a mediated change is more suited to the quiescent stem cell niches that are in hypoxic environments and reduces mitochondrial reactive oxygen species (ROS) mediated damage. In stem cells, Akt promotes differentiation by increased production of ROS. Similarly, differentiation in HSC and epidermal stem cells is characterized by the activity of Myc (Wilson et al., 2004). In addition, activity of Myc and/or mTOR signaling is needed for reprogramming into iPSCs (Cao et al., 2015; Ryall et al., 2015). Overall, during differentiation, these changes in metabolic environment of the cells are essential to meet the energetic and anabolic demands of the new cell state (Tatapudy et al., 2017).

Apart from the above described passive role of metabolism in the context of differentiation, it can also act as the driver for the change in cell fate through changes in cell signaling and gene expression. One of such examples is mammalian target of Rapamycin (mTOR) signaling, which is one of the key regulators of cell growth and proliferation. In ESCs, TOR has been shown to be involved in maintenance of pluripotency and repression of genes involved in differentiation (Hsu et al., 2016). Furthermore, activation of mTOR in quiescent

HSCs leads to differentiation by inducing mitochondrial biogenesis (Vannini et al., 2016). In addition, changes in pyruvate metabolism have also been shown to regulate proliferation and differentiation in epidermal and intestinal cell lineages (Flores et al., 2017; Schell et al., 2017). Pyruvate is produced in the cell by glycolysis, and can then be converted to lactate in the cytoplasm; or can enter mitochondria where it is converted to acetyl coA and enters the citric acid cycle. Studies carried out by Schell et al. and Sandoval et al. demonstrated that increased conversion of pyruvate to lactate drives proliferation, whereas increased mitochondrial oxidation of pyruvate promotes differentiation in epidermal and intestinal stem cells respectively (Schell et al.; 2017; Sandoval et al.; 2017). Overall, these studies demonstrate that changes in metabolism influence cell fate decisions by influencing cell signaling and gene expression (Tatapudy et al., 2017).

1.2.3 The role of metabolites in epigenetic regulation and cell fate

Recent studies on metabolism have highlighted its previously underrated role in influencing cell fate decisions by regulating the epigenetics and ultimately gene expression. This includes provision of the metabolites needed for chromatin modifications by the histone and DNA modifying enzymes (Ryall et al., 2015a; Stewart et al., 2018). DNA and histone modifications including the phosphorylation, crotonylation, succinylation, butyrylation, acetylation and methylation result in changes in chromatin accessibility and gene expression (Figure 1.6) (Ly et al., 2020).

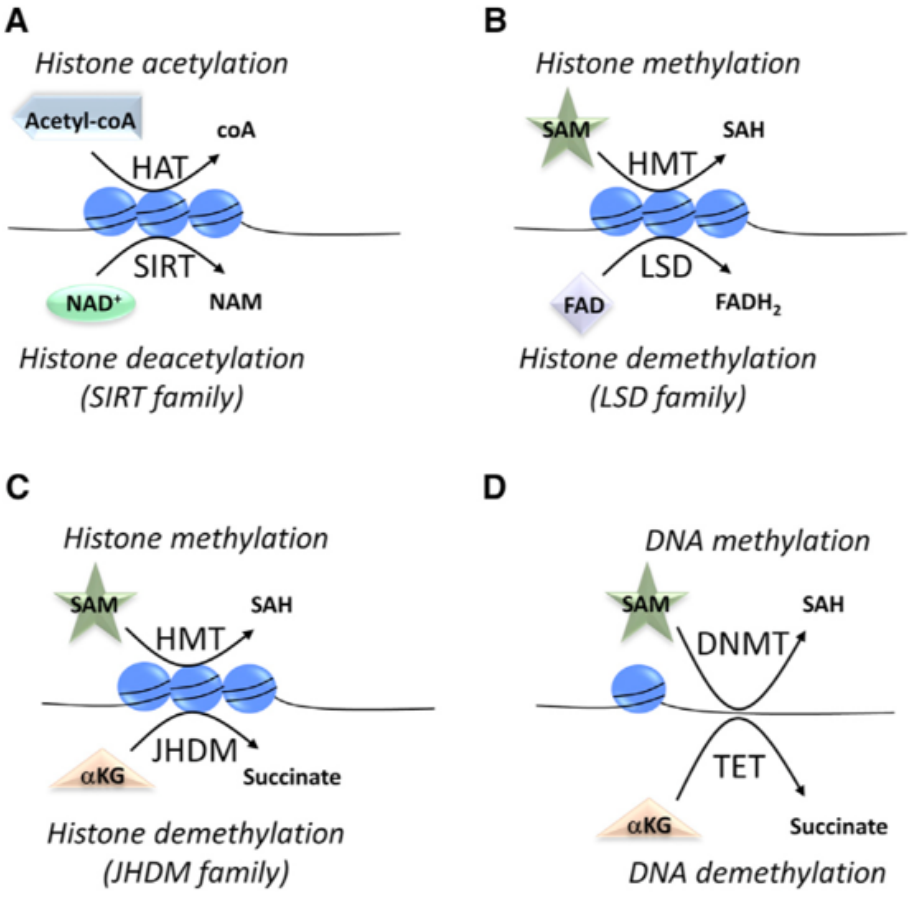

Figure 1.7: Metabolites as Essential Cofactors in the Epigenetic Regulation of Transcription. (A) Acetylation of histones occurs by the actions of histone acetyl- transferases (HATs), which attach an acetyl group to lysine residues and release co-enzyme A. In contrast, histone deactylation is performed by HDAC proteins, including the Sirtuin family. Activity of sirtuins is dependent on the availability of NAD^+ for their deacetylase activity. (B–D) Methylation of either histone proteins or DNA occurs via the attachment of a methyl group (from SAM) to either lysine or arginine residues in a reaction mediated via HMTs (B and C) or DNMT (D). Enzymes that perform histone demethylation belong to (B) the LSD family of demethylases, which require FAD as a cofactor, or (C) the JHDM family, which require aKG as a cofactor. The TET family of DNA demethylases also require aKG for their activity (D) (Reprinted from Ryall et al., 2015).

Histone acetylation:

Cellular enzymes termed histone acetyl transferases (HATs) can transfer the acetyl groups from acetyl CoA to the histone tails (Sabari et al., 2015). The acetylation of histones predominantly increases the chromatin accessibility and hence the gene transcription (Shahbazian and Grunstein, 2007). This reaction is reversed by the activity of histone deacetylases (HDACs) and are classified into four major classes in humans and require Zn^{2+} and NAD^+ for their activity (Figure 1.7). The acetylation of the histones is therefore dependent

on the availability of acetyl-CoA and the cofactors of deacetylases demonstrating global gene expression changes regulated by the availability of these metabolites. Acetyl-coA is produced in various metabolic reactions in the cell including fatty acid oxidation, amino acid breakdown and glycolysis. Interestingly, it has been shown that cells use glycolysis derived citrate to form acetyl-coA to utilize for histone acetylation (Figure 1.7) (Wellen et al., 2009). This link between glycolysis and histone acetylation has also been observed in ESCs, MuSCs and tumor cells (Moussaieff et al., 2015b; Ryall et al. 2015). In addition to histone acetylation, histones can be subjected to an interlinked modification of acylation involving the addition of short chain fatty acids including butyrylation, crotonylation, and succinylation. While this process shares the same machinery (enzymes HATs and HDACs) for the histone modifications, decrease in the levels of acetyl-coA, which results in decreased histone acetylation, results in increased crotonylation and vice versa (Wellen et al, 2009; Sabari et al., 2015). These studies demonstrate epigenetic effects resulting from the changes in the balance of metabolites derived from mitochondrial metabolism (acetylation) versus beta oxidation (crotonylation).

DNA and histone methylation/demethylation:

Methyl group can be added to both histones and DNA; and while methylation of DNA generally results in transcriptional repression, histone methylation can result both in increased and decreased gene expression (Bird, 2002; Kouzarides, 2002; Zhang and Reinberg, 2001). This methylation of DNA and histones utilizes the methyl group donated by SAM which is produced through the condensation of methionine and ATP; with the carbon backbone coming from threonine, glycine, and serine via the folate metabolism pathway (Kaelin and McKnight, 2013). This methyl group is added to a lysine or arginine amino acid on the histones or on cytosines of the DNA and is carried out by histone and DNA methyltransferases (HMTs and DNMTs), respectively. Methylation of DNA and histones is reversible and the removal of methyl group occurs by the activity of another set of enzymes- the Lysine specific demethylase (LSD1) and Jumonji family of histone demethylases; and members of TET family of DNA demethylases (DNMTs) (Figure 1.7). LSD1 requires FAD to carry out the demethylation and its activity is known to inhibit key metabolic enzymes and transcription factors thus influencing the cellular metabolic state (Hino et al., 2012). While a-KG is required by the DNMTs and Jumonji dioxygenases as a cofactor, succinate and fumarate inhibit this demethylation by acting as antagonists of a-KG (Figure 1.7, 1.8). Collectively, the activity of these methyl transferases and demethylases is therefore dependent on the intracellular levels of different metabolites

including SAM, serine, glycine and a-KG & its antagonists' (succinate and fumarate). Taken together, this links the cellular metabolism to histone and DNA modification (Shi et al., 2004; Tsukada et al., 2006).

a-KG is produced in the cell primarily during the TCA cycle and the glutamine metabolism. As mentioned earlier, it acts as a cofactor for a number of dioxygenases (Lunt and Vander Heiden, 2011). In order to be utilized by these enzymes, it is transported out of the mitochondria, into the cytoplasm where it can be converted to other metabolites including citrate, or for the generation of various non- essential amino acids (Ryall et al., 2015). In murine embryonic stem cells (mESCs), a-KG has been shown to promote self-renewal by maintaining demethylation of histones and DNA (Carey et al., 2015). However, in human pluripotent stem cells (hPSCs), increased levels of a-KG primed the cells towards differentiation (TeSlaa et al., 2016). In addition, decreased levels of a-KG compared to its antagonists' succinate and fumarate have been shown to promote metabolic switch to glycolysis in cancer associated fibroblasts (Zhang et al., 2015). Taken together, these studies show conflicting effects of the levels of the metabolite a-KG but demonstrate its role in regulating and influencing the cell fate by changes in the methylation status of the DNA and histones.

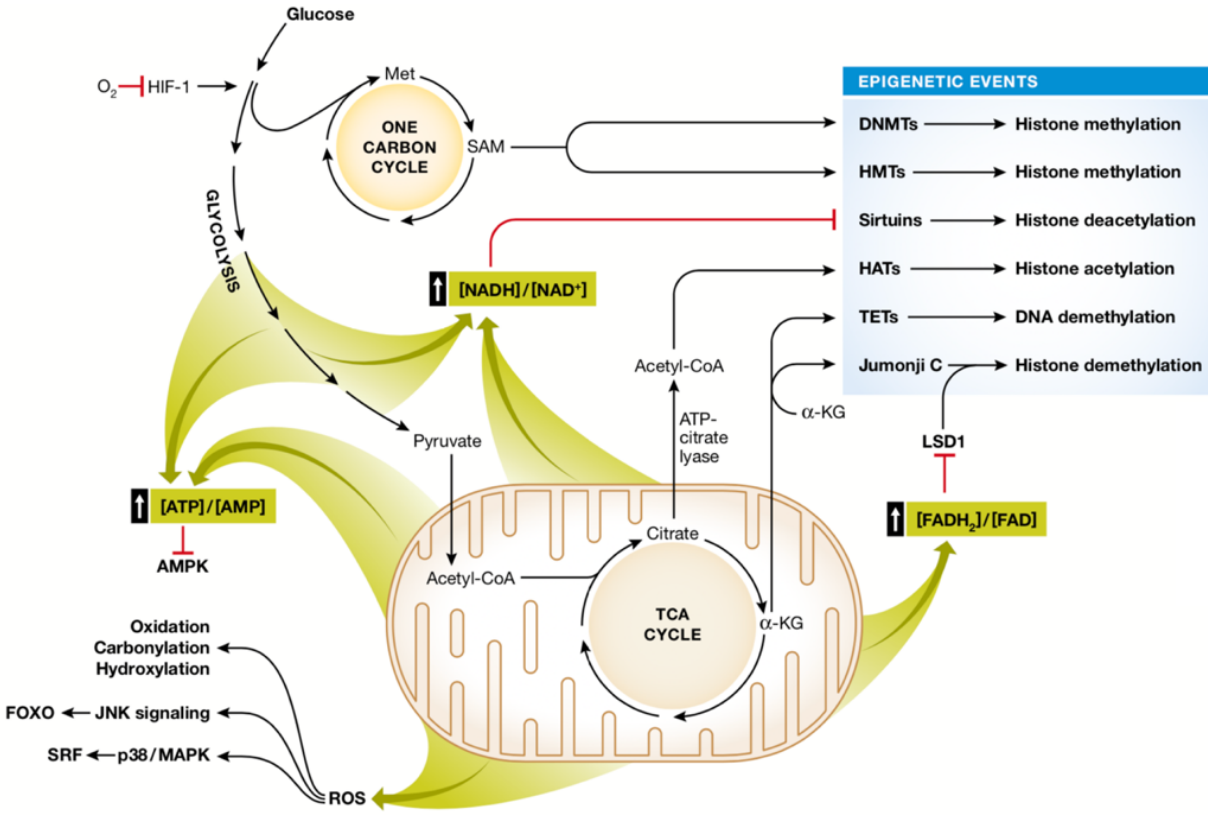

Figure 1.8: The connections between metabolism and cell fate decisions. Metabolic inputs regulate epigenetics and cell signaling that affect changes in cell fate. Metabolites generated by glycolysis feed into the folate and one carbon metabolism cycle to produce S-adenosylmethionine (SAM), which is a cofactor for DNA methyltransferases (DNMTs) and histone methyltransferases (HMTs). AMP and NAD+ are cofactors of AMPK and sirtuins respectively, and are also utilized during glycolysis and OXPHOS. Acetyl CoA produced after glycolysis and enters the TCA cycle to form citrate. This generated citrate can be converted back to acetyl CoA and contributes to the histone acetylation by histone acetyltransferases (HATs). A-KG, the intermediate of the TCA cycle, is a cofactor for TET and Jumonji C enzymes, which demethylate DNA and histones, respectively. Increased OXPHOS also generates reactive oxygen species (ROS), which promote oxidation, carbonylation, and hydroxylation as well as increase the levels of JNK and p38/MAPK pathway activity. (Reprinted from Tatapudy et al., 2017).

1.3 *C. elegans* as a model to study reprogramming

In the context of reprogramming, the model organism *C. elegans* has emerged as a powerful system to study cell fate conversion *in vivo*, and the genetic and microenvironmental factors that influence it. Tursun et al. and Patel et al. previously identified a conserved chromatin regulator LIN-53 (CAF-1p48/RBBP7) that acts as barrier of reprogramming of germ cells to neurons and muscle like cells (Tursun et al., 2011; Patel et al., 2012). Interestingly, in a later study by Cheloufi et al., CAF-1 (mouse ortholog of LIN-53), was shown to be involved in maintaining the somatic cell identity during reprogramming to neurons and iPSCs (Cheloufi et al., 2015). Furthermore, another study in *C. elegans* identified the chromatin regulator FACT complex involved in maintaining identities of intestinal and germ cells. FACT acts as a reprogramming barrier for their conversion to neuronal fate and this function of the FACT complex was shown to be conserved in human cells where its depletion enhanced the reprogramming of fibroblasts (Kolundzik et al., 2018). These findings highlight the potential of *C. elegans* in studying the process of reprogramming and identification of the conserved barriers that prevent it.

The nematode *C. elegans* is a free living, soil dwelling organism that is non-pathogenic and is found across the world. The nematode feeds on bacteria and is commonly found in rotten food that harbors their food source. In 1963, the Nobel Laureate Sydney Brenner introduced them as a genetic model to study development and neurobiology (Brenner, 1974; Corsi et al., 2015). Since then, extensive research has been carried out on the organism to answer questions related to basic cellular functions and interactions between eukaryotic cells, aging and evolution.

The features that make *C. elegans* a suitable system to study these processes is its short size, rapid life cycle, transparent body and a well annotated genome which shares conserved genes across species. Since the body of the worm is translucent, it allows the visualization of individual cells and sub-cellular components using the Nomarski imaging (Differential Interference Contrast, DIC). The transparent body also allows the use of florescent protein-based markers that can be used to tag sub-cellular compartments or proteins of interest. This florescent tagging of proteins has allowed the study of cell cycle, developmental processes, cell isolation, screens to identify mutants for cell development and function, and protein interactions *in vivo* (Corsi et al., 2015; Chalfie et al., 1994; Boulin et al., 2006).

C. elegans has a rapid life cycle of approximately 3 days in favorable conditions and exists primarily as a self-fertilizing hermaphrodite; although male arise at a frequency of <0.2 %. The animal has distinct tissues including the intestine, muscle, hypodermis, germ line, neurons and excretory system. In addition, owing to the fact the worm has an invariant number of somatic cells, researchers have been able to track the fate of each cell between fertilization and adulthood in live animals and generated a complete cell lineage (Sulston and Horvitz, 1977; Kimble and Hirsh, 1979; Sulston et al., 1983). Furthermore, the shape of each cell has been constructed from electron micrographs, including all the 302 neurons that the animal possesses in the adult hermaphrodite (White et al., 1986).

The life cycle of the worm consists of embryogenesis, four larval stages and adulthood. After fertilization, the embryos are retained inside the hermaphrodite until they reach the 24-cell stage after which they are laid. The laid egg has a virtually impermeable eggshell that allows the embryo to develop independent of the mother. After hatching, the animal passes through four larval stages (L1-L4) eventually reaching adulthood (Figure 1.9). Each of the larval stage ends with a period of inactivity in which a new cuticle is made (Raizen et al., 2008). The reproductive system gradually develops during the course of larval development, and is fully functional once adulthood is reached. Under unfavorable conditions such as starvation, the L2 larvae enter an alternative life cycle and molt into an alternative state- the *dauer*. In this state the animal can survive for several months and is characterized by an arrest in feeding and reduced locomotion (Golden and Riddle, 1984).

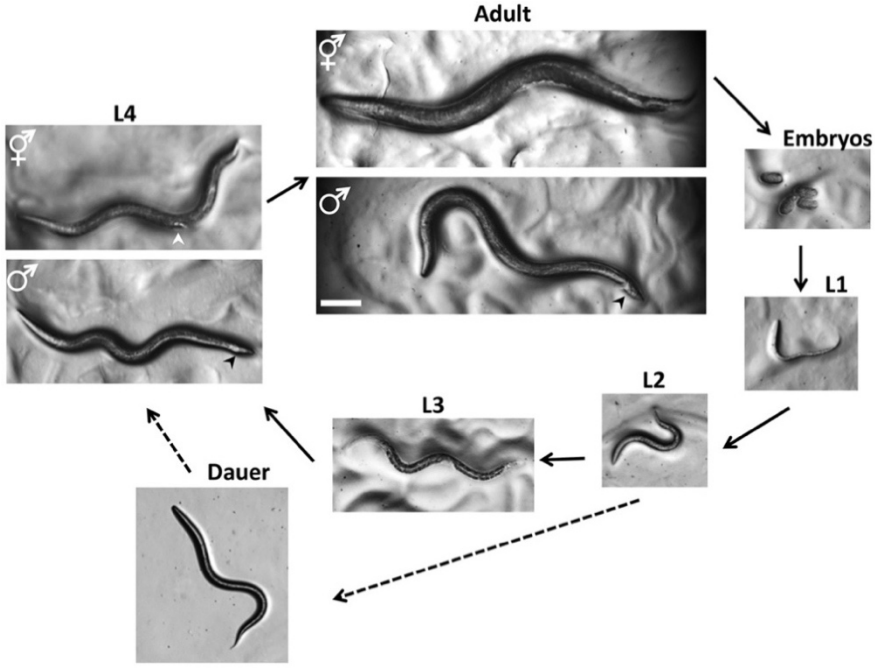

Figure 1.9: Life cycle of *C. elegans*. *C. elegans* has a rapid life cycle that consists of four larval stages and adulthood. At the L4 stage, hermaphrodites have a tapered tail and the developing vulva appears as a half circle in the mid body part of ventral side (white arrow). In contrast, the males have a wider tail (black arrow) but no obvious fan at this stage. In adults, the hermaphrodites and males can be distinguished by the wider girth and tapered tail of the hermaphrodite and slimmer girth and fan-shaped tail (black arrow) of the male. The *dauer* larvae are slimmer than all of the other larval stages. Bar: 0.1 mm (Reprinted from Corsi et al., 2015).

C. elegans was the first multicellular organism to have its genome sequenced. (*C. elegans* Sequencing Consortium 1998). This made possible the forward genetics-that rely on a genome wide mutagenesis in which unknown genes involved in a biological process are sought; as well as reverse genetics that works by knockdown of target genes (Kutscher and Shaham, 2014). This has enabled the identification and study of genes that play important roles in various developmental and cell biological processes. Remarkably, approximately 60 % of the *C. elegans* genes have homologs within the human genome (Sonnhammer and Durbin, 1997). In addition, molecular pathways that have been implicated in human diseases such as Notch, Wnt and insulin signaling are well conserved in *C. elegans* (Baumeister and Ge, 2002). Together these features make it an excellent model to study epigenetics, aging and cellular reprogramming.

In the field of reprogramming, *C. elegans* has been studied as an *in vivo* multicellular system since over two decades. One of the earliest studies by Jin et al. mis expressed transcription factor UNC-30, the terminal selector required for the specification of GABAergic neurons (Jin et al., 1994). It was shown that the upon the ectopic expression of the transcription factor, somatic cells displayed GABAergic neuronal characteristics. Subsequently, a number of other transcription factors have been shown to induce reprogramming. In developing embryos, the muscle fate inducing transcription factor MyoD homolog HLH-1 was shown to have reprogramming potential. However, this activity was limited only to the embryonic development, and was shown to be diminished or decreased in the later developmental stages (Fukushige and Krause, 2005). Similar to these findings, the reprogramming ability was shown to be restricted during the early development stages for the pharynx fate inducing transcription factor PHA-4, which is an ortholog of the vertebrate HNF-3 (Horner et al., 1998; Mango et al., 1994). Furthermore, expression of transcription factors END-1, END-2 and the downstream factor ELT-2, responsible for inducing endodermal fate also showed decreased reprogramming potential during later developmental stages (Zhu et al., 1998; Fukushige et al., 1998).

These findings highlighted the loss in cellular plasticity upon the establishment of differentiated cellular states. Yuzyuk et al. showed the role of Polycomb group complex 2 (PRC2) protein MES-2/E(Z) in this loss in plasticity (Yuzyuk et al., 2009). In the developing embryos, PRC2 performs chromatin structure reorganization that restricts the plasticity during the course of development. In addition, ubiquitous expression of HLH-1 was shown to not result in higher reprogramming efficiency in *pha-4* and *end-1* mutants, suggesting that this loss of plasticity is uncoupled from the cell fate specification (Yuzyuk et al., 2009).

Studies carried out by Tursun et al. made use of another transcription factor induced reprogramming system which employed the gustatory glutamatergic ASE neuron-specifying terminal selector TF CHE-1 (Tursun et al., 2011; Uchida et al., 2003; Etchberger et al., 2007). This system employed transgenic worm strains that carried a heat shock inducible promoter that drives *che-1* overexpression (CHE-1^{oe}), and a GFP reporter of a CHE-1 target gene, *gcy-5*, that is normally expressed in the right ASE neuron (Figure 1.10) (ASER; *gcy-5::GFP*) (Yu et al., 1997; Tursun et al., 2011; Patel et al., 2012).

Broad mis-expression of CHE-1 in early gastrula stage embryos results in the activation of ASE neuronal fate broadly (based on *gcy-5::GFP*) and the developmentally arrested embryos with deformations. However, during later developmental stages, the activation of the fate reporter upon CHE-1^{oe} becomes increasingly more restricted and eventually at the L4 and adult stages, when all tissues have differentiated, the only cells that express *gcy-5::GFP* are some anterior neurons (Patel and Hobert, 2017; Tursun et al., 2011). These are the RIS, CEP, ASK, and ASI neurons and suggest that these differentiated neurons provide some molecular context which allows the CHE-1-mediated reprogramming. However, it still unclear why these neurons are responsive to CHE-1 since they do not bear any obvious relationship to ASE (Patel and Hobert, 2017).

Using this CHE-1^{oe} system, a small-scale RNAi knock down-based screen was carried out to identify genes whose knock down allowed the CHE-1-based conversion to ASE-like neuronal cells in other cellular contexts. This screen identified a conserved histone chaperone LIN-53 (CAF-1p48/RBBP4/7 in mammals) and later, other members of the Polycomb repressive complex (PRC2) including *mes- 2*, *mes-3* and *mes-6* that act as barriers for conversion of germ cells into neuron- or muscle-like cells (Figure 1.10) (Tursun et al., 2011; Patel et al., 2012). Seelk et al. showed that this Polycomb mediated barrier to reprogramming

is antagonized by GLP-1/Notch signaling pathway (Seelk et al., 2016). Using the same system, the chromatin regulator FACT was identified to be a reprogramming barrier for the conversion of intestinal and germ cells to ASE neuron like cells; and human fibroblasts to iPSCs (Kolundzic et al., 2018).

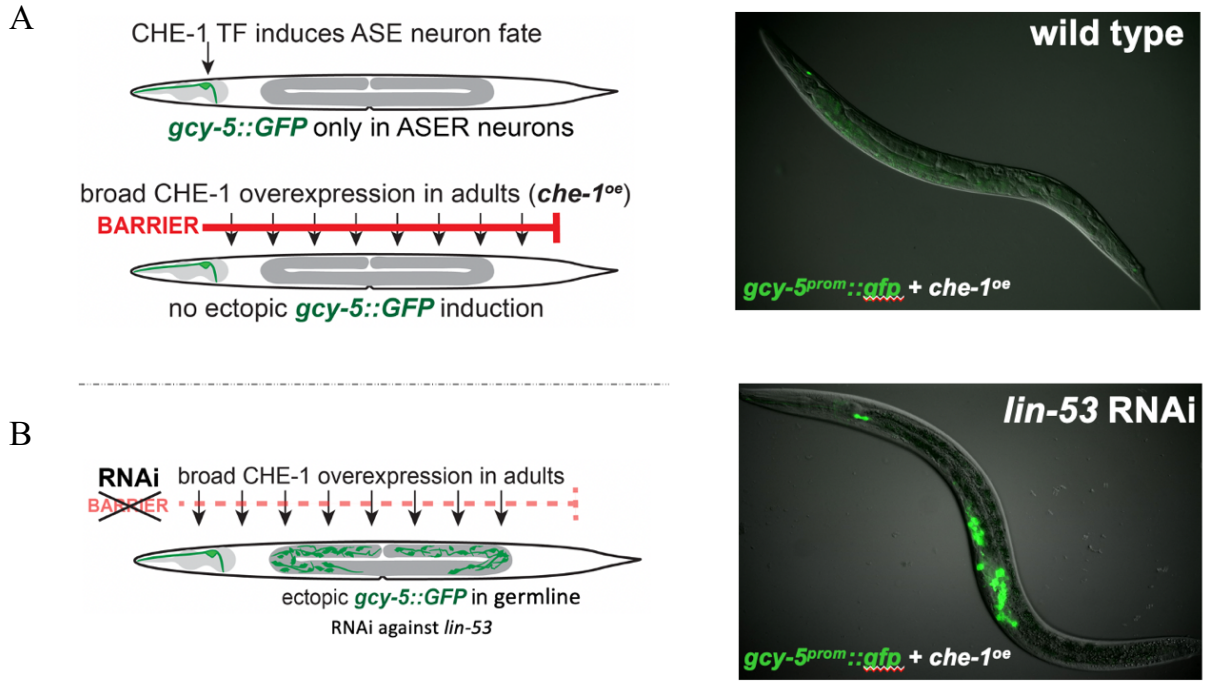

Figure 1.10: *C. elegans* as a model for reprogramming. (A) Schematic representation of transgenic animals expressing *gcy-5::GFP* reporter for ASE neuron fate induced by the zinc-finger TF CHE-1. Ubiquitous mis-expression of TF CHE-1 in the adult animals does not induce ectopic *gcy-5::GFP* except in some other head-neurons. (B) However, when a barrier, for example, *lin-53* is removed by RNAi, induction of ASE neuron fate in germ cells can be observed. Thus, upon overexpression of CHE-1, and knockdown of *lin-53*, germ cells convert to neuronal cells.

These findings demonstrate the role of histone modifiers and chromatin regulators in preventing cell fate conversion. In addition, since these reprogramming barriers are conserved across species, this highlights the potential of using *C. elegans* as a model organism to identify additional cell fate protecting factors that are conserved in mammals.

1.4 Aim of the project

Reprogramming barriers that have been identified and studied previously are in general proteins involved in chromatin regulation; and therefore, have a direct impact on chromatin accessibility for the fate inducing transcription factor. In order to identify additional factors that safe guard cell identity to TF- induced cell fate conversion, a whole genome RNAi screen in *C. elegans* was carried out and it identified 50 factors having function in mitochondria and/or metabolism. The aim of this project was to identify and characterize these factors that are involved in the mitochondrial and metabolic function as well as regulation of cell fate identities *in vivo*.

Mitochondrial function and its associated metabolism not only provide energy to drive cellular processes, but also metabolites that influence the activity of enzymes. Disturbances in cellular metabolic homeostasis can therefore have an impact on the functionality of proteins involved in various processes in the cell including chromatin modification and protein degradation. My work focuses on a conserved mitochondrial enzyme isocitrate dehydrogenase 3 (IDH3), which upon depletion, allows reprogramming of germ cells to neurons. The identified candidate functions in the mitochondria in the citric acid cycle which is the central metabolic hub of the cell. One part of my work focuses to characterize this IDH3 depletion mediated reprogramming with regard to the degree to which the germ cells are converted to neurons; as well as the cell types into which the germ cells can be converted. In a larger part of the study, I sought to understand the mechanistic basis of this IDH3 depletion mediated reprogramming event. I performed genetic screens to identify the potential players involved and carried out metabolic studies to understand the metabolic changes and compensatory mechanisms upon IDH3 depletion and link them with the cell fate safeguarding mechanisms.

2. RESULTS

2.1 Depletion of mitochondrial isocitrate dehydrogenase allows ASE fate marker expression in the germ cells

A whole genome RNAi screen was carried out in the lab previously to identify novel genes that safeguard the cell fate and pose a barrier to reprogramming. This was done in *C. elegans* using the previously described transgenic animals carrying the TF CHE-1 under a heat shock promoter, and the ASE neuronal fate marker *gcy-5^{prom}::GFP* (Tursun et al., 2011). The animals were fed with bacteria from the Ahringer RNAi feeding library (SourceBioscience) and CHE-1 expression was induced at L3/L4 stage followed by the screening for the ectopic expression of the ASE fate marker *gcy-5^{prom}::GFP* in the animals after 24 hours (Kolundzic et al., 2018). This whole genome RNAi screen identified approximately 170 candidate barriers out of which 50 were involved in mitochondrial function and/or metabolism. Since mitochondrial function has been shown to be involved in cell fate maintenance, pluripotency and differentiation (Xu et al., 2013), we decided to focus on these candidates.

Importantly, these candidates needed further validation as they were derived from a whole genome RNAi screen and could represent false-positive hits due to high-throughput procedures in handling around 20.000 bacterial RNAi clones. Out of the 50 candidates tested, (Table 2.1) *idha-1* gave a consistent and reliable phenotype. Depletion of this gene led to *gcy-5^{prom}::GFP* induction in up to 40% of the animals in the germline upon overexpression of CHE-1 (CHE-1^{oe}) similar to the previously described germ cell to neuron reprogramming upon depletion of *lin-53* and FACT complex members (Figure 2.1.1 B).

lpd-5	*mrpl-24*	*rab-10*	*gas-1*	*idha-1*
pyk-1	*cco-1*	F59C6.5	*pry-1*	*spg-7*
mrpl-17	T02H6.11	T14B4.2	*mrpl-10*	*bcs-1*
C18E9.4	R53.4	*plc-3*	*sfxn-1.2*	C34C12.8
gop-3	*ucr-1*	C16A3.5	*mrps-17*	*mrpl-32*
mrpl-11	*mrpl-12*	*wah-1*	*cco-2*	*ant-1.1*
Y82E9BR.3	M70.4	*mrps-21*	*ogdh-1*	*yars-1*
cyc-2.1	C06G3.5	*asb-2*	*mrps-33*	*mrpl-51*
hsp-1	CD4.3	*dlst-1*	*gfm-1*	*plc-1*
R04F11.2	*mrps-5*	*eft-4*	*eef-2*	*mrps-28*

Table 2.1: List of genes identified by the genome wide RNAi screen that upon knockdown allow expression of ASE neuronal marker reporter *gcy5^{prom}::GFP*.

The gene *idha-1* codes for the alpha subunit of mitochondrial isocitrate dehydrogenase (IDH3). This enzyme functions in the citric acid cycle (TCA) and catalyzes the conversion of isocitrate to alpha-ketoglutarate (a-KG) (Figure 2.1.1 C). The human homolog of the gene (IDH3A) shares a striking 96% nucleotide and amino acid homology (WormBase). In humans, the enzyme is a heterotetrametric complex, consisting of two alpha (IDH3A), one beta (IDH3B) and one gamma (IDH3G) subunit (Figure 2.1.1 D). Homologues of all three subunits (IDHA-1, IDHG-1, IDHB-1) exist in the worm and share >85% homology with the human counterparts (WormBase).

Since the knockdown of the alpha subunit *idha-1* gave a consistent phenotype, we knocked down other members of the complex to check if it resulted in the same effect (Figure 2.1.1 E). Knockdown of the gamma subunit *idhg-1* also showed similar *gcy-5*^{prom}*::GFP* induction in the germ line upon CHE-1^{oe}. However, we did not see reprogramming upon knockdown of IDHB-1 knockdown. This is possibly due to the fact that IDHB-1 plays a structural role in enzyme assembly, and the enzyme has been reported to have considerable basal activity in its absence, with alpha and gamma subunits (Ma et al., 2017). Interestingly, knockdown of the isozyme IDH-1 (functional in the cytoplasm) or IDH-2 (also operates in the mitochondria but does not function in the TCA cycle) does not result in the phenotype.

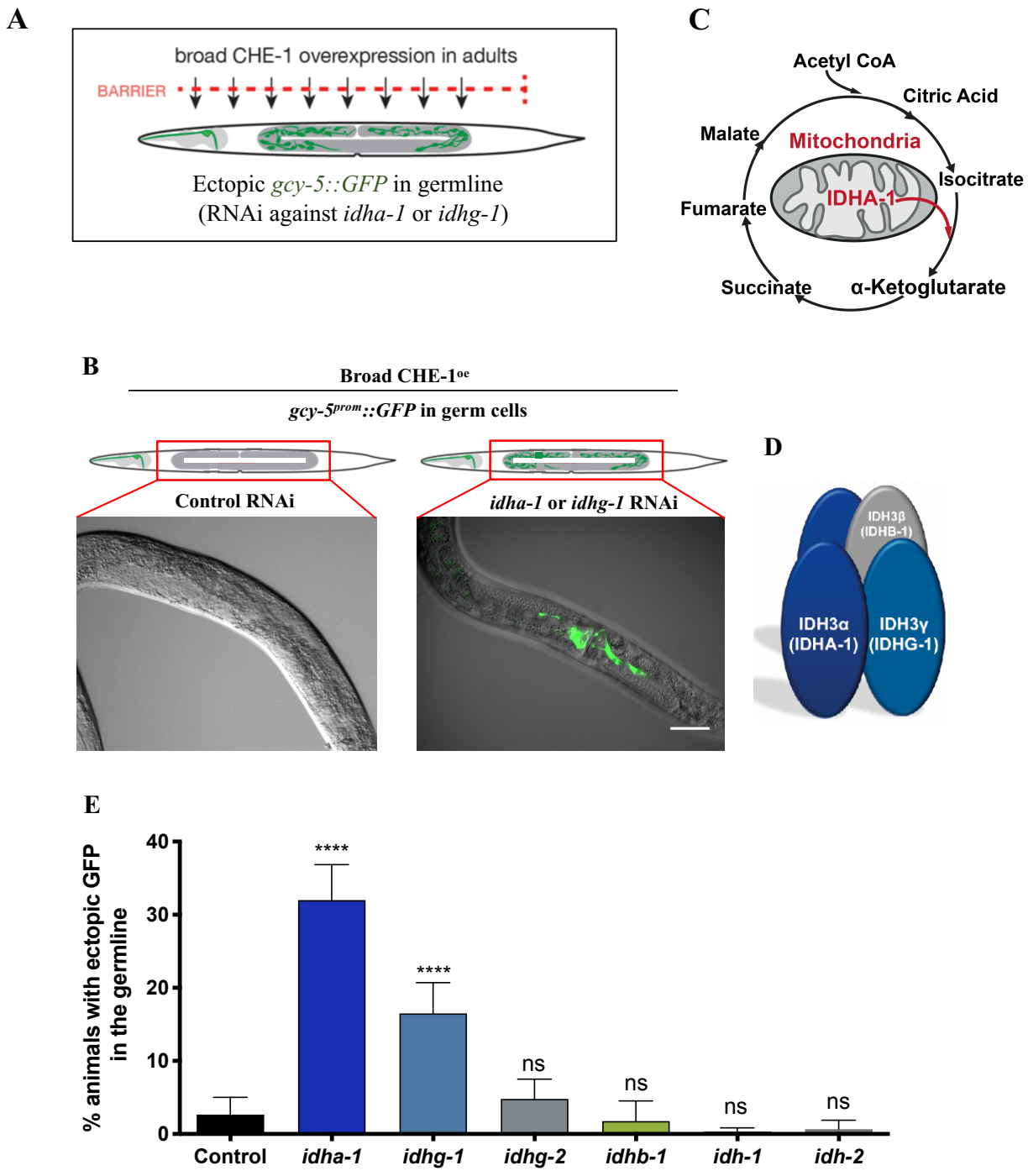

Figure 2.1.1 Depletion of the mitochondrial isocitrate dehydrogenase complex subunits allow TF induced ASE fate marker expression in the germ line. A) Schematic representation: *idha-1* or *idhg-1* RNAi allow TF CHE-1 mediated induction of ASE neuron fate in the germ line. **B)** Representative image of *idha-1* depletion mediated CHE-1 induced ASE marker expression in the germ line. Scale bar: 50 µm. **C)** Schematic drawing of the TCA cycle in the mitochondria; IDHA-1 mediates conversion of isocitrate to a-KG. **D)** Schematic representation of the isocitrate dehydrogenase complex consisting of two alpha, one beta and one gamma subunit. **E)** Quantification of the CHE-1^{oe} mediated ASE marker induction in the germ line upon depletion of putative isocitrate dehydrogenase subunits in *C. elegans*.

Knockdown of the subunits of the isocitrate dehydrogenase resulted in the ASE neuronal marker expression only in the germ line. Since no expression data is available for the proteins, we next analyzed the expression of the two subunits IDHA-1 and IDHG-1 by generating CRISPR strains whereby we tagged the two proteins at the C terminus with Human Influenza Hemagglutinin (3xHA) and 3xFLAG tag respectively (Figure 2.1.2 A). We next performed immunostainings and studied the expression of these proteins. Both the alpha and gamma subunit showed mitochondrial localization (Figure 2.1.2 D), as expected and show an overlap in expression (Figure 2.1.2 C). However, interestingly they were expressed throughout the worm body (Figure 2.1.2 B); although the conversion phenotype observed upon knockdown is only in the germ line.

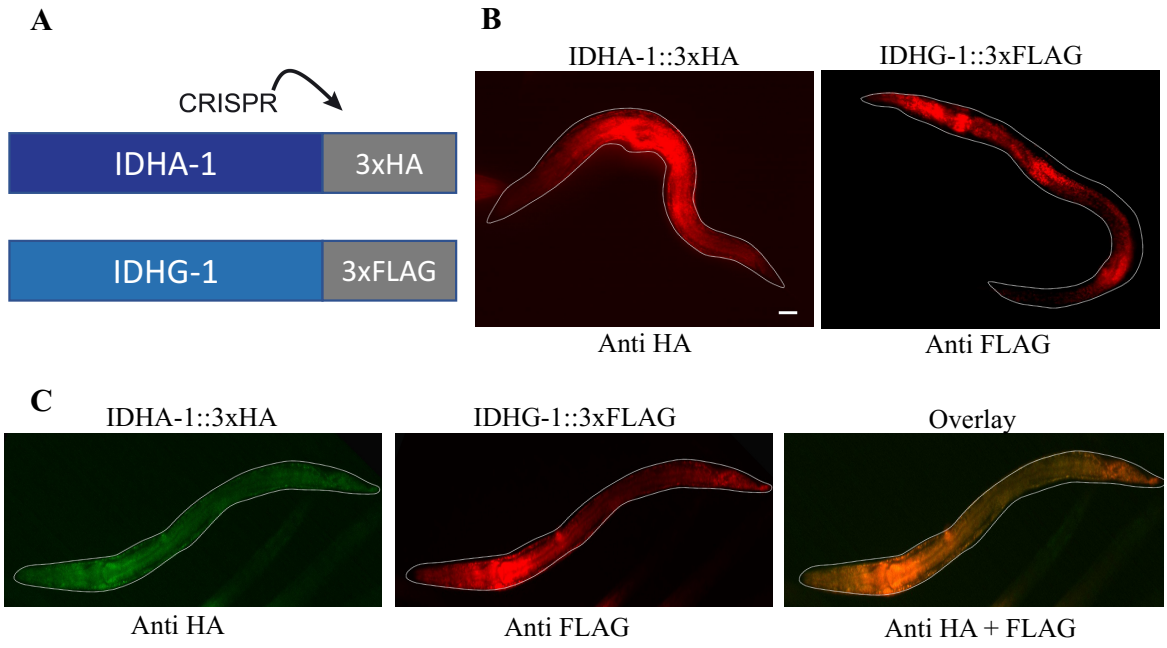

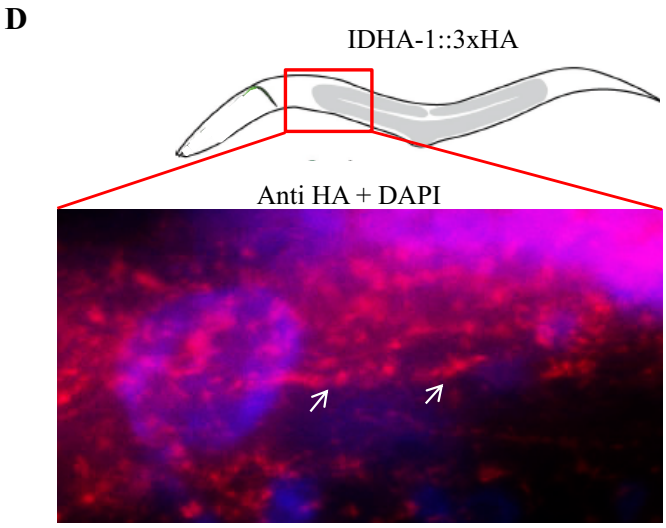

Figure 2.1.2 Expression patterns of IDHA-1 and IDHG-1. A) Schematic representation of endogenously tagged IDHA-1 and IDHG-1 using CRISPR mediated gene editing. **B)** Immunoflorescent stainings of the tagged IDHA-1 and IDHG-1 proteins showing their expression in *C. elegans* larvae. Scale bar: 50 µm. **C)** Immunoflorescent stainings of the tagged IDHA-1 and IDHG-1 proteins in a single worm showing co expression of the two subunits. White lines represent the outline of the worm. **D)** Immunoflorescent staining of the germ line region of a worm with tagged IDHA-1. White arrows indicate the mitochondrial expression in the cells.

IDHA-1 and IDHG-1 are homologs of the IDH3 complex subunits, which has not been characterized in *C. elegans* but is highly conserved. Given this unexpected role as a barrier for cell fate conversion, we further focused on characterizing IDH3 in worms in detail, as an *in vivo* model to understand the role of mitochondria in cell fate maintenance.

2.2 Converted germ cells express ASE-specific and pan-neuronal markers

Our first focus was to analyze the specificity and extent of this germ cell to neuronal conversion upon depletion of the IDH3 subunits. In order to study the extent of reprogramming, we examined the morphology of the converted cells and expression of other neuronal genes. Analysis of the *gcy-5^{prom}::GFP*-positive cells revealed that these cells underwent morphological changes exhibiting axo-dendritic like projections which are reminiscent of neuronal features (Figure 2.2.1 A).

In addition to *gcy-5^{prom}::GFP*, the germ cells also expressed the ASE/AWC-specific gene reporter *ceh-36^{prom}::RFP* (Hobert, 2016). Also, the marker *ift-20^{prom}::NLS::RFP* is activated which is specific for ciliated neurons such as ASE neurons (Inglis, 2006). In addition, we also detected the expression of a pan-neuronal reporter gene *rab- 3^{prom}::NLS::RFP* in the germ cells upon treatment with *idha-1* RNAi (Figure 2.2.1 B, C) - overall demonstrating an extensive conversion of the cells into neuron-like cells.

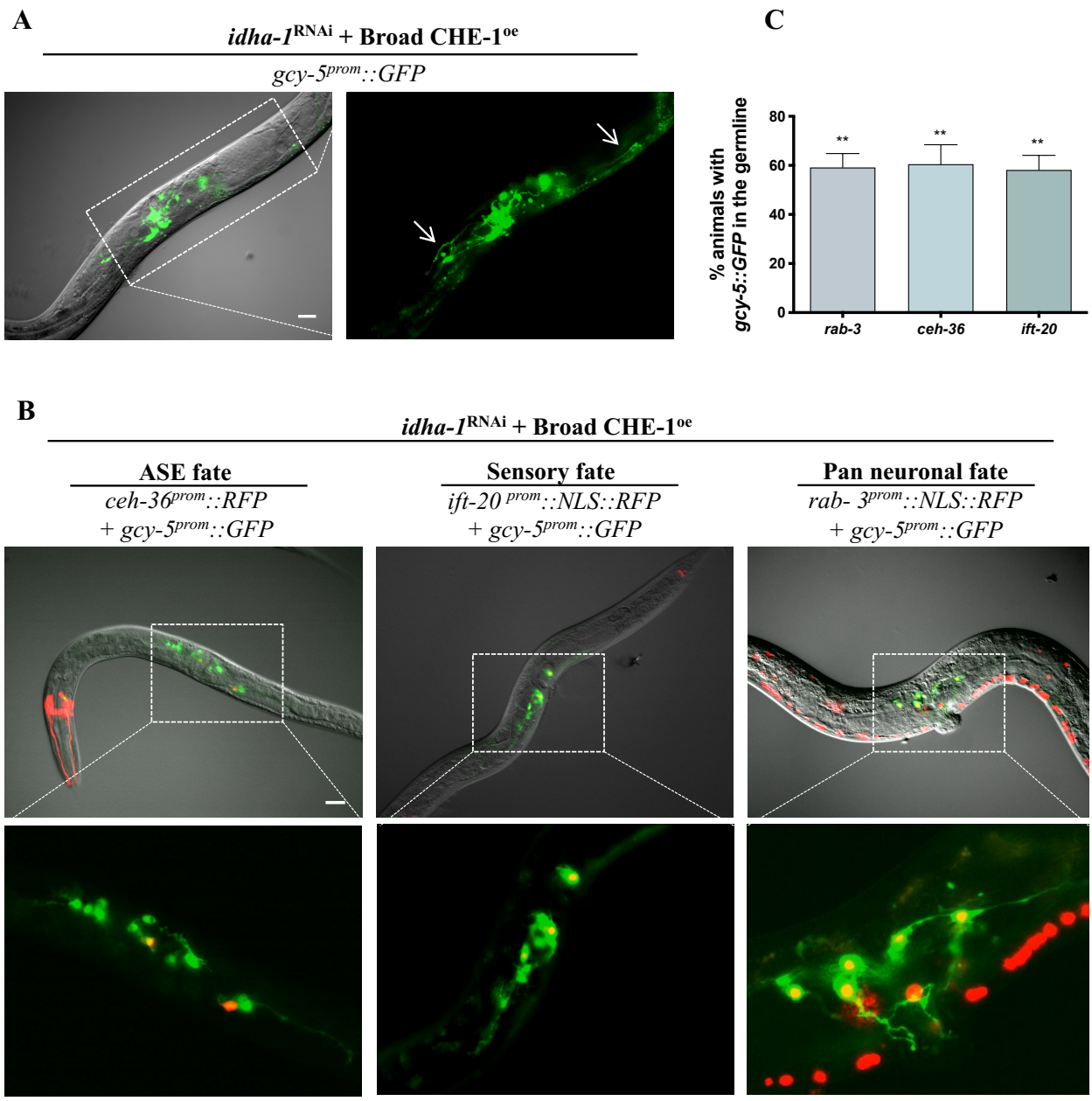

Figure 2.2.1 IDH3 depletion allows germ cell conversion to neurons. A) *gcy-5^{prom}::GFP* positive germ cells of *idha-1*^{RNAi} animals show axo-dendrite like projections after CHE-1^{oe}. **B)** Expression of ASE/AWC marker *ceh-36*, sensory neuronal marker *ift-20*; and pan neuronal fate marker *rab-3* can be detected in animals displaying *gcy-5^{prom}::GFP* in the germ line. Dashed boxes represent magnified area. Scale bars: 50 µm. **C)** Quantification of neuronal markers *rab-3^{prom}::NLS::RFP, ceh-36^{prom}::RFP, ift-20^{prom}::NLS::RFP* in germ line of *idha-1*^{RNAi} animals showing *gcy-5^{prom}::GFP.* Ordinary one-way ANOVA was used for statistical comparison, ** p<0.01. At least 150 animals were counted for each condition. Error bars represent SEM.

In order to test whether the expression of the transgene reporters also reflected the endogenous gene expression, we performed single molecule Florescent In Situ Hybridization (smFISH). We analyzed the expression of the endogenous neuronal genes *gcy-5, rab-3, unc-119* and conserved synaptic protein coding gene *unc-10 (RIM)* using smFISH. Expression of all these neuronal genes was indeed detected in the reprogrammed germ cells upon *idha-1*

RNAi treatment (Figure 2.2.2 A) providing evidence that expression of the reporter transgenes reflect expression of the endogenous neuronal genes. Furthermore, by performing immunostaining, we were able to detect the expression of the conserved pre-synaptic protein UNC-10 (RIM) in the converted germ cells (Figure 2.2.2 B).

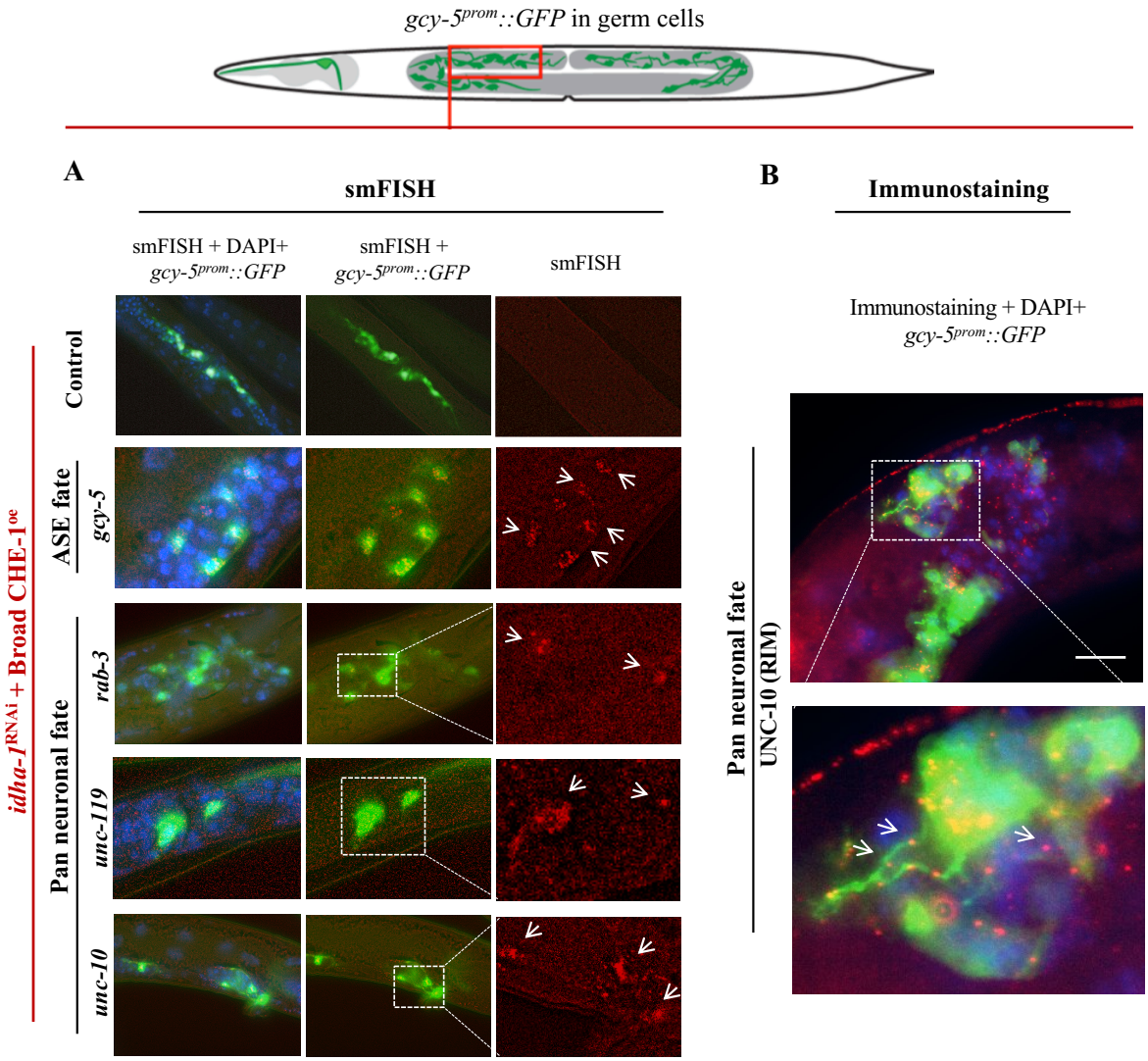

Figure 2.2.2 Converted germ cells endogenously express neuronal genes. A) smFISH based visualization of transcripts derived from endogenous neuronal genes *gcy-5, rab-3, unc-119* and *unc-10* in germ cells of *idha-1*^{RNAi} CHE-1^{oe} animals. mRNAs are visualized by red dots. Controls were treated with mock hybridizations. Dashed boxes represent magnified area. smFISH probes used in the study are listed in Table 4.9. **B)** Immunostaining of neuronal synaptic protein UNC-10 (RIM) in *gcy-5*^{prom}*::GFP* expressing converted germ cells upon *idha-1*^{RNAi} and CHE-1^{oe}. Scale bar: 50 µm.

Taken together, these results indicate that germ cells become neuron-like cells at the morphological and molecular level since the converted cells displayed neuron-like morphology, expressed neuronal reporters as well as endogenous neuronal gene and protein expression.

2.3 *idha-1* depletion allows germ cell conversion to GABAergic neurons

Given that the depletion of *idha-1* allowed the conversion of the germ cells to neurons, and since the CHE-1 TF used to drive this conversion specifies the identity of a specific type of Glutamatergic neurons, we next wondered whether *idha-1* played a general role in safeguarding the germ cell identity; or whether this was specific for conversion to neurons by CHE-1. In order to study this, we made use of another TF UNC-30 which controls terminal differentiation of GABAergic motor neurons (Jin et al., 1994) and was shown previously to convert germ cells to GABAergic neurons upon depletion of the reprogramming barrier *lin-53* (Tursun et al., 2011). We studied the conversion of the germ cells based on the expression of the marker *unc-25^{prom}::GFP* in a strain expressing the TF UNC-30 under control of a heat shock inducible promoter (Figure 2.3 A). Upon depletion of *idha-1* and ectopic expression of UNC-30, approximately 50% of the animals expressed the marker expression in the germ cells (Figure 2.3 B, D).

Further, we asked whether it is possible to convert germ cells into fates other than the neuronal fate upon depletion of *idha-1*. To this end, we mis-expressed the basic helix loop helix (bHLH) TF HLH-1 (MyoD homolog) (Harfe et al., 1998) in the animals and studied the expression of the reporter *myo-3* in the germ line (Figure 2.3 A, C). However, we failed to observe any reprogramming to muscle cells upon depletion of *idha-1* and expression of the TF HLH-1 (Figure 2.3 C, D). These results hint towards specificity of IDHA-1-mediated restriction of germ cell reprogramming to other cell types as its depletion appears to create permissiveness for reprogramming primarily to neuronal cells.

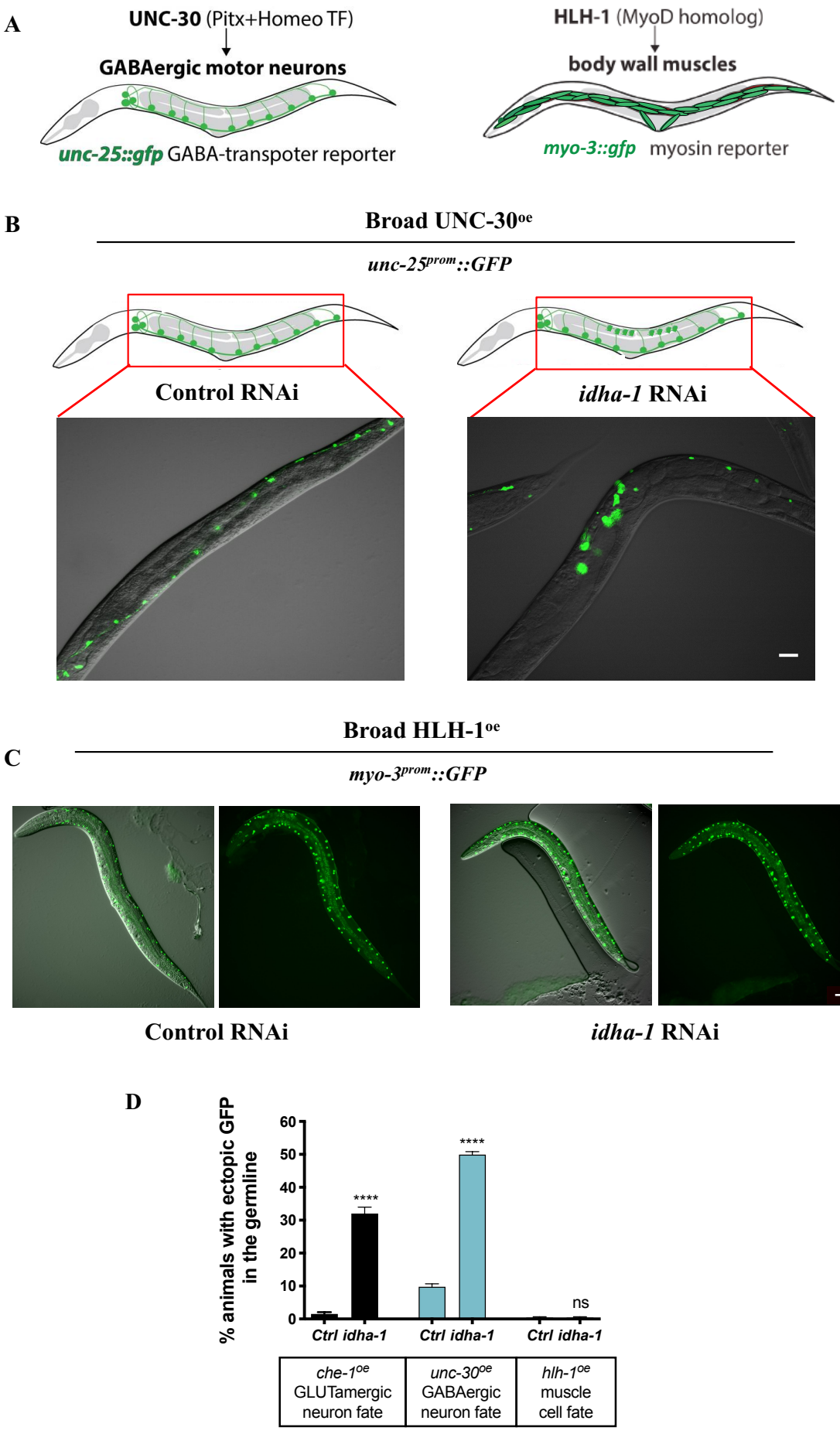
A
UNC-30 (Pitx+Homeo TF)
GABAergic motor neurons
unc-25::gfp GABA-transpoter reporter
HLH-1 (MyoD homolog)
body wall muscles
myo-3::gfp myosin reporter
B
Broad UNC-30oe
unc-25prom::GFP
Control RNAi
idha-1 RNAi
C
Broad HLH-1oe
myo-3prom::GFP
Control RNAi
idha-1 RNAi
D
% animals with ectopic GFP in the germline
60
50
40
30
20
10
0
****
****
ns
Ctrl idha-1
Ctrl idha-1
Ctrl idha-1
che-1oe GLUTamergic neuron fate
unc-30oe GABAergic neuron fate
hlh-1oe muscle cell fate

Figure 2.3 Depletion of IDHA-1 allows conversion to GABAergic neuronal fate but not to muscle fate in germ cells. A) Schematic representation of TFs UNC-30 and HLH-1 mediated induction of GABAergic neuron fate and muscle fate in the animals respectively visualized by the respective reporters. **B)** Representative images of induction of GABAergic neuronal fate reporter *unc-25^{prom}::GFP* upon TF UNC-30^{oe} in control and *idha-1*^{RNAi} treated animals. **C)** Overexpression of muscle fate inducing TF HLH-1 does not convert germ cells in *idha-1*^{RNAi} animals. **C)** Quantification of germ cell conversion to other fates upon induction of respective TFs. Neuronal induction can be achieved in 30-35% of the animals after CHE-1^{oe} and 45-50% of the animals after UNC-30^{oe} but no muscle induction is observed upon HLH-1^{oe}. Ordinary one-way ANOVA was used for statistical comparison, **** $p<0.0001$, ns not significant. At least 600 animals were counted for each condition. Error bars represent SEM. Scale bar: 50 μm

2.4 HIF-1 plays a role in IDHA-1 mediated germ cell conversion phenotype

IDH3 is a mitochondrial enzyme, and the germ cell conversion upon its depletion suggests its involvement in safeguarding the cell fate of germ cells. We reasoned that depletion of this mitochondrial protein results in signaling events from the mitochondria to the nucleus, that allow TF CHE-1 to initiate the transcription of neuronal gene program, eventually leading to the conversion of the germ cell to neuronal cell (Figure 2.4 A). We next sought to elucidate the mechanistic basis of this *idha-1* depletion mediated germ cell reprogramming.

The transcription factor hypoxia inducible factor (HIF-1) has been described to have a role in the attainment of plasticity in cancer associated fibroblasts which have depletion of IDH3a (homolog of IDHA-1); as well as in gliomas with IDH1 depletion (Zhang et al., 2015; Zhau et al., 2009) (Figure 2.4 B). We next asked if HIF-1 has a role in this context of IDH3 depletion mediated germ cell reprogramming. For this, we studied the effects on the germ cell conversion (GeCo) penetrance in *hif-1(ia4)* null mutants. Interestingly, in the *hif-1* mutant background, the phenotype penetrance dropped to about a half (approx. 13%) compared to the wild type. This is indicative of the involvement of HIF-1 in the germ cell conversion (Figure 2.4 B).

In order to rule out the possibility that this drop in the number of animals showing germ cell conversion is due to decrease in the levels of CHE-1, we performed western blots to analyze the levels of ectopic CHE-1 expression (Figure 2.4 C). The levels of ectopic CHE-1 are comparable between the wildtype and *hif-1* mutants indicating that mutation in *hif-1* does not affect the ectopic CHE-1 expression.

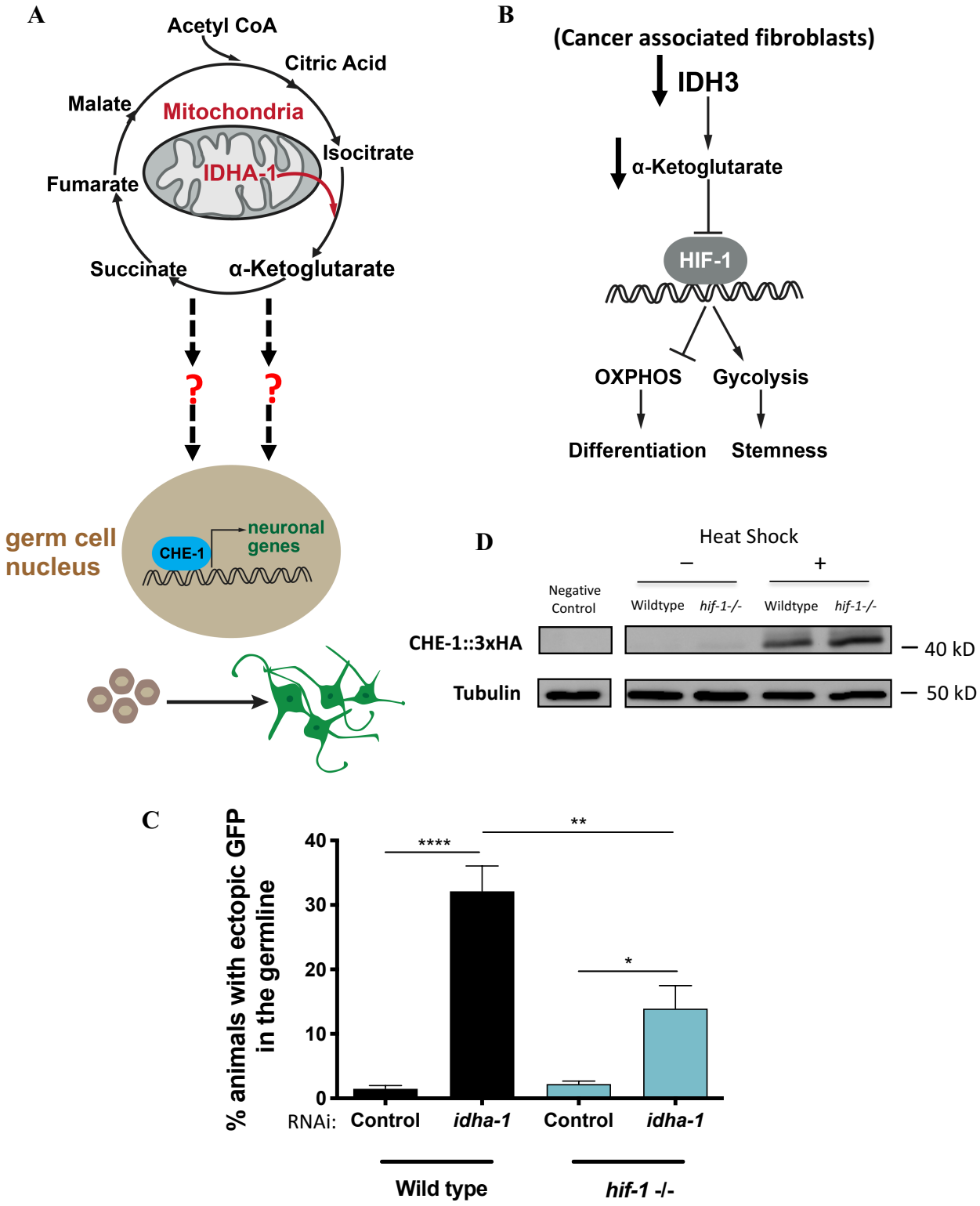

Figure 2.4 Underlying events of IDHA-1 depletion mediated germ cell conversion. A) Schematic model outlining the events leading to germ cell to neuronal reprogramming upon *idha-1*^{RNAi}. Depletion of mitochondrial TCA cycle enzyme IDH3 subunit IDHA-1 leads to retrograde signaling from the mitochondria to the nucleus leading to changes in nuclear chromatin accessibility. This allows CHE-1^{oe} mediated germ cell conversion to

neuronal fate. **B)** Previously described role of TF HIF-1 in cancer associated fibroblasts where it is shown to be stabilized upon IDH3 depletion and leads to the transcription of genes that favor glycolysis in the cell, and promote stemness (Modified from Zhang et al., 2015). **C)** Quantifications shows 13% of *hif-1* mutants compared to 30% of wildtype in *gcy-5*^{prom}*::GFP* induction upon *idha-1*^{RNAi} and CHE-1^{oe}. Ordinary one-way ANOVA was used for statistical comparison, **** $p<0.0001$, ** $p<0.01$, * $p<0.05$. At least 1000 animals were counted for each condition. Error bars represent SEM. **D)** Western blot analysis reveals no differences in heat shock inducible ectopic CHE-1 induction in HIF-1 mutants and the wildtype animals.

Together, these results implicate involvement of HIF-1 in the mitochondrial to nuclear signaling upon depletion of *idha-1*. However, the partial drop in germ cell conversion phenotype observed in HIF-1 mutants suggests the involvement of additional pathways.

Since the identified factor HIF-1 is actively degraded in the cell and is stabilized under low oxygen (<1%) conditions (hypoxia), we next asked if it is possible to achieve increased reprogramming under hypoxic conditions due to increased HIF-1 stability. Furthermore, identification of HIF-1 as an enabling factor raises the possibility that hypoxia response pathways underlie the IDH3 depletion mediated reprogramming. In order to test this, we exposed the worms to hypoxic conditions (in a hypoxia chamber). However, exposing the animals of different larvae and adult stages for varying time points resulted in death. The experimental setup thus did not allow us to study this, and the answers remain inconclusive.

2.5 Altered histone methylation upon *idha-1* depletion and role of Jumanji proteins of histone demethylases

Since the drop observed in germ cell conversion phenotype penetrance in the *hif-1* mutants was partial, we sought to find the additional players in the IDH3 depletion mediated conversion process. a-KG, which is the product of IDH3, acts as a co-factor in the functioning of various dioxygenase enzymes, which are proteins including Jumanji family of histone demethylases. In mammalian system, depletion of IDH3a (Homolog of IDHA-1) have been shown to affect the activity of these proteins due to alterations in effective a-KG levels (Zhang et al., 2015). We next undertook a suppressor/enhancer screen in which together with *idha-1*, we depleted members of the Jumanji protein family. If upon co-depletion of any candidate, the phenotype is decreased, it is indicative of the requirement of the candidate for the conversion to occur. Whereas candidates which upon depletion allow enhanced reprogramming, act to inhibit the reprogramming process. We found that co-depletion of *idha-1* together with *jmjd-3.3* or *jmjd-4* resulted in a reliable decrease in the levels of germ cell conversion phenptype penetrance (Figure 2.5.1 A).

Further, to validate the results obtained from the screen, we created RNAi plasmids whereby we stitched these identified candidates individually with *idha-1*. This allows for simultaneous knockdown of *idha-1* with each of the identified Jumanji members to study double knockdown effects in a more reliable manner. By using these RNAi plasmids and the resulting double knockdown of *idha-1* with either *jmjd-3.3* or *jmjd-4*, we were able to detect a decrease in the penetrance of the conversion phenotype which is consistent with the results obtained previously (Figure 2.5.1 B).

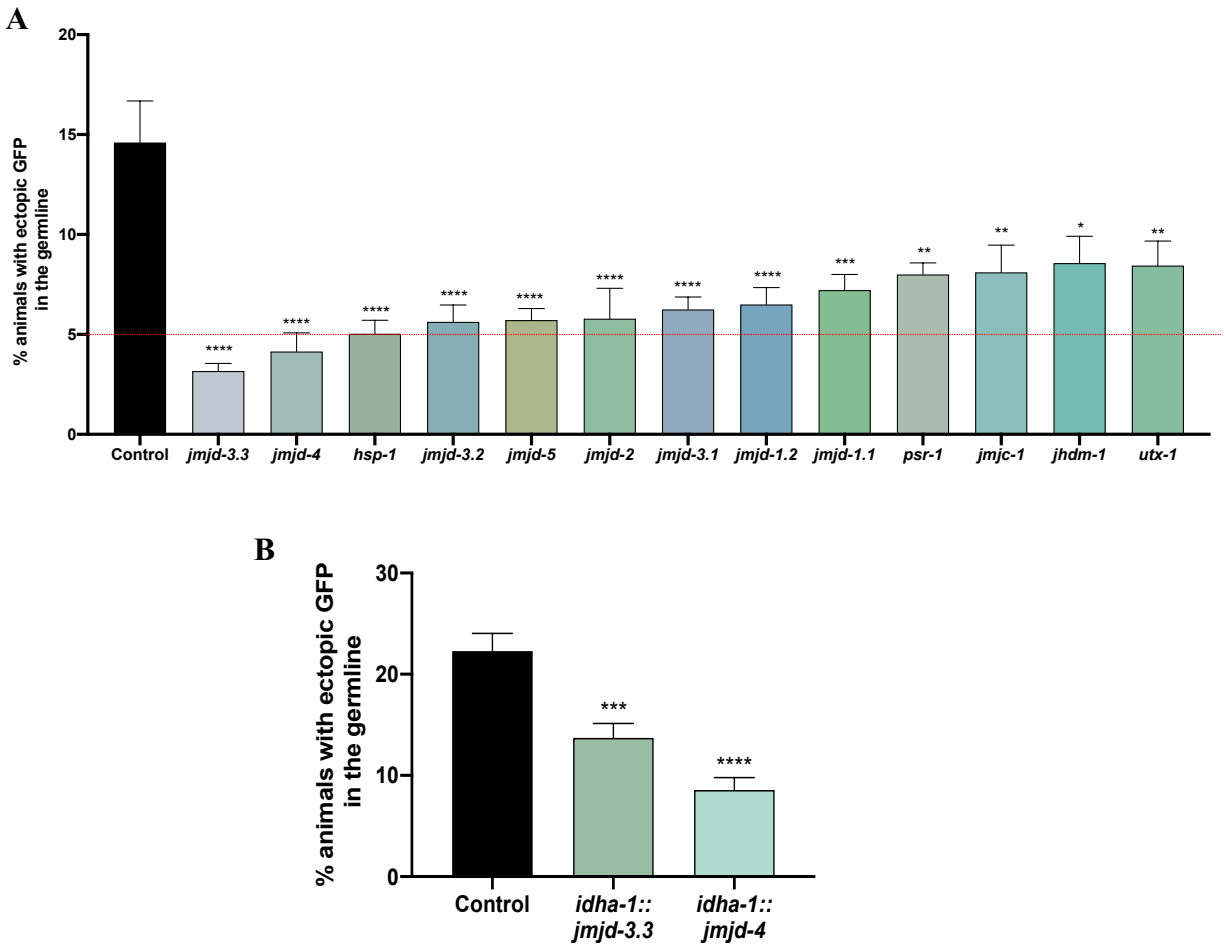

Figure 2.5.1 Members of Jumanji protein of histone demethylases are implicated in IDHA-1 depletion mediated germ cell reprogramming. A) Quantification of animals showing *gcy-5*^{prom}*::GFP* induction upon CHE-1^{oe} in the germ line upon double RNAi knockdown with *idha-1* and candidate Jumanji protein coding genes. Ordinary one-way ANOVA was used for statistical comparison, **** p<0.0001, *** p<0.001, ** p<0.01, * p<0.05, ns non-significant. At least 1000 animals were counted for each condition. Error bars represent SEM. **B)** Quantification shows 12% of the *idha-1::jmjd-3.3*^{RNAi} and 8% of the *idha-1::jmjd-4*^{RNAi} (stitched RNAi plasmids for simultaneous knockdown) animals are positive for *gcy-5*^{prom}*::GFP in* the germ line upon CHE-1^{oe} compared to 22% in control. *idha-1* and Rluc RNAi treated animals were used as control. Ordinary one-way ANOVA was used for statistical comparison, **** p<0.0001, *** p<0.001. At least 1500 animals were counted for each condition. Error bars represent SEM.

Furthermore, we tested mutants for the candidate Jumanji members *jmjd-3.3* and *jmjd-4* obtained from Japanese Consortium (partial deletion) as well as created in the lab using CRISPR (complete gene deletion). Results from *jmjd-4* mutants confirmed the suppression observed in the germ cell conversion as seen previously. However, we failed to observe such suppression effects for the *jmjd.3.3* mutants (Figure 2.5.2 A, B, C).

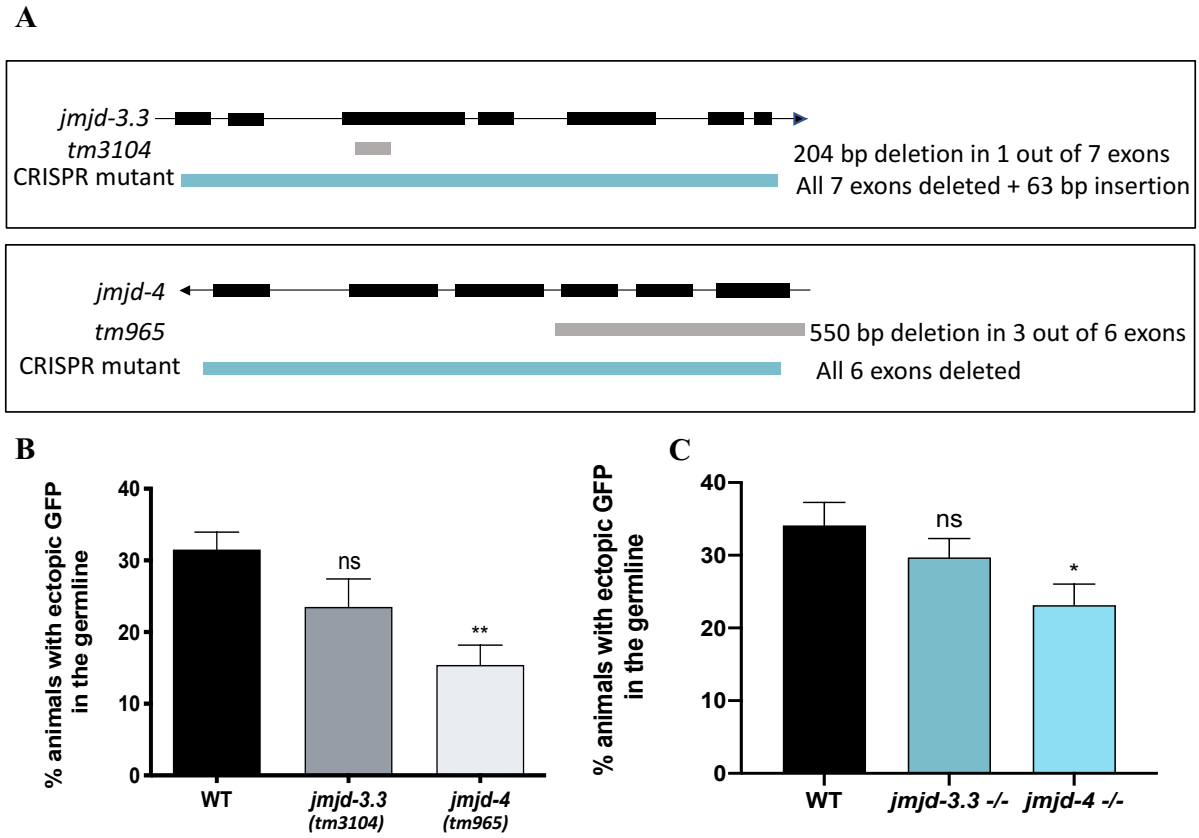

Figure 2.5.2 Members of Jumanji protein of histone demethylases are implicated in IDHA-1 depletion mediated germ cell reprogramming. A) Schematic illustration of the deleted genomic regions in the *jmjd-3.3* and *jmjd-4* mutants obtained from the Japanese consortium (*tm3104, tm965*) and null mutants created by CRISPR in the lab. **B,C)** Quantification of *jmjd-3.3* mutants shows no difference and *jmjd-4* mutants show reduced expression compared to wildtype for number of animals showing *gcy-5*^{prom}*::GFP* induction upon CHE-1^{oe} in the germ line. Mutants were obtained **B)** from Japanese Consortium and **C)** generated by CRISPR in the lab. Ordinary one-way ANOVA was used for statistical comparison, ** $p<0.01$, * $p<0.05$, ns non-significant. At least 400 and 700 animals were counted for each condition respectively. Error bars represent SEM.

Results obtained from the depletion of JMJD-4 by RNAi knockdown and mutants consistently show suppression in the germ cell conversion phenotype in *idha-1*^{RNAi} treated animals. Taken together, these results strongly indicate that JMJD-4 is required for the *idha-1* depletion mediated reprogramming to occur. The function of JMJD-4 remains unknown in *C. elegans* as well as humans but it shares a strikingly 98% homology between the two species (WormBase).

Depletion of IDH3 in *jmjd-3.3*, *jmjd-4* or previously identified candidate *hif-1* mutant background resulted in a partial suppression of the conversion phenotype. We next exposed the *hif-1* mutant to RNAi mediated co-depletion of *idha-1* with either *jmjd-3.3* or *jmjd-4* to study the effects on the suppression of germ cell conversion phenotype (Figure 2.5.3). We observed no change in the penetrance of the phenotype compared to HIF-1 mutant alone.

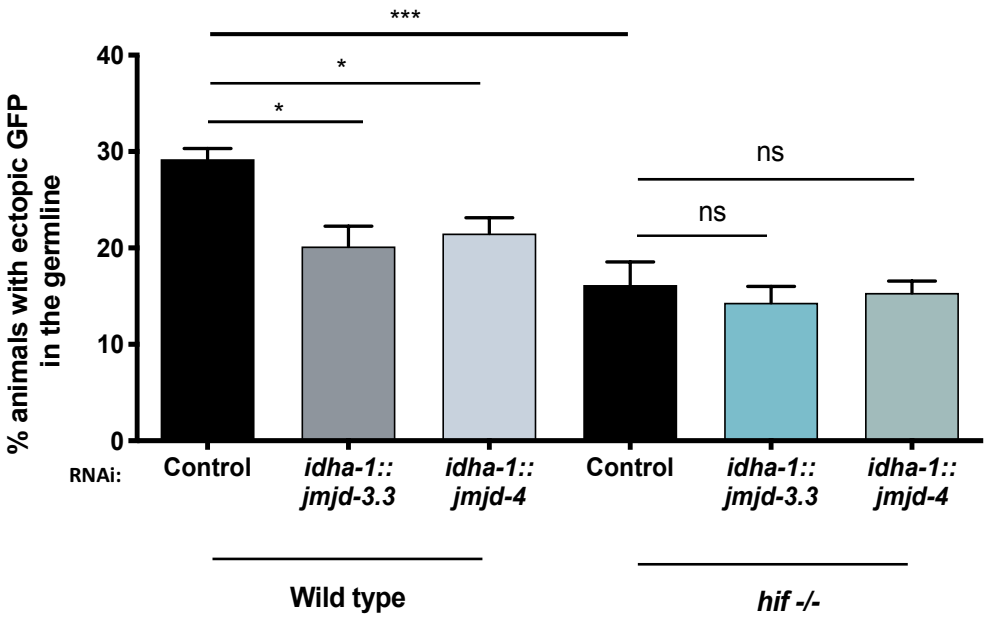

Figure 2.5.3 HIF-1 and candidate Jumanji members are involved in the same pathway. Quantification of wildtype and *hif-1* mutant animals treated with double RNAi plasmids of *idha-1* and *jmjd-3.3*; and *idha-1* and *jmjd-4* shows no difference in the number of animals showing *gcy-5*^{prom}*::GFP* induction upon CHE-1^{oe} in the germ line. *idha-1* and Rluc double RNAi treated animals were used as control. Ordinary one-way ANOVA was used for statistical comparison, *** $p<0.001$, * $p<0.05$, ns not significant. At least 600 animals were counted for each condition. Error bars represent SEM.

These results point towards the possibility of the previously identified candidate HIF-1 and candidate Jumanji proteins operating in the same pathway.

In context of TF mediated reprogramming, chromatin state of the given cell type and accessibility of the target genes of the fate inducing TF are deterministic of the reprogramming potential of the cell. One of the mechanisms that control chromatin accessibility is the methylation of histones; and since the Jumanji proteins are involved in histone demethylation, we next asked what happens to the chromatin methylation state upon knockdown of IDH3. In order to study this, we performed whole worm western blots and immunostaining analysis of germ lines to analyze histone methylation levels (Figure 2.5.4 A, B, C). Western blot analysis showed that upon depletion of *idha-1,* the levels of repressive histone marks histone 3 lysine 9 trimethylation (H3K9me3) and histone 3 lysine 27 trimethylation (H3K27me3) are decreased; whereas the active chromatin mark histone 3 lysine 4 trimethylation (H3K4me3) remains

unaltered (Figure 2.5.4 A). Such decrease in H3K9me3 was also observed in the germ line immunostainings (Figure 2.5.4 B, C).

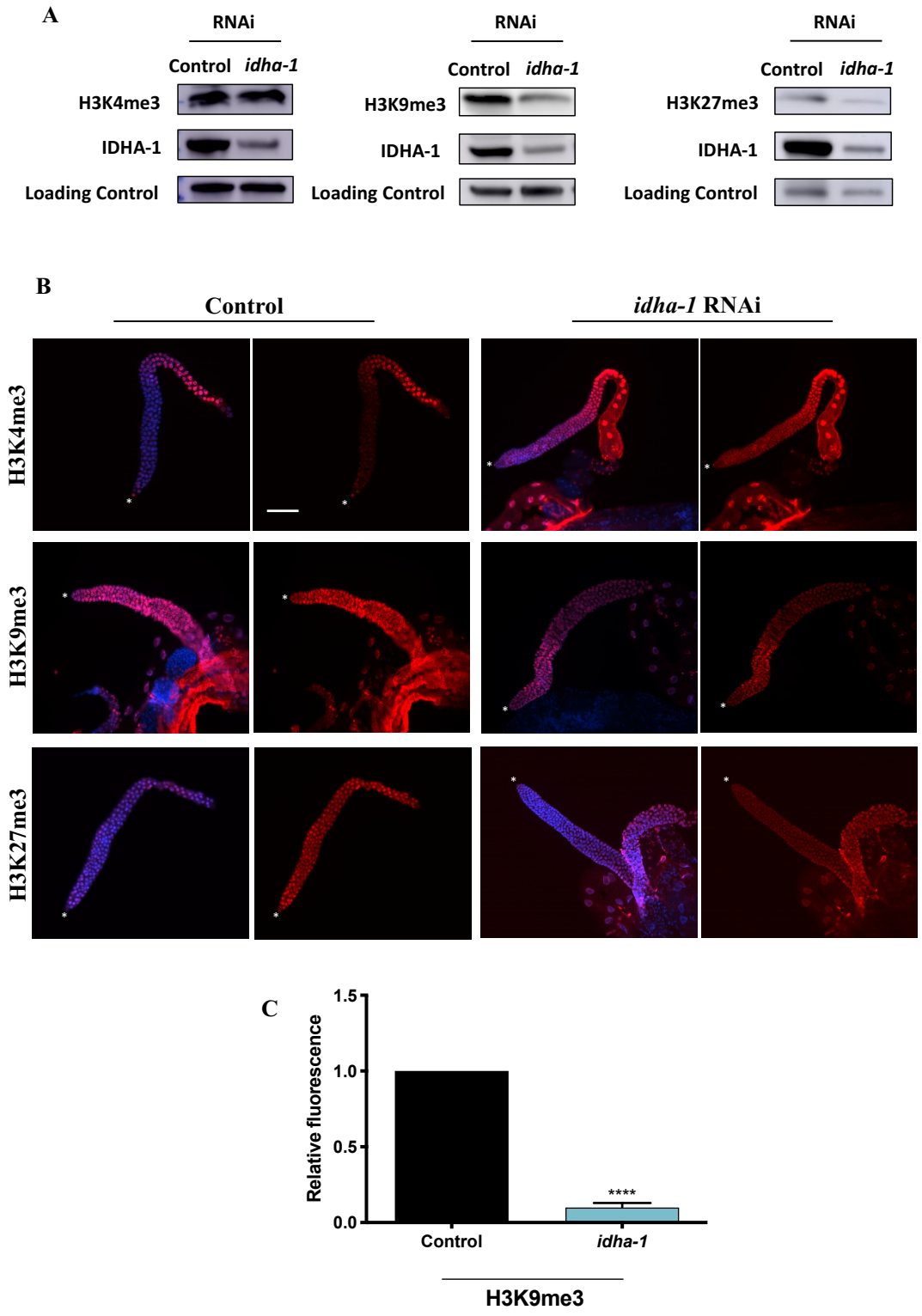

Figure 2.5.4 *idha-1* depletion alters histone methylation status. A) Western blot analysis of H3K4me3 and H3K9me3 levels of whole worms treated with control and *idha-1*^{RNAi}. **B)** Immunostaining of germ lines against the histone methylation H3K9me3 and H3K4me3 upon control and *idha-1*^{RNAi} treatment. Distal tip cell is marked

with an asterisk. **C)** Quantification of fluorescence intensities of germlines immunostained for H3K9me3. Paired t-test was used for statistical comparison, **** $p<0.0001$; n:9. Error bar represents SEM. Scale bar: 50 μm

These results not only strongly suggest the involvement of Jumanji proteins but also demonstrate the general increase in the permissiveness of the chromatin upon IDH3 depletion. Since the ability of a TF to initiate transcription is dependent on the accessibility of its target genes, such increase in chromatin permissiveness sets the landscape for the TF mediated conversion.

In IDH3 depleted worms, the suppression effects observed upon co-depletion of Jumanji genes (in the RNAi screen) and in particular *jmjd-4* indicate that the Jumanji proteins are not only active, but also required for the reprogramming to occur. Furthermore, the increased histone demethylation observed upon *idha-1*^{RNAi} treatment is also supportive of increased Jumanji activity. This is unanticipated, since knockdown of IDH3 is expected to decrease the levels of its product a-KG, and therefore result in decreased functionality of the Jumanji enzymes that require a-KG as a cofactor.

2.6 Exogenously provided metabolites enhance germ cell reprogramming

Since a-KG is the product of IDH3, we hypothesized that upon knockdown of IDH3 the levels of a-KG drop, and this is the underlying cause of the changes that eventually allow CHE-1-mediated reprogramming. Interestingly, a-KG levels influence the stability of the identified factor HIF-1, since it is actively degraded by the a-KG dependent prolyl-hydroxylases (EGLN) (Kaelin and Ratcliffe, 2008; Klimova and Chandel, 2008). However, the increased activity of the Jumanji proteins (that require a-KG as a co-factor) observed in our previous results was in contradiction of this hypothesis. Therefore, we sought to understand if the levels of a-KG are causative for the germ cell conversion upon IDH3 depletion.

Based on this concept, we fed the animals with exogenously provided a-KG and studied the effects on the germ cell conversion (Figure 2.6 A). Surprisingly, such feeding resulted in increased conversion in *idha-1* depleted animals (Figure 2.6.1 C). Germ cell conversion by *lin-53* depletion was chosen as control to test for specificity of the effects and these animals fed with a-KG did not show the increase in germ cell reprogramming as observed for *idha-1* depletion. This increased reprogramming efficiency observed upon a-KG feeding in *idha-1* depleted animals was unexpected and suggested that a-KG levels are not decreased upon IDH3 depletion; and/or decreased level of a-KG is not the underlying cause of the phenotype.

The former prospect raises the possibility that even upon IDH3 knockdown, the TCA cycle is active and hence its functionality and levels of its other metabolites may also have implications on the reprogramming phenotype.

In order to explore this aspect further, we performed additional feeding experiments of metabolites belonging to the TCA cycle including succinate, fumarate, malate and citrate (Figure 2.6.1 C). Furthermore, we co-depleted *idha-1* with additional enzymes functioning in the TCA cycle, including aconitase (*aco-2*) which catalyzes citrate to citric acid conversion; oxoglutarate dehydrogenase (*ogdh-1*) which converts a-KG to succinate; succinate to fumarate converting enzyme succinate dehydrogenase (*sdhb-1*) as well as fumarate hydratase (*fum-1*) which is responsible for fumarate to malate catalysis (Figure 2.6.2 A, D). Upon IDH3 depletion, if the TCA cycle is indeed functional and required for the reprogramming phenotype, alterations in levels of its metabolites and disruption in its functioning caused by depletion of its enzymes is expected to influence the reprogramming potential of cells. While we observed no reprogramming upon these treatments without *idha-1* depletion, fumarate and malate feeding resulted in a significant increase in the number of animals showing the germ cell conversion phenotype upon co-depletion with *idha-1* (Figure 2.6.1 B, C). Correspondingly, knockdown of TCA cycle enzymes *ogdh-1*, *sdhb-1* and *fum-1* did not show any effects, while upon co-depletion with *idha-1* showed a significant suppression in conversion phenotype (Figure 2.6.2 C, D). Taken together, these results suggest that the TCA cycle is functional and parts of the cycle are required for the germ cell reprogramming upon *idha-1* depletion. Furthermore, we did not observe any reprogramming upon exogenous metabolite feeding or depletion of TCA cycle enzymes without *idha-1* depletion, thus suggesting that upon these treatments, the enhancement/suppression observed is for IDH3 depletion mediated reprogramming.

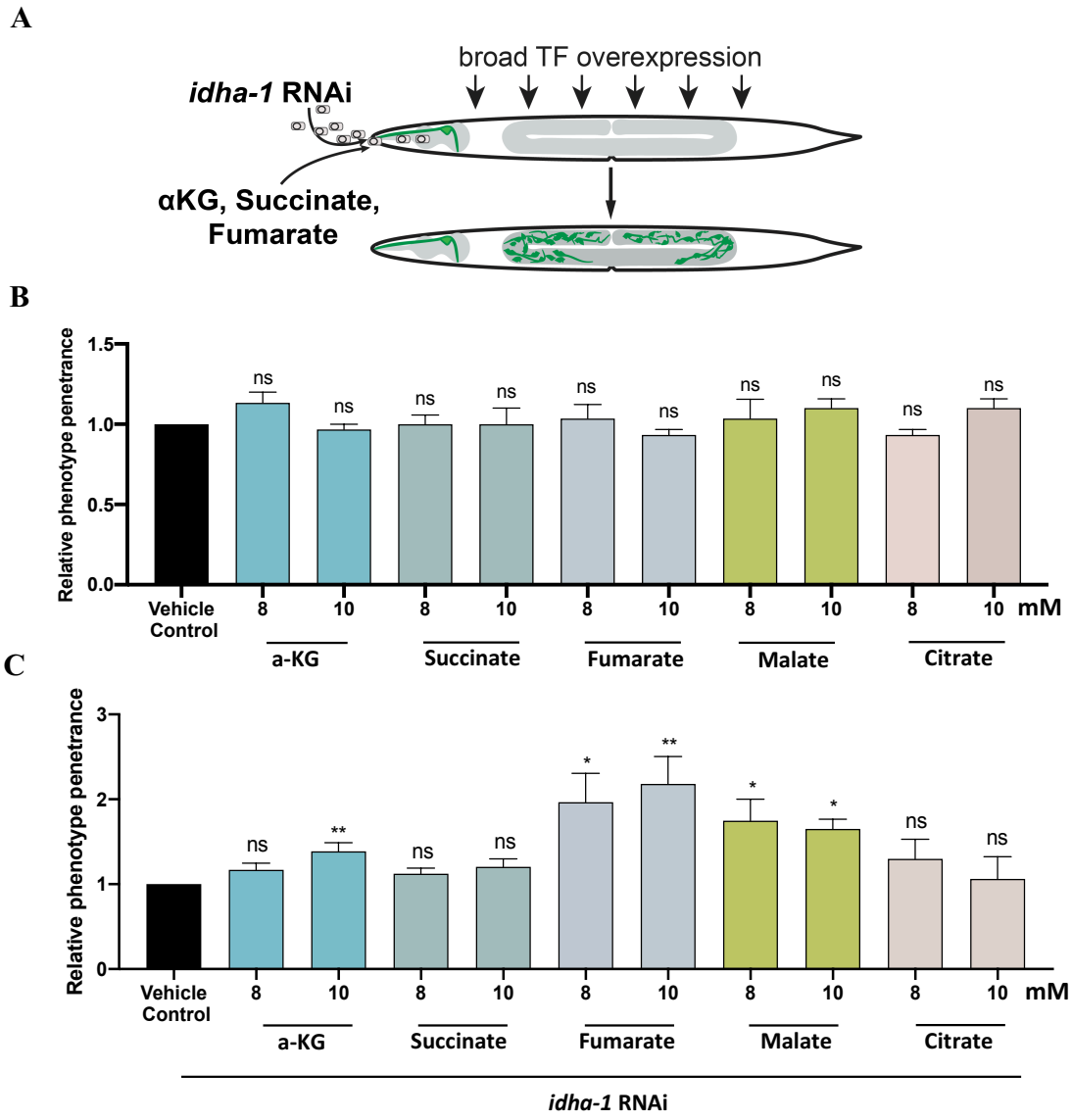

Figure 2.6.1 Exogenously provided TCA cycle metabolites enhance germ cell to neuronal conversion. A) Design of the metabolite feeding experiments. Animals were fed with the respective metabolite and treated with *idha-1*$^{RNAi;}$ and *gcy-5*^{prom}*::GFP* induction in the germ line was observed upon CHE-1^{oe}. **B,C)** Quantification of animals showing *gcy-5*^{prom}*::GFP* induction upon CHE-1^{oe} in the germ line after feeding on exogenously provided metabolites relative to the control **B)** alone **C)** and with co-depletion of *idha-1*. At least 600 animals were counted for each condition. Ordinary one-way ANOVA was used for statistical comparison, ** $p<0.01$, * $p<0.05$, ns not significant. Error bars represent SEM.

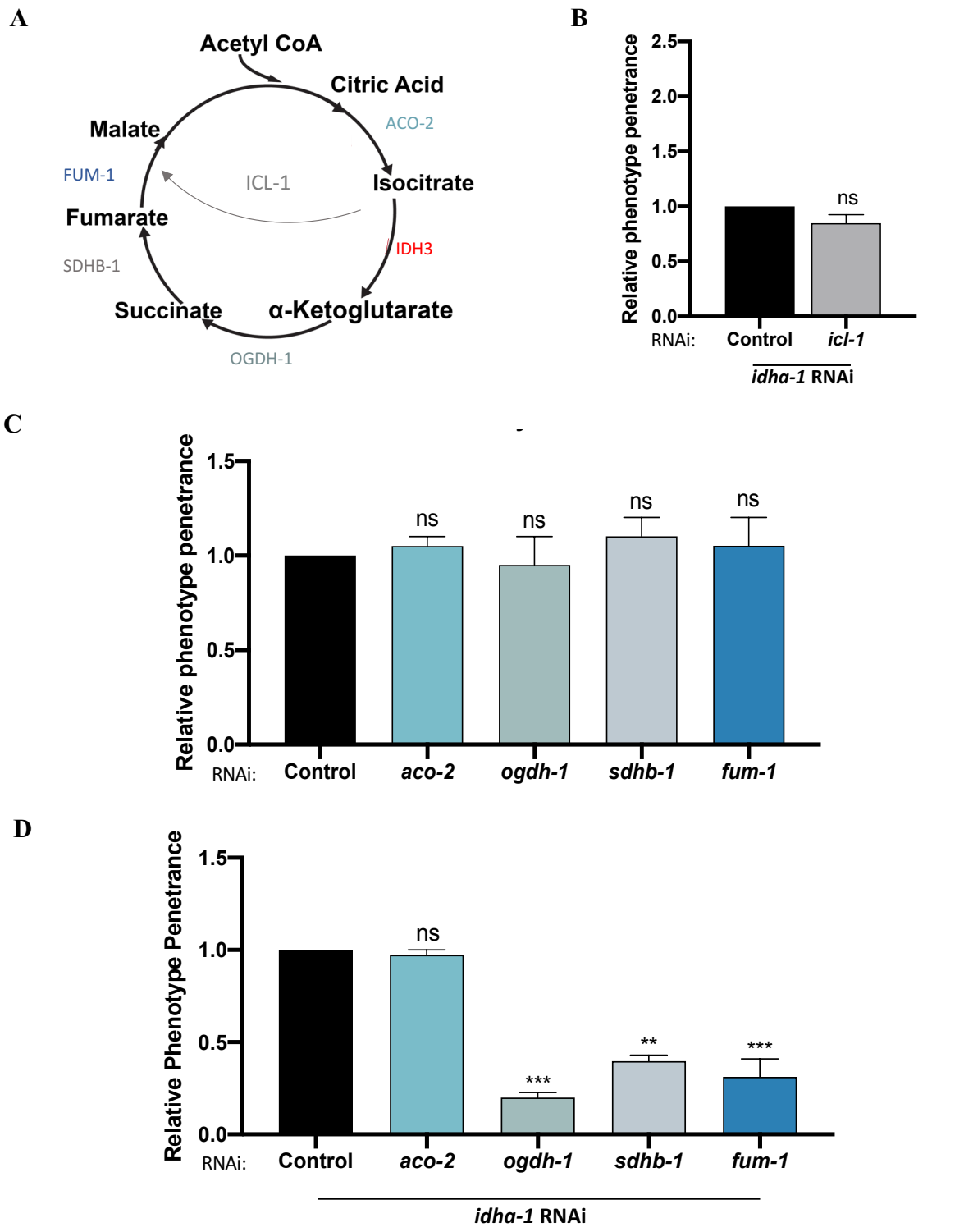

Figure 2.6.2 Effects of knock down of TCA cycle and glyoxylate shunt enzymes on germ cell to neuronal conversion. A) Schematic diagram showing reactions and their enzymes of TCA cycle and the shortcut glyoxylate shunt. **B,C,D)** Quantification of animals showing *gcy-5*^{prom}*::GFP* induction upon CHE-1^{oe} in the germ line upon RNAi knockdown of **B)** glyoxylate shunt enzyme *icl-1* with co-depletion of *idha-1;* and TCA cycle enzyme coding genes **C)** alone **D)** and with co-depletion of *idha-1*. Ordinary one-way ANOVA was used for statistical comparison, ***p<0.001, ** p<0.01, * p<0.05, ns not significant. At least 200 animals were counted for each condition. Error bars represent SEM.

IDH3 catalyzes one of the earliest chemical reactions in the TCA cycle and its depletion is expected to block the cycle. Since our results suggested that the cycle is functional, we next asked how cells are able to by-pass the block in the cycle caused upon IDH3 depletion. Under certain conditions such as desiccation, *C. elegans* employ a biochemical shortcut of the TCA cycle, called the glyoxylate shunt that allows production of malate directly from isocitrate; thereby by-passing multiple steps in the cycle; including the IDH3 mediated conversion of isocitrate to a-KG. (Erkut et al., 2016) (Figure 2.6.2 A). It is thus likely that upon IDH3 depletion, cells utilize this shortcut and keep the TCA cycle functional this way. In order to test this, we next depleted the enzyme responsible for catalyzing this reaction, the isocitrate lyase (*icl-1*), together with *idha-1.* If the cells indeed utilize the glyoxylate shunt as means to evade the TCA cycle block posed by IDH3 depletion, and this underlies the reprogramming phenotype, co-depletion of the enzyme *icl-1* with *idha-1* is expected to decrease the conversion efficiency. However, we did not observe any such effects in the *idha-1* depletion mediated reprogramming phenotype (Figure 2.6.2 B).

Taken together, these results suggest that the cells are able to by-pass the IDH3 depletion mediated disturbance in the TCA cycle by means other than the glyoxylate shunt, and likely keep the cycle functioning; at least partially. In addition, at least part of the TCA cycle (from a-KG to malate production) is required for the IDH3 depletion mediated reprogramming to occur.

2.7 GC-MS based metabolomic analysis shows altered metabolism upon *idha-1* depletion

Previous experiments with metabolite feeding upon *idha-1* depletion showed unexpected outcomes regarding the germ cell reprogramming efficiencies, and suggested an, at least, partially functional TCA cycle. Furthermore, our data indicated seemingly counterintuitive results of increased activity of a-KG dependent Jumanji proteins upon *idha-1* depletion. In order to understand how cells are able to by-pass the block upon depletion of IDH3, we investigated the metabolic changes resulting from the depletion of IDH3. For this, we collaborated with the Kempa lab at the BIMSB to perform Gas Chromatography-Mass Spectrometry (GC-MS) based metabolomic studies. Analysis of the metabolome of animals of both P0 and F1 RNAi revealed changes in the levels of a number of metabolites (Figure 2.11 A).

The levels of citric acid were significantly higher in both P0 and F1 *idha-1* RNAi-treated animals compared to the controls (Figure 2.11 B). This suggests a block in the TCA cycle at this point, which is expected since the step of isocitrate conversion to a-KG is disrupted upon *idha-1* depletion. Surprisingly, the levels of a-KG showed no significant difference in the levels of the metabolite in the treated vs control fraction (Figure 2.11 B). Further, other than malate, levels of no other TCA cycle metabolite were detected to be altered. This outcome was not anticipated since the disruption of the TCA cycle at the level of *idha-1* was expected to cause a marked decrease of a-KG and ensuing metabolites.

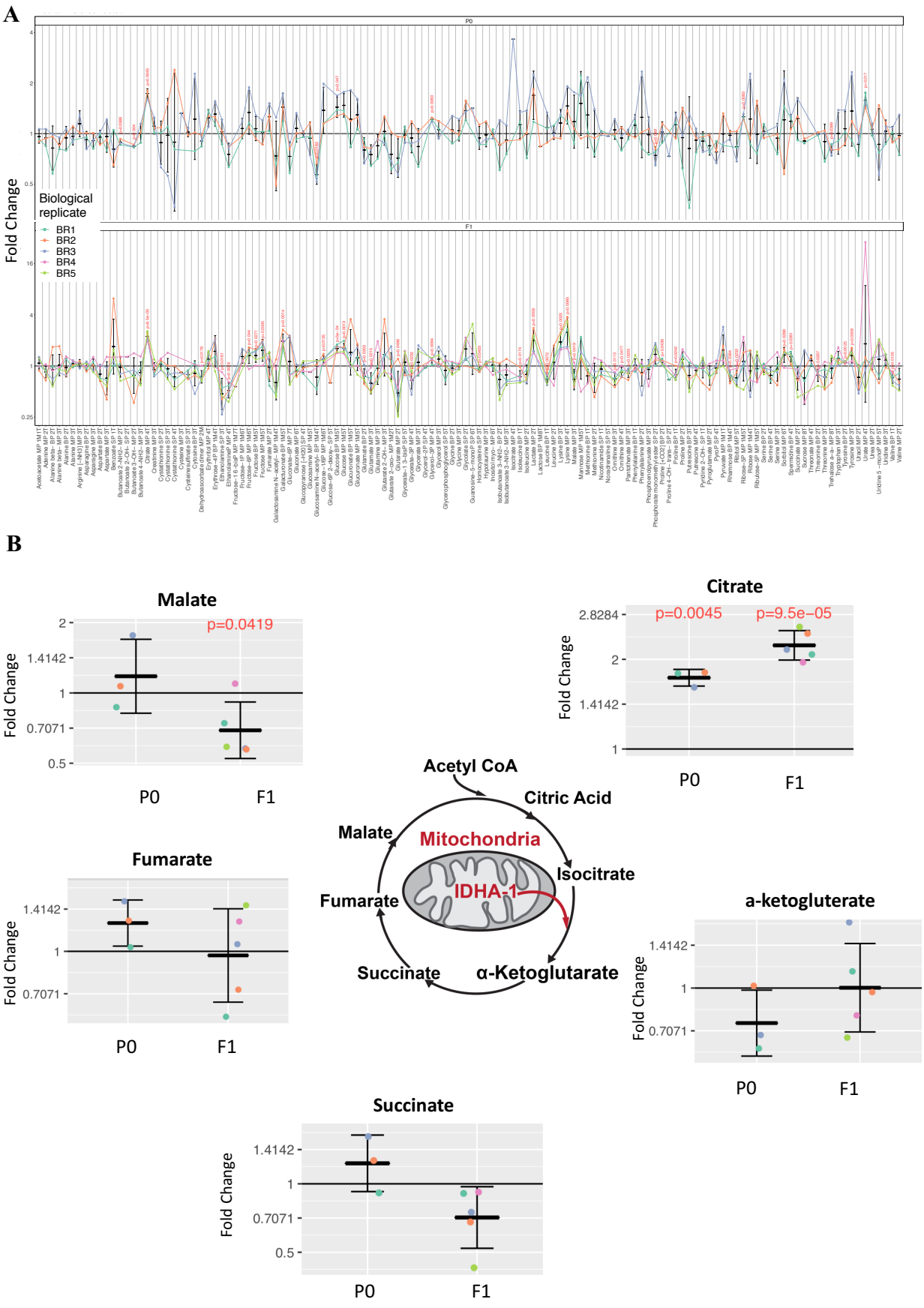
A
P0
F1
Fold Change
Biological replicate
BR1
BR2
BR3
BR4
BR5
B
Malate
p=0.0419
Fold Change
P0
F1
Citrate
p=0.0045
p=9.5e−05
Fold Change
P0
F1
Acetyl CoA
Citric Acid
Malate
Mitochondria
Isocitrate
Fumarate
IDHA-1
Succinate
α-Ketoglutarate
Fumarate
Fold Change
P0
F1
a-ketogluterate
Fold Change
P0
F1
Succinate
Fold Change
P0
F1

Figure 2.7 Metabolomic analysis reveals altered metabolite levels upon *idha-1* depletion. A) Overview of the metabolite changes in P0 and F1 *idha-1*^{RNAi} treated animals compared to control. **B)** Analysis of TCA cycle metabolites reveals high citrate levels indicating cycle blockade; whereas a-KG, fumarate and succinate levels remain unaltered in P0 and F1 *idha-1*^{RNAi}. Graph represents fold change compared to control.

These results indicate that the TCA cycle is blocked (based on the high citrate levels) upon knockdown of *idha-1*, and alternative metabolic side reactions are feeding into the TCA cycle thus making it partially functional and resulting in unaltered levels of a-KG and the ensuing metabolites.

2.8 Glutamine anaplerosis may contribute to germ cell reprogramming

Results from the metabolic analysis revealed no significant differences in the levels of a-KG upon depletion of *idha-1*. In addition, the results explained in section 2.6 suggested that part of the TCA cycle is not only functional, but also required for the IDH3 depletion-mediated reprogramming to occur. This is possible only when the cells, upon IDH3 depletion, are able to by-pass the block in a-KG production by IDH3 and are able to replenish a-KG levels by alternative reactions to keep the cycle functional beyond this point.

In the cell, glutamine is metabolized to glutamate by the action of glutaminases (*glna-1; glna-2* and *glna-3*). The glutamate generated can then be converted to a-KG by the action of enzyme glutamate dehydrogenase (*gdh-1*). However, the reverse reaction of glutamate to glutamine can also be carried out and is catalyzed by the enzyme glutamine synthase (*gln-2*) (Xiao et al., 2016). This breakdown of glutamine to generate a-KG is called glutamine anaplerosis or glutaminolysis and is utilized extensively by cancer cells (Bott et al., 2019). In addition to glutamine, 2-Hydroxyglutarate can also be utilized to produce a-KG by the action of D2HG dehydrogenase (F54D5.12, Y45G12B.3).

We next explored the involvement of these reactions that can regenerate a-KG levels to maintain the TCA cycle and are known as anaplerotic pathways. To this end, we performed an RNAi screen in which we depleted enzymes responsible for metabolic reactions related to the a-KG metabolism together with *idha-1* (Figure 2.8 A, C). We found that knockdown of D2HG dehydrogenase (F54D5.12 or Y45G12B.3) involved in 2-Hydroxyglutarate to a-KG production did not result in a change in the germ cell conversion phenotype. However, knockdown of glutaminases (*glna-1* or *glna-3*); or glutamate dehydrogenase (*gdh-1*) together with *idha-1* leads to a suppression in the reprogramming phenotype compared to the control (Figure 2.8 A, C). This means that these enzymes are required by the cells to generate a-KG upon IDH3

knockdown and are involved in germ cell reprogramming; and upon their depletion, cells are no longer able to undergo conversion. On the other hand, depletion of glutamine synthetase (*gln-2),* which catalyzes the reverse reaction of glutamate to glutamine production, leads to increased reprogramming efficiency; providing further evidence that glutamine breakdown is indeed utilized by the IDH3 depleted cells. Furthermore, the levels of glutamate were reduced as revealed in the metabolomic analysis suggesting its metabolism to a-KG in the absence of IDH3 (Figure 2.8 B). To further analyze the role of glutamine anaplerosis in IDH3 depletion mediated reprogramming, we fed the *idha-1* depleted animals with exogenously provided glutamine. However, we did not observe any further increase in the reprogramming penetrance upon such treatment (Figure 2.8 C). This points towards the possibility that in addition to glutamine anaplerosis, an additional factor/pathway is required for the germ cell conversion. Alternatively, intracellular a-KG levels and/or signaling events resulting from the glutamine breakdown upon depletion of IDH3 alone are sufficient to allow reprogramming and any additional supply of glutamine therefore does not have any effect.

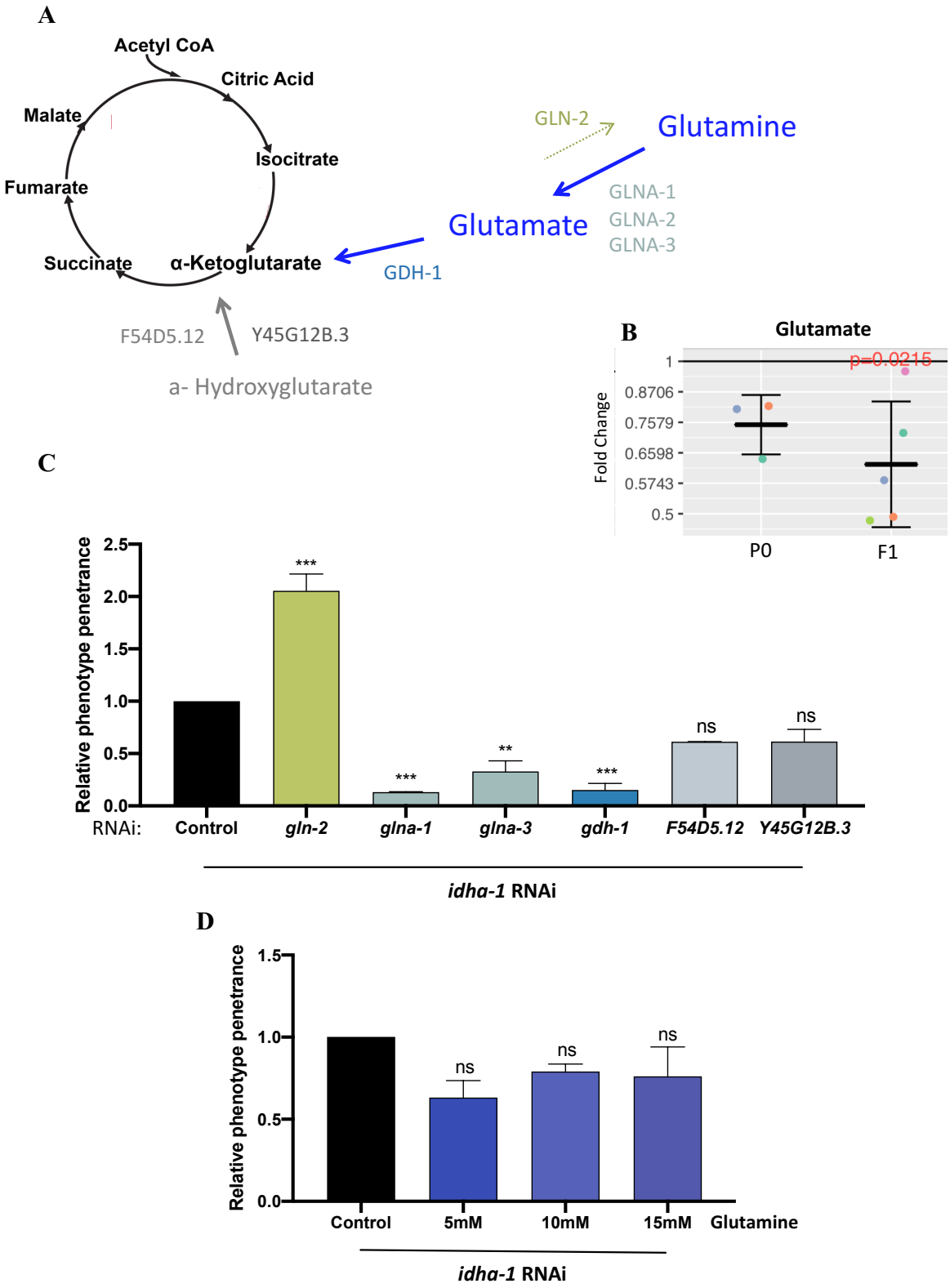

Figure 2.8 Glutamine anaplerosis replenishes a-KG levels. A) Schematic diagram showing anaplerotic reactions and their enzymes feeding into the TCA cycle by forming a-KG. **B)** Metabolomic Analysis shows significantly decreased glutamate levels upon *idha-1*^{RNAi} indicating increased metabolism. **C)** Quantification of animals showing *gcy-5*^{prom}*::GFP* induction upon CHE-1^{oe} in the germ line upon double RNAi knockdown with

idha-1 together with genes coding for glutamine (*gln-2, glna-1, glna-3, gdh-1*) and hydroxyglutarate (F54D5.12, Y45G12B.3) metabolism . **D)** Quantification of animals showing *gcy-5^{prom}::GFP* induction upon CHE-1^{oe} in the germ line after feeding on exogenously provided glutamine relative to the control. Ordinary one-way ANOVA was used for statistical comparison, *** $p<0.001$ ** $p<0.01$, ns not significant. At least 200 animals were counted for each condition. Error bars represent SEM.

Taken together these results indicate that the intracellular levels of a-KG are replenished by the glutamine anaplerosis upon depletion of IDH3. It also raises the possibility that this pathway of metabolic reactions can contribute towards the IDH3 depletion mediated germ cell to neuron reprogramming. Although it cannot be ruled out that the cells also utilize a-hydroxyglutarate to produce a-KG upon depletion of IDH3; our results suggest that it does not contribute to the reprogramming phenotype.

2.9 Metabolic Flux analysis using stable isotopes

To further investigate the possibility that anaplerotic pathways such as glutamine breakdown contribute to the observed germ cell reprogramming phenotype upon IDH3 depletion, we started performing metabolic flux analysis (MFA). For flux analysis studies, stable isotopes such as carbon-13 (^{13}C) is utilized. When a compound such as glucose containing ^{13}C isotopes is taken up by the cells, it is metabolized and the enzymatic reactions incorporate the carbon units. This results in specific labelling patterns in downstream metabolites that can be measured by Mass Spectrometry (MS) (Antoniewicz et al., 2018) (Figure 2.9). In this way, the isotopic tracer ^{13}C-containing glucose is used to both trace metabolic pathways as well as quantification of flux through these pathways (Dieuaide-Noubhani et al., 2007).

Since metabolomic flux analysis has not been performed in *C. elegans* before, we first needed to establish a protocol for these studies. We decided to inactivate the bacteria by Ultra violet radiation (UV) on which the worms feed in order to prevent the metabolization of the ^{13}C labelled glucose by the bacteria itself; and make it available exclusively for the worms. In addition, in order to encourage the worms to ingest the ^{13}C glucose solution, we introduced a brief starvation step just before glucose feeding. However, we optimized to keep the starvation window short since it may induce metabolic changes in the animal. Furthermore, we performed metabolomic analysis before and after the starvation; in order to evaluate any changes in the metabolome caused due to starvation (Figure 2.9 A).

We fed the animals with the ^{13}C and control (^{12}C) glucose solution for different time points including 60, 180, 360 and 840 minutes. This allows for the increasing assimilation of

^{13}C units into the metabolites of the animals over the given time period to later trace the flux of the labelled metabolites. This was followed by metabolic analysis by GC-MS carried out by Tobias Opialla from the Stephan Kempa group at the MDC.

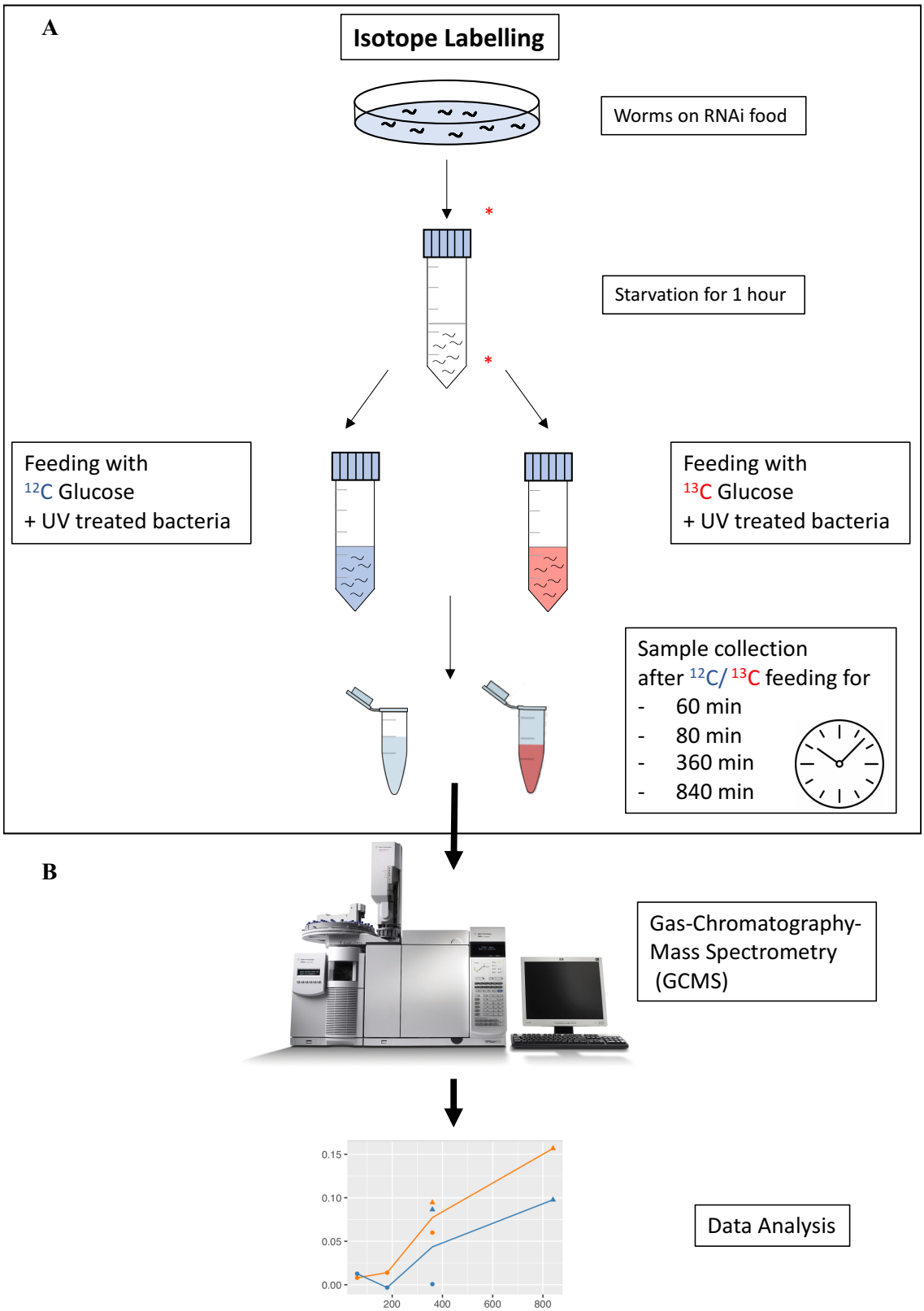

Figure 2.9.1 Metabolic Flux Analysis (MFA) in *C. elegans* A) Schematic diagram of the method developed to study MFA in *C.elegans.* Animals are exposed to the RNAi mediated knockdown by growing on bacterial food. At the desired stage, animals are washed off in M9 buffer (explained in methods section) and starved for one hour. After starvation, animals are fed on ^{12}C or ^{13}C containing glucose solution containing UV treated dead bacteria. At the respective time points, samples are collected and the worm pellet is immediately flash frozen in liquid nitrogen to preserve the metabolomic content. Asterisks represent time points before and after starvation where samples are collected in order to later analyse and eliminate the effects of starvation on the metabolism profile of the worms. **B)** The frozen samples are subjected to GC-MS based metabolomic analysis and the data is analyzed to determine the ^{13}C labelled metabolite profile compared to unlabeled control (^{12}C). Analysis is carried out by Tobias Opialla from the Stephan Kempa group at the BIMSB. (Figure modified from prodigy scientific).

Glucose enters the cells and undergoes a series of reactions called glycolysis whereby energy and metabolic precursors for various processes are generated. The end product of glycolysis, pyruvate is converted to acetyl Co-A and enters the TCA cycle, which is the central hub of cellular metabolism involved in energy production and biosynthesis (Figure 2.9.2 A). For the initial analysis, we therefore focused on the flux through these two major metabolic pathways glycolysis and TCA cycle and their related metabolites.

We treated the animals with the control and *idha-1* RNAi and collected the samples at the abovementioned time points. Overall, we detected a decrease in ^{13}C labelled metabolites associated with glycolysis including fructose 6 phosphate, glycerate and phosphoenolpyruvate in worms with IDH3 depletion compared to control; thereby suggesting a decreased glycolysis flux (Figure 2.9.2 B). This is also consistent with decreased ^{13}C labelled detected in lactate and the amino acids alanine and serine in IDH3 depleted worms (Figure 2.9.2 B). Lactate and alanine are produced by the glycolysis intermediate pyruvate; whereas serine is generated by metabolism through glycerate (Figure 2.9.2 A). Overall, these results suggest that metabolic flux through glycolysis and its linked pathways is reduced in animals with IDH3 depletion. This is in contrast to the findings for the TCA cycle, where we detected increased ^{13}C-labelled metabolites such as citrate, fumarate, malate and succinate in IDH3 depleted worms (Figure 2.9.2 C). While the difference observed in IDH3 treated versus controls in ^{13}C-labelled metabolites of TCA cycle is not as pronounced as observed for the glycolysis, it nonetheless points towards comparable, if not increased, TCA cycle flux in IDH3 depleted animals.

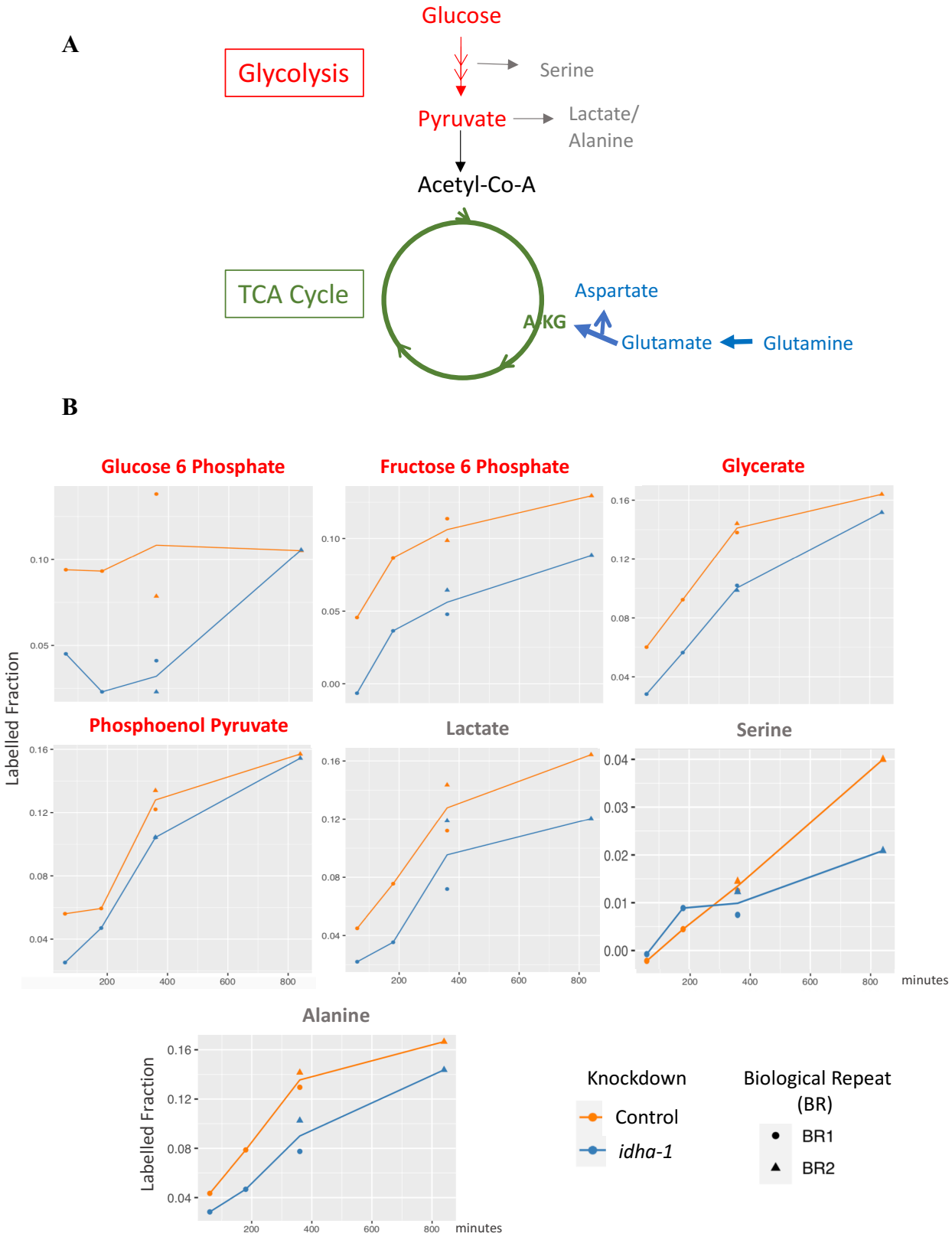

Figure 2.9.2 Metabolic Flux Analysis (MFA) reveals decreased glycolysis flux upon IDH3 depletion A) Schematic diagram of the analyzed glycolysis and TCA cycle. Glucose undergoes a series of metabolic reactions to generate pyruvate which is converted to acetyl co-A and enters the TCA cycle. Both of these processes generate energy and metabolic precursors for various processes of the cell. Strength of the line represents the increased/decreased flux upon IDH3 depletion. Glycolysis generated metabolites are represented in grey. Blue

metabolites represent the glutamine metabolism pathway to generate a-KG. **B)** Fold change in ^{13}C labelled glycolysis and its associated metabolites in *idha-1* depleted animals compared to control. Glycolysis intermediates glucose 6 phosphate, fructose 6 phosphate, glycerate and phosphoenol pyruvate; and metabolites derived through glycolysis show decreased ^{13}C labelling upon IDH3 depletion.

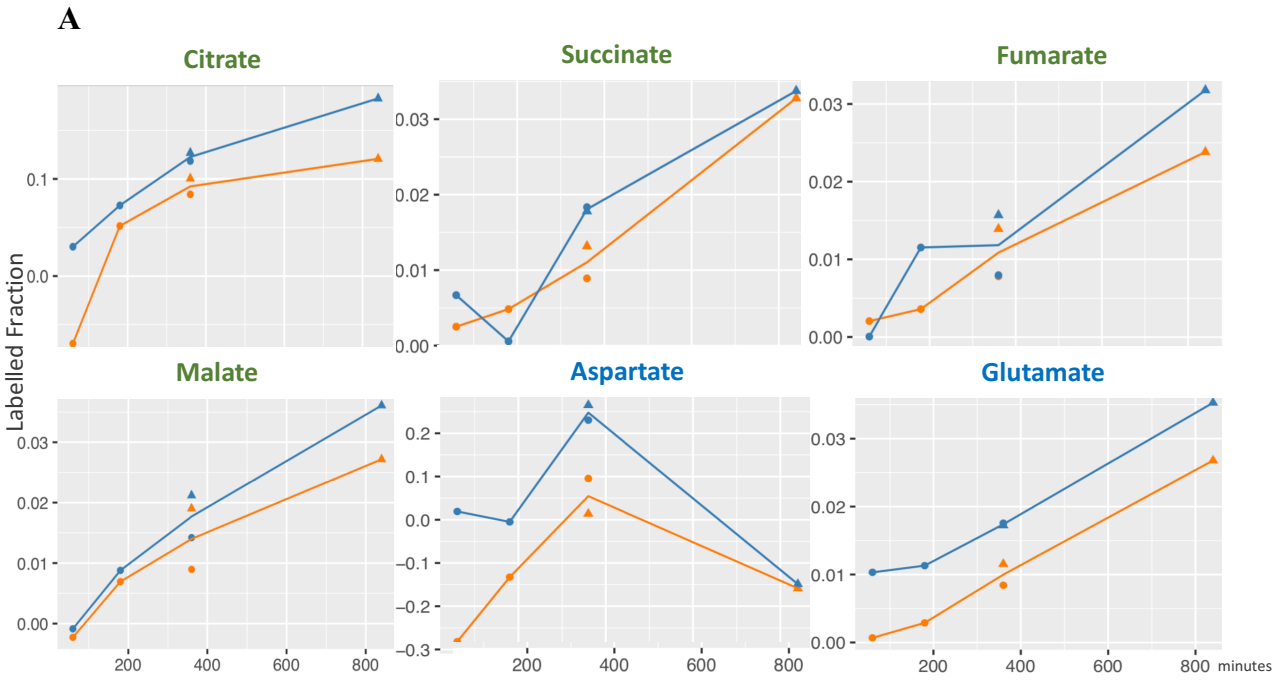

Figure 2.9.3 Metabolic Flux Analysis (MFA) reveals a functioning TCA cycle upon IDH3 depletion A) Fold change in ^{13}C labelled TCA cycle and glutamine anplerosis associated metabolites in *idha-1* depleted animals compared to control. ^{13}C labelling is increased in TCA cycle metabolites and glutamine anaplerosis related metabolites glutamate and aspartate.

Taken together, our metabolomic flux analysis revealed a decreased glycolysis and slightly increased TCA cycle based on the ^{13}C -labelled metabolites detected for the respective processes. These results are consistent with our previous findings whereby we determined that TCA cycle is active in worms with IDH3 depletion and is required for the reprogramming to occur (Section 2.6).

We previously identified that cells utilize glutamine metabolism as the alternative source of a-KG production when IDH3 is depleted. In order to validate these results, we next analyzed the levels of metabolites involved in glutamine to a-KG production. In the cells, glutamine is metabolized to glutamate, which is converted to a-KG while generating aspartate. Interestingly, we were able to detect increased ^{13}C-labelled glutamate as well as aspartate in IDH3 depleted worms (Figure 2.9.2 A, C). Taken together, this indicates that in worms with

IDH3 depletion, an increased metabolic flux exists for glutamine metabolism; and it can be concluded that the a-KG produced is then utilized to overcome the block in TCA cycle.

Furthermore, in these preliminary results with this method that we developed for the flux analysis in *C. elegans*, we detected comparable TCA cycle function in the IDH3 depleted and control worms despite decreased glycolysis occurring in IDH3 depleted animals. Since the TCA cycle is itself fueled with pyruvate, the end product of glycolysis, this raises the question of how IDH3 depleted cells with reduced glycolysis are able to sustain a TCA cycle flux that is slightly elevated than the control. A detailed analysis of other metabolic side reactions is required to answer this question. Another interesting observation is the increased ^{13}C -labelling of aspartate in *idha-1* depleted animals as a possible acute response, but the levels become comparable to the control in the later time points (Figure 2.9.2). As this analysis is ongoing, detailed result of this part of the study will be presented in the near future in a manuscript.

2.10 Trans tissue effects

The CHE-1 mediated cellular conversion observed upon knockdown of IDH3 is observed only in the germ line. Based on the results obtained from immunostainings of IDHA-1 and IDHG-1 (Figure 2.1.2), we were able to determine that these proteins are expressed in multiple tissues of the animal. We next asked if knockdown of these IDH3 subunits in the germ line alone is sufficient to allow reprogramming (cell type autonomous). In order to study this, we made use of RNA dependent RNA polymerase 1 (*rrf-1)* mutant background which is permissive for RNAi predominantly in the germ line (Kumsta and Hansen, 2012). We used *lin-53* RNAi treated animals as controls since the germ cell conversion occurring upon knockdown of *lin-53* is known to be cell type autonomous (Figure 2.10.1). We found that while the percentage of animals showing germ cell conversion remained unaltered in the control *lin-53* RNAi treated animals, the numbers dropped significantly upon *idha-1* RNAi treatment. This suggests that knockdown of IDH3 in the germ line alone is not sufficient for the germ cells to reprogram. Furthermore, we used the mutants for Piwi like protein 1 (*ppw-1)* which are resistant to RNAi knockdown in the germ line. Using this strain, the *lin-53* treated animals showed a significant drop in the percentage of animals showing germ cell conversion. Although the phenotype penetrance in the *idha-1* RNAi treated animals was lower compared to the control, this decrease was not significant. Taken together these results illustrate that the germ cell conversion observed upon drop of *idha-1* is not cell type autonomous.

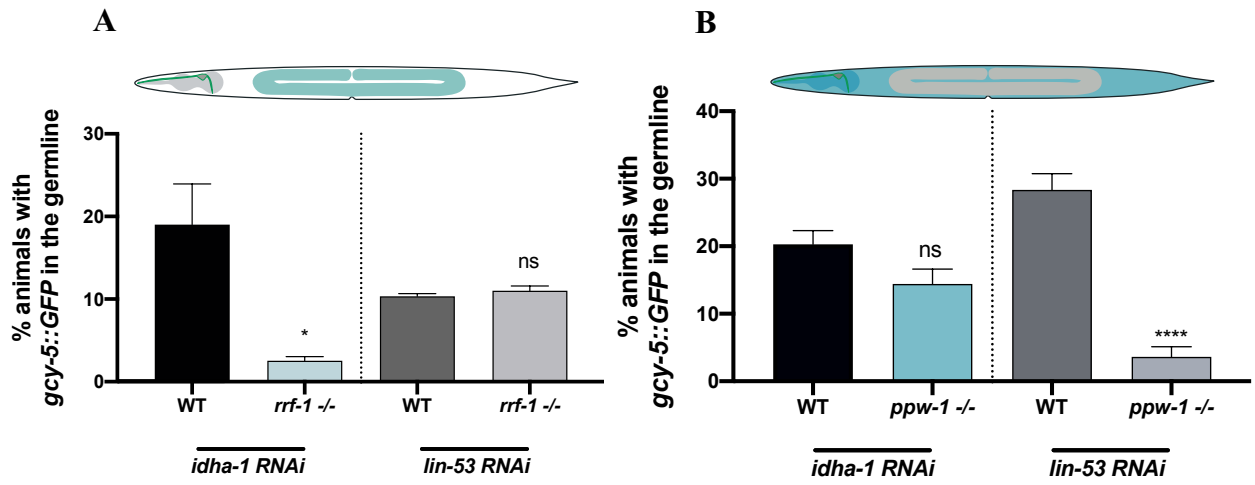

Figure 2.10.1 Soma and germ line RNAi mutants reveal cell- non autonomous nature of the germ cell conversion. A,B) Quantification of animals showing CHE-1^{oe} mediated *gcy-5^{prom}::GFP* induction in the germ line in mutants with RNAi depletion predominantly in the **A)** germ line and **B)** soma. Suppression in germ line specific RNAi mutants *rrf-1* provides indication that *idha-1*^{RNAi} depletion mediated germ cell reprogramming is cell non- autonomous. Previously described germ cell reprogramming barrier *lin-53* was used as control. Ordinary one-way ANOVA was used for statistical comparison, **** $p<0.0001$, * $p<0.05$, ns not significant. At least 300 animals were counted for each condition. Error bars represent SEM.

We further sought to identify the tissue responsible for contribution in the IDH3 depletion mediated germ cell conversion. Since the mutant of *idha-1* or *idhg-1* is not viable, we opted for the tissue specific Auxin inducible degradation system. For this, we tagged the endogenous IDHA-1 with the Auxin inducible degron (AID) and Human Influenza Hemagglutinin (3xHA). The auxin inducible degron makes the protein subject to degradation by the plant-based protein TIR1 in the presence of auxin (Figure 2.10.2 A). When such degron tagged worms are combined with transgenic strains expressing TIR1 in specific tissues, the effects of knockdown of the protein of interest can be observed in that particular tissue (Zhang et al., 2015).

Since IDH3 is localized to the mitochondria, and the TIR1 mediated proteasomal degradation occurs in the cytoplasm, we first analyzed the degradation of the degron tagged IDHA-1 by the AID system. Western blot analysis in the strain expressing TIR1 under a soma specific promoter revealed depletion of IDHA-1 upon treatment with 4mM auxin (Figure 2.9.2 B).

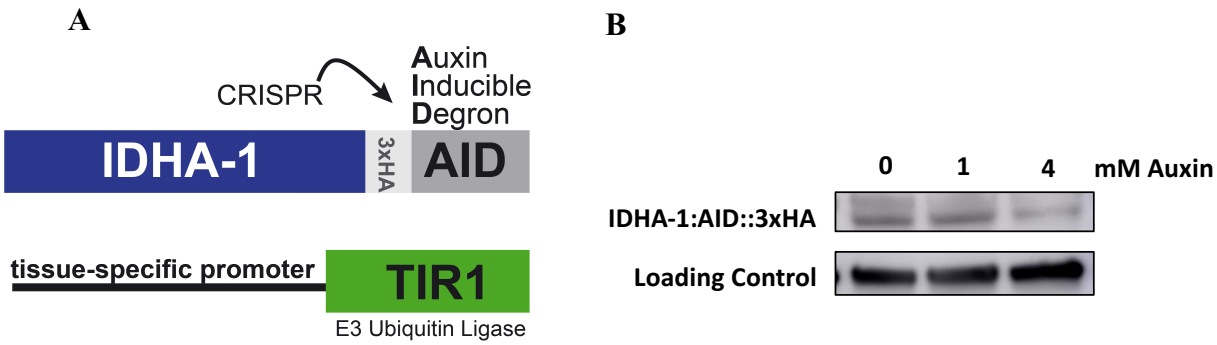

Figure 2.10.2 Tissue specific knockdown by Auxin Inducible Degradation system. A) Schematic diagram showing CRISPR mediated tagging of endogenous IDHA-1 locus with AID degron and HA tag. This strain is combined with strains expressing AID recognizing TIR1 E3 ubiquitin ligase expressed under tissue specific promoters to achieve protein degradation in a specific tissue. **B)** Western Blot analysis shows depleted IDHA-1 levels upon treatment with 4mM Auxin.

In order to validate the results obtained previously that showed cell non-autonomous nature of the *idha-1* depletion mediated phenotype, we next tested the AID tagged IDHA-1 strain with soma specific and germ line specific TIR1 expressing worm strains. However, the auxin mediated depletion of IDHA-1 in somatic tissue was not sufficient to induce reprogramming. We next exposed these worms to *idha-1* RNAi (systemic knockdown) and auxin treatment (tissue specific knockdown) together. When exposed to 4mM auxin and *idha-1* RNAi, soma expressing TIR1 animals show enhanced germ cell conversion phenotype penetration; whereas no significant differences were observed in animals expressing TIR1 in the germ line alone (Figure 2.10.3 A, B). These results are in line with the ones obtained from the *rrf-1* and *ppw-1* mutants and demonstrate the cell non- autonomous nature of IDH3 depletion mediated reprogramming phenotype.

The enhancement observed upon auxin mediated depletion of IDH3 in the soma (together with *idha-1* RNAi) demonstrates not only the requirement of the IDH3 depletion in the soma, but also its strong contribution for the germ cell reprogramming to occur. We next sought to identify the specific somatic tissue(s) involved. In *C. elegans*, inter-tissue communication, involving intestine and germ line has been known to occur to regulate stress resistance in the animal (Nono et al., 2020). We therefore asked if intestine is also involved in this IDH3 depletion mediated germ cell conversion. To test this, we combined AID tagged *idha-1* strain with intestine specific TIR1 expressing worms, to study the effects of IDHA-1 knockdown in the intestine. However, no significant differences could be observed in the phenotype penetrance upon treatment of the worms with auxin (Figure 2.10.3 C).

Another probable cell-type that could be involved in soma to germ line signaling is gonadal sheath cells since they are somatic in nature, are in close contact with the germ line and involved in several aspects of its development. Therefore, we created worm strains with somatic gonad expressing TIR1 in the lab (*lim-7*^{prom}::TIR1). Interestingly, by using this strain that allowed auxin mediated depletion of IDHA-1::AID in the somatic gonad, significant increase in germ cell conversion phenotype was observed (Figure 2.10.3 D).

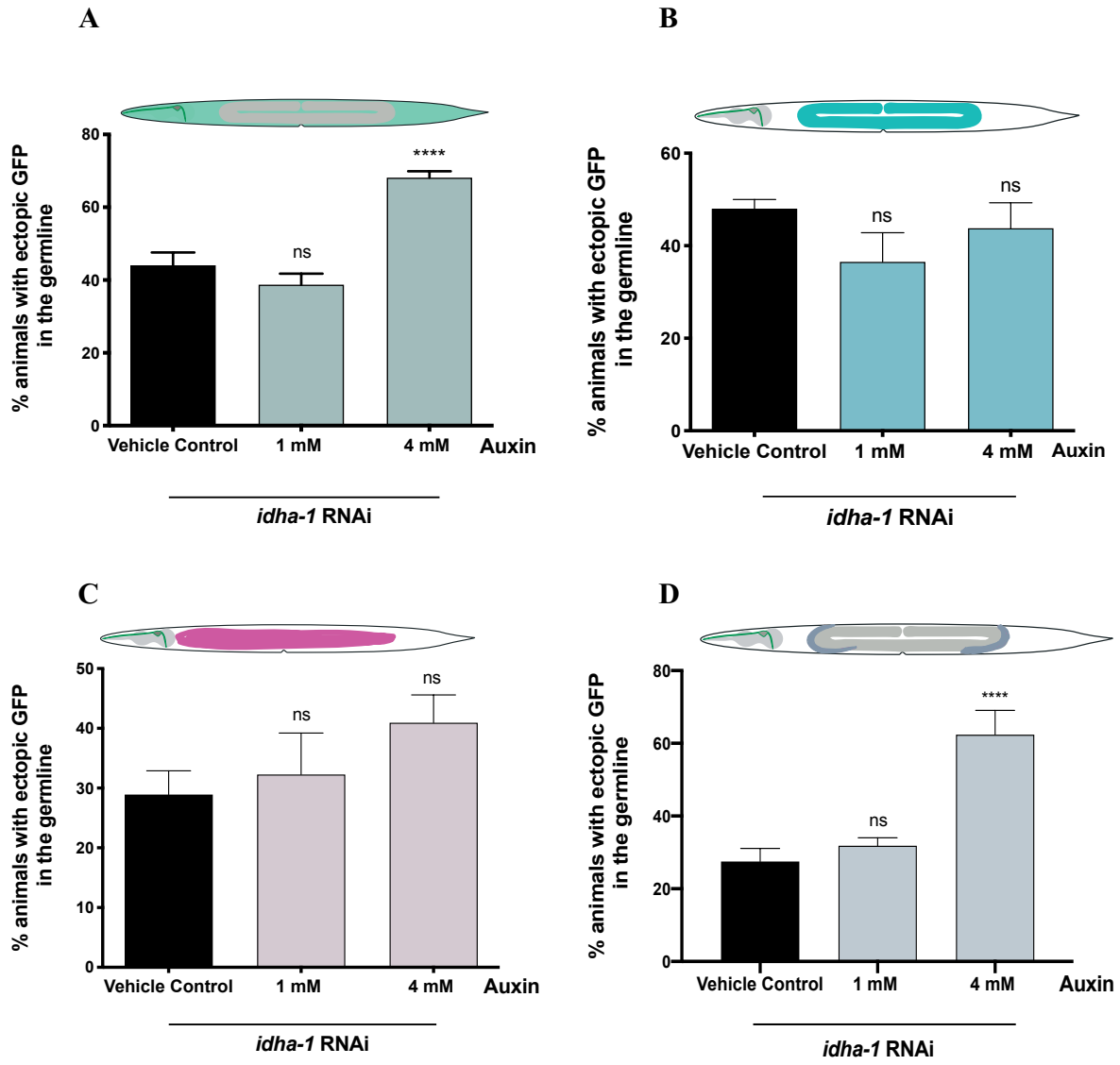

Figure 2.10.3 Cell non-autonomous effects using Auxin Inducible Degradation system. A,B,C,D) Quantification of animals showing CHE-1^{oe} mediated *gcy-5*^{prom}*::GFP* induction in the germ line upon *idha-1*^{RNAi}, and AID mediated IDHA-1 depletion in **A)** soma, **B)** germ line, **C)** intestine and **D)** somatic gonad indicates possible involvement of somatic tissue esp. somatic gonad. Ordinary one-way ANOVA was used for statistical comparison, **** $p<0.0001$, ns not significant. At least 300 animals were counted for control and 1mM auxin treatments, and 100 animals were counted for 4mM auxin treatments. Error bars represent SEM.

Overall, the reprogramming phenotype upon IDH3 knockdown is observed in the germ line of the animal. However, the results from the RNAi mutants and AID depletion experiments

demonstrate that this germ cell conversion phenotype observed upon IDH3 depletion is not cell type autonomous and simultaneous knockdown in germ line as well as somatic tissue is required for the germ cells to reprogram. Furthermore, results from the AID mediated tissue specific depletion indicate possible involvement of somatic gonad in signaling to the germ line to enable the reprogramming upon IDH3 depletion.

2.11 Enhanced glucose transport inhibits reprogramming

The results from section 2.10 indicated that upon IDH3 depletion, there is a signaling event from somatic gonad to the germ line. Furthermore, the results also demonstrated that this signaling between tissues enables the germ cell to neuronal reprogramming upon IDH3 depletion.

We next sought to understand the nature of this cross tissue signaling that occurs upon depletion of IDH3. Signaling between cells can occur from direct interaction of a cell with its neighbor or by secreted signaling molecules (Cooper, 2000). In both of these cases, a number of different agents including hormones, neurotransmitters, amino acids as well as small molecules function to signal between cells. We therefore performed a suppressor/enhancer RNAi screen in which we co-depleted *idha-1* with transporters and receptors of different signaling molecules and scored the germ cell conversion phenotype penetrance compared to the control. If upon co-depletion of any candidate, the phenotype is decreased, it is indicative of the requirement of the candidate for the conversion to occur. Whereas candidates which upon depletion allow enhanced reprogramming, act to inhibit the reprogramming process.

Since IDH3 is an important metabolic enzyme, its depletion is expected to alter the metabolomic processes of the cell. This was also demonstrated in the metabolomic analysis carried out on *idha-1*^{RNAi} treated worms as explained in section 2.7 & 2.9. Based on this, we hypothesized that the signaling resulting due to depletion of this important metabolic enzyme IDH3 could also involve a metabolite. This is likely in an event in which cells try to 'compensate' the disturbance of metabolism and can involve import of a metabolite that is needed or depleted; or export of ones that are produced in excess. Our metabolomic analysis revealed very high intracellular citrate levels. We therefore depleted the enzymes *nac-1, nac-2, nac-3* as well as B0285.6 that are homologs to the human Na+ coupled dicarboxylate transporters (NADC) and belong to the SLC13 family of solute carriers involved in citrate and succinate transport. Another interesting candidate is the transmembrane Solute carrier family

6 (SLC6) that is involved in the transport of multiple amino acids including alanine, serine and tryptophan. We therefore co-depleted members of the amino acid transporters *aat-1* and *aat-2* together with *idha-1*. In addition, since we detected decreased levels of malate in the metabolomic analysis in *idha-1* depleted worms, we also co-depleted *mdh-1* & *mdh-2* which code for malate dehydrogenase and work with amino acid transporter *aat-1* and *aat-2* as part of the aspartate/malate shuttle. However, depletion of any of these enzymes belonging to the SLC13 and SLC6 family of transporters did not cause significant change in the phenotype penetrance (Figure 2.11). While these results do not rule out the possibility that aberrant transport of any of these metabolites can occur upon IDH3 depletion, it does demonstrate that such transport does not have an effect on the ability of the cells to be reprogrammed.

Another interesting candidate and one of the main metabolites that fuels the energy generating pathways in the cell is glucose. Multiple families of transmembrane transporters are involved in the transport of glucose across the plasma membrane. We selected F14E5.1 (homolog of human GLUT1) that is one of the most abundantly expressed glucose transporters and has been reported to be altered in conditions of cellular differentiation and transformation (Jun et al., 2011). Interestingly, we observed more than 2-fold increase in the phenotype penetrance upon co-depletion of F14E5.1 with *idha-1* (Figure 2.11). These results suggest that upon depletion of *idha-1,* the cells utilize increased glucose transport possibly in order to overcome the effects of defective metabolism. This increased glucose transport is able to 'rescue' the disturbances created in the metabolism by the IDH3 depletion. However, upon co-depletion of *idha-1* and F14E5.1, the rescue effect of glucose is alleviated, possibly resulting in increased and/or further alterations in the cellular metabolic environment thus enabling efficient reprogramming.

Since we observed increased reprogramming upon the depletion of the glucose transporter, the results obtained from co-depletion of *idha-1* and F14E5.1 suggested that the glucose transport inhibits cellular reprogramming. Our initial motivation was to identify the signaling between tissues (somatic gonad and germ line) that enables reprogramming; we therefore continued exploring possible signaling mediators. Since we detected no change in reprogramming phenotype in any tested metabolite (other than glucose) we made an attempt to understand if signaling other than metabolite in nature is involved. For this, we depleted member of SLC6 dopamine transporter (*dat-1),* which is involved in transmission of neurotransmitters including dopamine. No change was observed in the phenotype penetrance

upon its co-depletion with *idha-1* (Figure 2.11). Another possible candidate is the family of receptor tyrosine kinases that are involved in cell-to-cell communication for a variety of cellular processes including growth, differentiation and metabolism (Du & Lovly, 2018). We co-depleted *tdc*-1 (tyrosine decarboxylase), *tph-1* (tryptophan hydroxylase) and tyramine receptor *tyra-3* together with *idha-1.* As depicted in figure 2.11, we did not detect any change in penetrance of reprogramming phenotype upon any of these treatments.

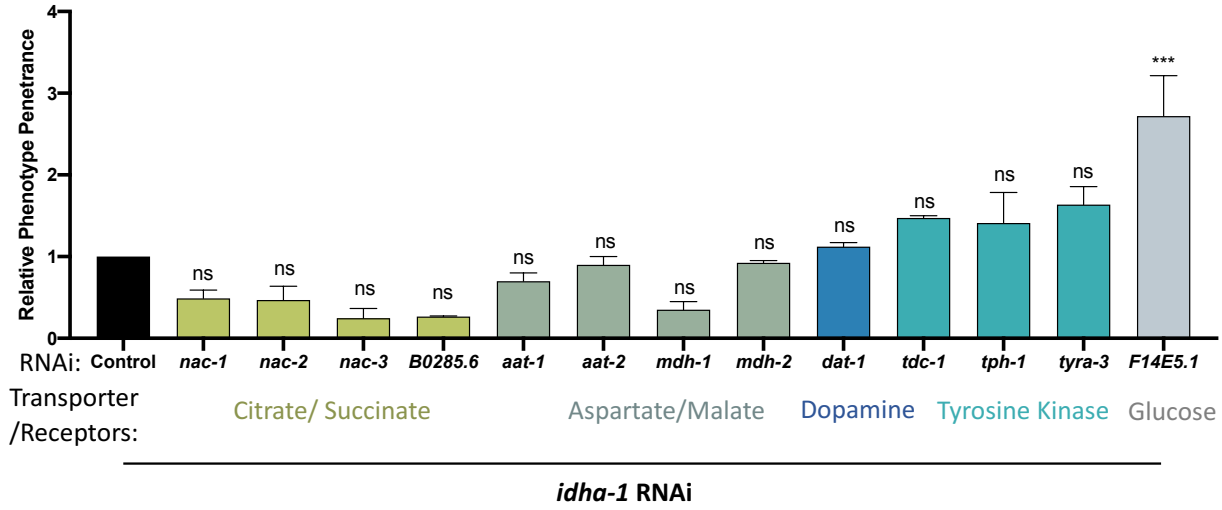

Figure 2.11 Double RNAi screen of IDHA-1 depletion and candidate members of metabolite transporters and receptors. A) Quantification of animals showing *gcy-5*^{prom}*::GFP* induction upon CHE-1^{oe} in the germ line upon double RNAi knockdown with *idha-1* and genes coding for the indicated metabolites' transporter and receptor proteins. Ordinary one-way ANOVA was used for statistical comparison, *** $p<0.001$, ns non-significant. At least 200 animals were counted for each condition. Error bars represent SEM.

Taken together, the RNAi screen results suggest that increased glucose transport occurs upon IDH3 depletion. This glucose transport, however, acts to rescue the effects of IDH3 depletion which causes limited germ cell reprogramming. Furthermore, in the conducted experiments, the RNAi knockdown of the identified glucose transporter F14E5.1(as well as *idha-1*) was in the entire animal; therefore, additional experiments that allow tissue specific knockdown are required to identify the tissues involved in the putative transport of glucose among tissues. Overall, the nature and mechanism of the signaling event that occurs between somatic gonad and germ line (described in the previous section) remains to be elucidated and is subject to continued research.

2.12 Changes in transcriptome upon IDH3 depletion

We found changes in the metabolome of the animals upon depletion of IDH3. This is expected since the enzyme is functional in a central metabolic pathway. In context to reprogramming, these metabolic changes are eventually expected to alter the epigenetic state of the cell that primes the cell towards reprogramming. Our results from histone methylation analysis also revealed decreased levels of repressive histone marks H3K9me3 and H3K27me3. Additionally, this alteration in chromatin accessibility may also result in transcriptional changes which could contribute to the reprogramming potential of the cell.

Keeping this in view, we next asked if IDH3 depletion also results in changes in gene expression in the animals. For this, we performed RNA sequencing (RNA-seq) on animals treated with control and *idha-1* RNAi without the induction of CHE-1 overexpression in order to determine if the depletion of *idha-1* leads to transcriptional changes that may prime the cells towards TF mediate reprogramming. The number of reads mapping to the genome was highly concordant between the replicates, indicating reproducibility and good quality of the experiment. (Figure 2.12.1 A). Surprisingly, principial component analysis (PCA) of the normalized read counts obtained from RNA-seq revealed that the samples clustered based on the biological repeats (BR) (Figure 2.12.1 B). Consistently, based on differential expression analysis, heatmap of unsupervised hierarchical clustering of the top 100 genes with most variant gene expression across control and *idha-1* RNAi also revealed that control and *idha-1* RNAi samples of the same biological replicates clustered together and are similar to each other (Figure 2.12.1 C).

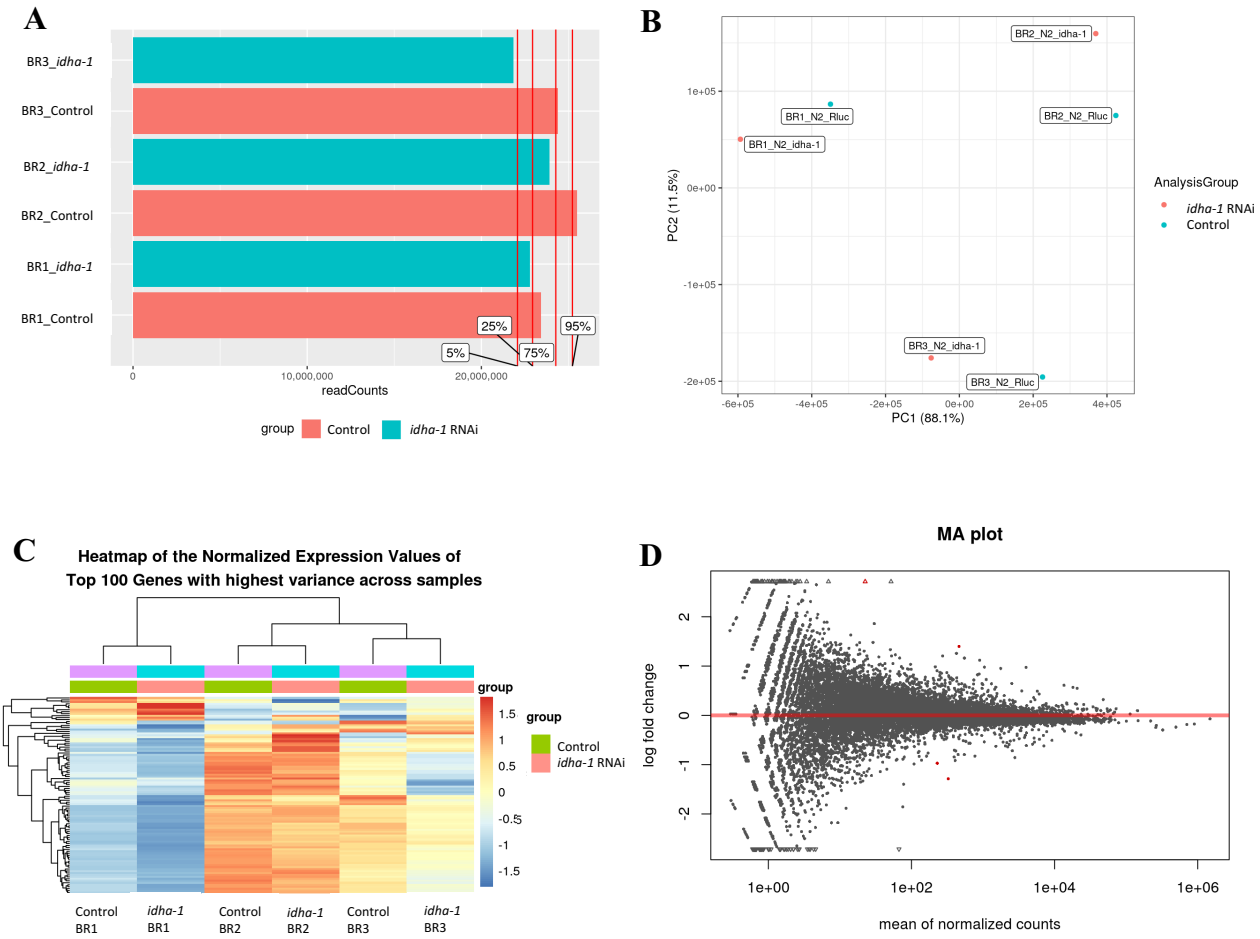

Figure 2.12.1 Transcriptome analysis of *C.elegans* upon IDH3 depletion A) Principal component analysis **(**PCA plot) showing the clustering of samples based on biological repeats. **B)** Plot showing number of reads obtained from each sample that were assigned to genes. **C)** A heatmap of unsupervised hierarchical clustering of the top 100 genes with most variant gene expression across control and *idha-1* RNAi samples shows that samples in each biological repeat (BR) are similar to each other. Independently generated biological replicates clustered together and are indicated. **D)** The MA plot showing the difference in log2 fold-change compared to the average normalized expression values per gene. Genes showing significant differential expression between *idha-1* vs control RNAi samples are indicated in red. Data analysis was performed by Mr. Alexander Blume.

Based on the differential gene expression analysis, we did not observe substantial differences upon *idha-1* depletion compared to control (Figure 2.12.1 D) suggesting that *idha-1* depletion does not cause drastic or apparent changes in gene expression. Yet, four candidate gene changes expression levels: infection response gene *irg-5*, amino methyltransferase *amt-1,* dietary restriction down regulated gene *drd-50,* and a gene of unknown function C07G1.7 that were detected based on the differential expression criteria of adjusted p-value below 0.1 and a log2 fold-change increase of at least +/-1, which corresponds to a two-fold increase or decrease in expression levels. However, analysis of the differential transcript usage based on the same criteria resulted in identification of 25 genes with one or more transcripts differentially expressed between *idha-1* and control RNAi samples (Figure 2.12.2) (Table 2.1).

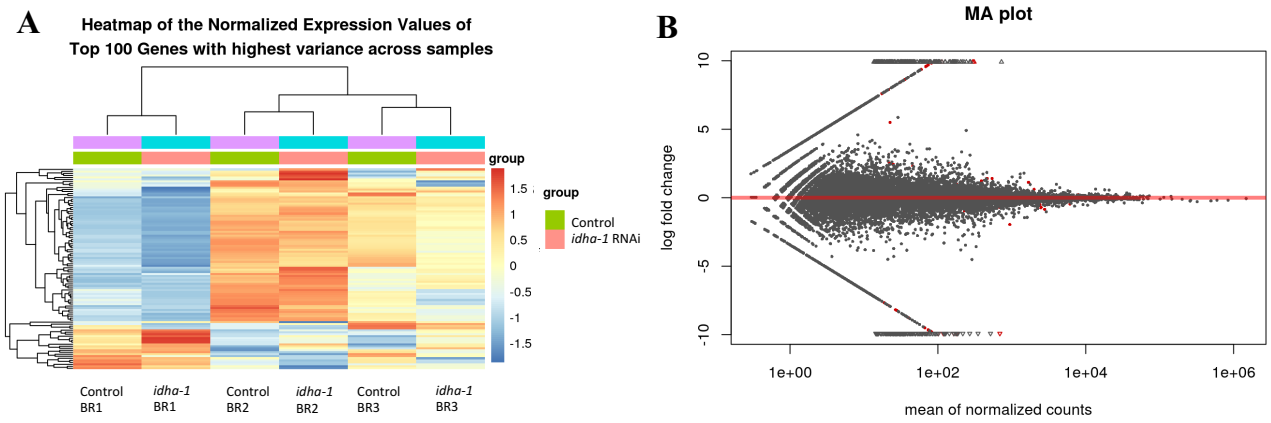

Figure 2.12.2 Analysis of differential transcript usage upon IDH3 depletion A) A heatmap of unsupervised hierarchical clustering of the top 100 genes with most variant transcript expression across control and *idha-1* RNAi samples. Independently generated biological replicates clustered together and are indicated. **B)** The MA plot showing the difference in log2 fold-change compared to the average normalized expression values per transcript. Genes showing significant differential transcript expression between *idha-1* vs control RNAi samples are indicated in red. Data analysis was performed by Mr. Alexander Blume.

A) Up-regulated

Sr. #	Gene name	log2 Fold Change	p value
1	K07E3.4	2.52582516	0.01092086
2	T11G6.2	2.43611315	0.02076246
3	*bcl-11*	2.33732269	0.06364359
4	*daf-15*	1.40633809	0.02076246
5	*rskn-1*	1.23037577	0.08091884
6	T19B10.2	1.22941234	0.00040666
7	*sec-16*	1.12344942	0.01114727
8	Y43F8C.7	1.0113895	0.0098674
9	C18B2.3	0.92366665	0.00054505
10	T12G3.2	0.78575166	0.00576241
11	*pst-2*	0.75442824	0.09155299
12	T04F3.1	0.60772396	0.00348777
13	Y43F8B.1	0.27908035	0.07578946
14	*mup-2*	0.2205277	0.0063605

B) Down-regulated

Sr. #	Gene name	log2 Fold Change	p value
1	*rpt-1*	-0.2322007	0.03471189
2	*rab-14*	-0.4229317	0.07578946
3	*hmp-1*	-0.4551586	0.09256189
4	*cka-1*	-0.699182	0.00346514
5	*dars-1*	-0.6999074	0.00013413
6	D1086.11	-0.7018181	0.00011673
7	F55B11.3	-0.7262073	0.0098674
8	*pst-2*	-0.7509261	0.0001405
9	*itr-1*	-0.8605617	0.0098674
10	C42C1.19	-1.2246697	0.02367485
11	*pcp-3*	-1.9535202	0.09155299

Table 2.2 A,B) List of genes with differential transcript usage upon *idha-1* depletion detected based on the differential expression criteria of adjusted p-value below 0.1 and a log2 fold-change increase of at least +/-1. Genes coding for transporters/receptors are highlighted in yellow; and for enzymes in grey.

Candidates that show differential transcript usage include genes coding for enzymes (10 out of 25) including K07E3.4 involved in formate-tetrahydrofolate ligase activity; methenyltetrahydrofolate cyclohydrolase activity; and methylenetetrahydrofolate dehydrogenase (NADP+) activity; as well as transporters (6 out of 25) such as T11G6.2 from the solute carrier family (SLC) 37 involved in phosphosugar/phosphate transport, and C42C1.19 belonging to solute carrier family SLC 34 involved in transport of glucose 6 phosphate (Table 2.2). The 'isoform-switches' observed in these genes could potentially lead

to biological consequences by for example skipping a functional domain in enzymes. These candidates are needed to be analyzed in further detail and validated to understand their possible role in IDH3 depletion mediated reprogramming.

Overall, we did not detect drastic transcriptome changes upon IDH3 depletion. This suggests that although chromatin changes occur upon IDH3 depletion, this does not lead to changes in gene expression. It can be proposed that this poised chromatin is available and utilized upon the induction of the fate inducing TF CHE-1 which initiates transcription of neuronal gene program for the cellular conversion process.

3. DISCUSSION

3.1 Mitochondrial Isocitrate Dehydrogenase safeguards germ cell identity

Cellular reprogramming has great potential for cellular replacement therapies and for disease modelling, however, it suffers from low efficiency. Tursun et al. demonstrated the presence of 'barriers'; safeguarding mechanisms that prevent cellular conversion to other identities, and described the role of histone chaperone LIN-53 in this context (Tursun et al., 2011). Since then, a number of other studies have identified additional cell fate safeguarding factors in *C. elegans* but also in other species and cell types (Reviewed by Ebrahimi et al., 2015; Kolundzic et al., 2018; Hajduskova et al., 2019). While the studies focusing on identification of fate safeguarding mechanisms have extensively explored the role of epigenetic regulation, our knowledge of other cellular functions and processes in cell fate maintenance is relatively limited. In an effort to identify further mechanisms involved in the protection of cell fate, a whole genome RNAi screen was carried out in the lab, that employed the transcription factor (TF) CHE-1 mediated direct reprogramming system described before (Figure 2.2.1) and identified a number of genes related to mitochondrial function and cellular metabolism. A follow up screen on these identified candidates revealed that knock down of alpha subunit of the mitochondrial isocitrate dehydrogenase coding gene *idha-1* gave a consistent germ cell conversion (GeCo) phenotype upon ectopic expression of the TF CHE-1. Identification of this key mitochondrial and metabolic enzyme subunit IDHA-1 as a cell fate safeguarding factor gave a unique opportunity to explore and study the role of mitochondria and metabolism using this TF CHE-1 mediated direct reprogramming system. Furthermore, knock down of other mitochondria and metabolism related genes did not allow germ cell reprogramming (Table 2.1). This highlights the specificity of cell fate protecting function of IDHA-1 in germ cells, and negates the possibility that the conversion occurred due to an overall general disturbance of mitochondrial function or metabolic state of the cell.

The identified reprogramming barrier IDHA-1 is the alpha subunit of isocitrate dehydrogenase 3 (IDH3) that belongs to a highly conserved family of enzymes isocitrate dehydrogenases (IDH) and has two other isoforms IDH1 and IDH2. Interestingly, we observed no reprogramming phenotype upon depletion of IDH1 or IDH2 (Figure 2.1.1). Together, these two isoforms share multiple differences from IDH3 and that provides possible explanations to this failure to achieve reprogramming upon their knockdown. One possibility is that depletion of a-KG is the main driver of reprogramming; and depletion of IDH1 or IDH2 does not result

in sufficient disturbance in the a-KG levels. Furthermore, unlike IDH3, IDH1 and IDH2 catalyze the reverse reaction of a-KG to isocitrate conversion as well, it is thus likely that their depletion results in increased levels of a-KG (as opposed to expected decrease in a-KG levels upon IDH3 depletion) and hence does not allow reprogramming (Kaminska et al., 2019). However, levels of a-KG have been shown to reduce upon depletion of IDH1 and IDH2 thus suggesting an alternative prospect (Calvert et al., 2017).

Another possibility is the co-factor requirement of these different isoforms. While IDH1 and IDH2 are NADPH+ dependent, IDH3 uses NAD+ as a co-factor and reduces it to NADH. NAD+ also acts as a co-factor for a number of other enzymes in the cell including histone deacetylases such as sirtuins and its intracellular levels and availability thus affect the chromatin state (Imai et al., 2014). Furthermore, NADH acts as a competitive inhibitor of sirtuins and thus the disturbance in the balance of NAD+/NADH due to IDH3 depletion could therefore result in altered activity of other cellular processes and may contribute to reprogramming (Lin et al., 2014). Another possible explanation to the reprogramming observed upon knockdown of IDH3 and not by IDH1 or IDH2 is the differences in their downstream effectors. Since IDH3 functions in the TCA cycle, depletion of this isoform and the resulting disruption of the TCA cycle and its related pathways/processes could be responsible for the reprogramming to occur. Our results favor this role of IDH3 in the TCA cycle to be underlying the germ cell reprogramming (explained in later sections). However, it is also likely that a combination of changes (involving for example NAD+/NADH levels) that occur only when IDH3 is depleted are responsible for mediating germ cell reprogramming.

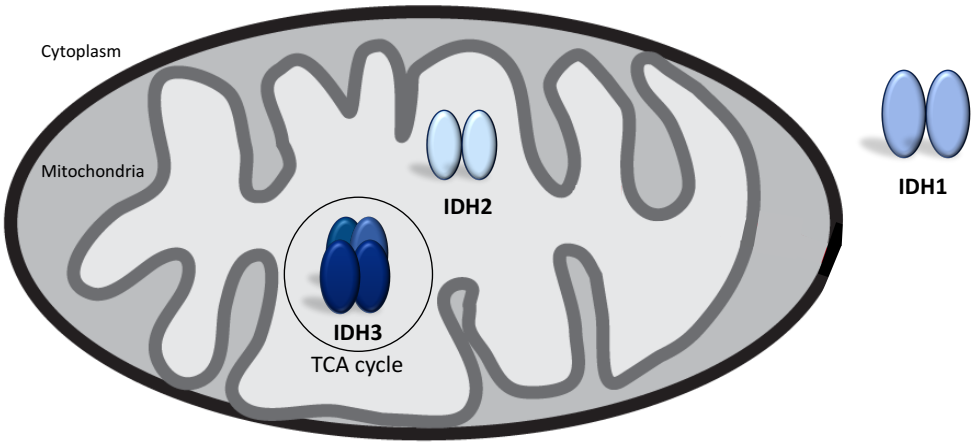

Figure 3.1 Isocitrate Dehydrogenases in the cell. IDH1 occurs predominantly in the cytoplasm; whereas IDH2 and IDH3 localize to the mitochondria. IDH3 is heterotetrameric unlike IDH1 and 2; and functions in the TCA cycle.

3.2 Cellular safeguard mechanisms may be cell type-specific and protect against specific fates

IDH3 depletion in the entire worm allowed reprogramming only in germ cells. Such phenotype is also seen upon depletion of the previously reported histone chaperone LIN-53 and FACT complex members (Tursun et al., 2011; Kolundzic et al., 2018). Together, these observations point to possible tissue-specific cell fate maintenance mechanisms that have developed in the organism. However, it cannot be ruled out that additional cell fate protection pathways operate in other tissues and thus depletion of IDH3 alone is not sufficient to overcome the cell fate barriers. Alternatively, it could be a result of the inherent plasticity of the germ cells that allows them to be reprogrammed, upon perturbation, relatively easier compared to other cell types. This notion is further supported by the results from the whole genome RNAi screen carried out by Ena Kolundzic in the lab (Kolundzic et al., 2018). It showed the tissue that exhibited highest percentage of conversion phenotype is the germ line which accounted for about 58% of the total number of reprogramming events observed.

Our results suggest that IDH3 safeguards cell fate against conversion to at least neuronal fates (ASE, GABAergic neuron). However, we failed to observe TF HLH-1 mediated reprogramming to muscle fate. These results are similar to ones reported from depletion of FACT complex members, which allows reprogramming to neuronal fates, but not to muscle (Kolundzic et al., 2018). This failure to achieve reprogramming to muscle could be due to reasons including the stability, or the pioneering ability of the TF HLH-1 for muscle fate induction. However, this seems unlikely since HLH-1 has been shown to successfully convert germ cells to neurons upon *lin-53* depletion. Furthermore, the mammalian homolog of HLH-1, MyoD was one of the earliest shown TF that achieved direct reprogramming and has been extensively used for this purpose since then (Tursun et al., 2012; Davis et al., 1987). The negative results thus raise the possibility that IDH3 may only restrict the reprogramming trajectory towards a neuronal developmental program while other factors may prevent the induction of non-neuronal differentiation programs.

3.3 Role of IDH and a-KG in reprogramming and cell fate

Isocitrate dehydrogenases have been extensively described for their role in cancer development and progression (Reviewed by Dang et al., 2016). Since cancer development is associated with the loss of original cell fate, cellular reprogramming and cancer exhibit

similarities in terms of erasure of existing cellular identity. Gain of function mutations in IDH1 and IDH2 isoforms have been associated with various cancers especially gliomas, secondary glioblastomas and acute myeloid leukemias; and have been extensively studied (Parsons et al., 2008; Yan et al., 2009; Kang et al., 2009; Madal et al., 2018). Interestingly, however, although mutations in IDH3 subunits have been identified in some cancers, they are not as recurrent and were previously considered to be the consequence rather than the cause of cancers (Krell et al., 2011). Recent studies, however have increasingly identified the role of IDH3 mutations in cancer development and progression (Molenaar et al., 2015; Stegh., 2017; Du et al., 2018; Lui et al., 2020). A recent analysis of the data from cBioPortal for Cancer Genomics revealed that the mRNA levels of IDH3a (homolog of IDHA-1) are upregulated in multiple types of cancers including colorectal, adenocarcinoma, hepatocellular carcinoma and lung adenocarcinoma among others. (Liu et al., 2020). Furthermore, studies have also reported correlation between IDH3a levels and poor outcomes in breast and lung cancer patients, thus highlighting its tumor promoting properties (Zeng et al., 2015). However, while the association of IDH1 and IDH2 with cancer is largely linked to gain of function mutation in these enzymes that generates the oncometabolite a-hydroxyglutarate, IDH3 and its role in cancer is defined by the alterations of its product a-KG or its metabolic analogs.

Intermediate of TCA cycle and product of IDH3, a-KG has been described to have an important role in the context of reprogramming and differentiation. This impact of a-KG on cell fate is related to its function as a co-factor for dioxygenases, which are involved in different cellular functions ranging from DNA and histone demethylation to targeting proteins for degradation (Markolovic et al., 2015; Walport et al., 2012). However, the exact effect of a-KG as an enabler or inhibitor of reprogramming has been found to be conflicting and dependent mainly on cellular context: in primed pluripotent stem cells, a-KG has been found to both accelerate differentiation as well as support the undifferentiated state (TesLaa et al., 2016; Zhu et al., 2017); whereas in naïve pluripotent stem cells, a-KG has been shown to be required to maintain pluripotency (Carey et al., 2014; Hwang et al., 2016). Interestingly, in both naïve and primed stem cells, the same mechanism of a-KG to succinate (metabolic homolog and inhibitor of dioxygenases) ratio is proposed to be responsible; which however, results in different outcomes in cell fate (Reviewed by Haniuda et al., 2020). Similarly, for induced reprogramming, a-KG dependent DNA and histone demethylation have been shown to be required for the acquisition of pluripotency, maintenance of pluripotent state as well as differentiation in vitro (reviewed by Tran et al., 2018).

A number of studies describe the role of IDH3 in cancer due to alterations of its product a-KG or its metabolic analogs. Diminished IDH3 activity in fibroblasts has been shown to result in slightly elevated a-KG levels. However, due to overall reduced a-KG to succinate ratio, the activity of dioxygenases is inhibited and promotes the transformation of these fibroblasts to cancer associated fibroblasts (Zhang et al., 2015). Further, in cervical epithelial carcinoma cells, downregulation of IDH3 has also shown to increase a-KG levels, however this results in delayed tumor growth (Zeng et al., 2014). However, our IDH3 depletion based direct reprogramming system represents one fundamental difference from these reports. While these previous studies on cancer directly link levels of a-KG or its antagonists' succinate/ fumarate to downstream effector function and cellular outcomes, we detected no severe changes in the levels of these metabolites upon IDH3 depletion (Figure 2.7). The possible explanation for this difference could be that these studies focusing on involvement of a-KG in cell fate and cancer are predominately carried out in cell culture systems. *In vivo* models including *C. elegans* exhibit cross tissue communication and compensatory and/or signaling mechanisms that add to the complexity and may therefore result in different outcomes. It should however be noted that our metabolomic analysis was carried out on whole worms. Therefore, while levels of metabolites such as a-KG overall show no significant difference in the animals, it is possible that changes occur in specific tissues such as the germ line. Tissue specific metabolomic analysis is required to address this possibility. However, current applications do not allow collection of sufficient number of cells that can be analyzed for metabolic content and therefore pose limitations to such studies at present.

Overall, our finding of maintained a-KG levels observed upon IDH3 depletion raise two questions: first, how is the cellular a-KG levels replenished to near normal levels in the absence of IDH3 activity? Secondly, given that the levels of these metabolites (a-KG, fumarate, succinate) do not change - what underlies the IDH3 depletion mediated conversion? Our results of enhancer/suppressor RNAi screen and isotope labelled metabolomic studies suggest the glutamine breakdown pathway as an alternative a-KG generating mechanism employed by the cells upon IDH3 depletion (Results section 2.8). Similar mechanism of glutamine break down has also been proposed to occur in cervical epithelial carcinoma where a-KG levels are not decreased, as would be expected upon depletion of IDH3 (Zeng et al., 2014). In an attempt to answer the second question, our experiments demonstrated that while a-KG levels are replenished by alternative means, the effects of glutamine anaplerosis itself, as well as a

number of other metabolic and epigenetic changes that result upon IDH3 depletion (will be discussed later in detail) provide possible mechanisms that prime germ cells to reprogramming.

3.4 Transcription Factor HIF-1 enables IDH3 depletion mediated reprogramming

The identification of the TF HIF-1 as an enabling factor for the IDH3 depletion mediated reprogramming is in line with the reports from reprogramming of dermal fibroblasts to iPSCs. Similar function of HIF-1 has been described early during the reprograming process, thus making it an enabling regulator during cell fate conversion (Prigione et al., 2014).

In cells, HIF-1 activity is regulated at multiple levels including transcriptional and translational regulation as well as proteasomal degradation (Reviewed by Nagao et al., 2019). Proteasomal degradation of HIF-1 is brought about by enzymes that require a-KG. Since a-KG is the product of IDH, the activity of IDH is therefore directly linked to the HIF-1 stability (Semenza et al., 2003). While a number of studies report HIF-1 activation upon depletion of IDH1 and IDH2 and show mixed results; the relationship between IDH3 activity and HIF-1 activation is relatively less studied, but follows a trend of HIF-1 activation (Reviewed by Liu et al., 2020). In these cases, the underlying cause of this increased HIF-1 stability is the overall reduction in a-KG levels, or decreased a-KG levels compared to its structural metabolic analogs' succinate and fumarate (effective a-KG) (Zeng et al., 2015; Zhang et al., 2015). Keeping this view, while the decreased a-KG or increased succinate/ fumarate levels upon IDH3 depletion appear to be the most obvious underlying cause of this identified HIF-1 activity, in our system, no such differences in the levels of these metabolites were observed, thus suggesting an alternative model of HIF-1 activation upon IDH3 depletion.

A recent study described activation of HIF-1 upon IDH2 depletion in prostate cancer (Wang et al., 2020). The described mechanism of HIF-1 activation and activity by perturbance of IDH2 shares similarities with our IDH3 depletion mediated HIF-1 dynamics based on the following reasons: First, this activation of HIF-1 was shown to be dependent on Reactive Oxygen Species (ROS) and not a-KG levels. Previously, similar activation of ROS has been reported upon depletion of IDH3 in mammalian systems (May et al., 2019). Second, this ROS mediated activation of HIF-1 was observed only upon perturbation of mitochondrial IDH2 and not of cytosolic IDH1. We also did not observe any reprogramming upon depletion of IDH1. More Importantly, this increased HIF-1 levels by ROS were shown to result in pseudo-hypoxia response; whereby there was no detectable increase in mRNA as well as protein levels of a

number of established HIF-1 target genes. These included enzymes such as hexokinase functional in glycolysis; as well as pyruvate dehydrogenase kinase which inhibits conversion of pyruvate to acetyl-coA for entry into the TCA cycle. In our results, while we observed increased activity of some established HIF-1 targets including Jumonji proteins as well as glucose transporter F14E5.1 (homolog of GLUT1); we also noted decreased glycolysis and increased mitochondrial TCA cycle flux (the reverse of which is established to be a hallmark of HIF-1 mediated hypoxia response; but is consistent with the observations in IDH2 depletion mediated pseudo-hypoxia response) (Results section 2.9). This model therefore explains not only the activation of HIF-1, but also its functionality, which is distinct from its described function under hypoxic conditions and in cancer. However, it cannot be ruled out that other known mechanism(s) of HIF-1 activation including microRNAs or Phosphoinositide 3-kinase pathway (PI3k) may underlie its activation upon IDH3 depletion (Kilic et al., 2013; Serocki et al., 2018).

3.5 Increased Jumonji activity as an enabler of IDH3 depletion mediated reprogramming

Results of the RNAi suppressor enhancer screen revealed requirement of Jumonji proteins for the reprogramming process (Figure 2.5.1). Furthermore, the decreased histone methylation observed does not only further confirm the involvement of these histone demethylases but also point to their increased activity upon depletion of IDH3 (Figure 2.5.4). a-KG acts as a co-factor for the Jumonji enzymes, and therefore these results are surprising since upon depletion of IDH3, levels of its product a-KG are expected to decrease, which should in return lead to a decrease in the activity of Jumonji enzymes.

A number of studies have reported the altered functionality of Jumonji proteins linked to IDH1 and 2 mutations in various cancer types (Reviewed by Madala et al., 2018). However, to our knowledge, only one study on IDH3 and its direct link to Jumonji protein activity has been conducted, and shows contradictory results to IDH1 and IDH2 depletion effects. IDH3a (IDHA-1 in worms) downregulation in primary fibroblasts increases the activity of Jumonji proteins as seen by increased demethylation of histone 3 lysine 4 trimethylation marks. (Zhang et al., 2015). This IDH3 depletion-mediated increase in Jumonji activity has been attributed to relative increased levels of succinate or fumarate (structural metabolic analogs of α-KG) compared to a-KG, which inhibits a-KG dependent enzymes. Our metabolomic analysis revealed comparable levels of a-KG as well as succinate and fumarate with and without IDH3

depletion. This finding thus provides explanation to the 'normal' functioning of the Jumonji proteins. However, it still fails to explain the increased Jumonji based demethylation observed upon IDH3 depletion.

One possible model has been described previously during embryonic development in mice, where increased histone demethylation by Jumonji proteins is achieved by the transport of mitochondrial enzymes to the nucleus (Nagaraj et al., 2017). Furthermore, multiple studies in mammalian systems have reported the transcriptional activation of the Jumonji genes including JMJD3 (*jmjd-3.3* in worms) in a HIF-1 dependent manner (Bayer et al., 2008; Pollard et al., 2008; Xia et al., 2009; Lee et al., 2014). The former prospect seems unlikely due to the following reasons: the increased Jumonji activity observed necessitates the requirement of transport of mitochondrial IDH3 in the nucleus to provide a-KG. However, our reprogramming model is based on the depletion of IDH3. Furthermore, this transport of IDH3 to the nucleus is dependent on high pyruvate levels whereas our metabolomic analysis revealed no detectable differences in the levels of pyruvate. Of these two possibilities, the latter seems more likely, since we also identified HIF-1 to be required for the IDH3 depletion mediated reprogramming; and our results suggested their functioning in the same pathway (Figure 2.5.3). It can therefore be suggested that IDH3 dependent activation of HIF-1 leads to increased Jumonji activity, resulting in increased histone demethylation.

One of the identified Jumonji candidates *jmjd-3.3* (JMJD3 in mammals) codes for conserved Jumonji protein, which is involved in H3K27-specific histone demethylation and is decreased upon IDH3 depletion as shown in Figure 2.5.3. In mammalian systems, JMJD3 regulates the transcriptional activation of genes involved in various processes including development, reprogramming and cancer (Burchfield et al., 2015). In mice, it has been shown that JMJD3 removes the H3K27me3 mark from promoters involved in reprogramming of bone marrow progenitor cells to hepatocytes (Kochat et al., 2014). Decreased expression of JMJD3 has been associated with the decreased H3K27 demethylation at the INK4A–ARF tumor suppressor locus leading to development of several human cancers including lung, liver and hematopoietic malignancies (Agger et al., 2009). Together with histone methyltransferase EZH2 and demethylase UTX, it has been shown to regulate hepatic plasticity and proliferation of liver cells (Pediconi et al., 2019). A recent study has shown the role of JMJD3 in activation of epithelial and pluripotency genes in mouse reprogramming with the Yamanaka TFs (Huang et al., 2020). In line with previous reports, the decreased H3K27 tri-methylation levels that we

observed upon *idha-1* depletion further confirms its involvement in this direct reprogramming system (Figure 2.5.3).

Another identified Jumonji candidate JMJD-4 (JMJD4 in mammals) is relatively less studied and is proposed to be involved in regulation of mRNA translation (Feng et al., 2014). JMJD4 was found to be overexpressed in human colon adenocarcinomas and this increase correlated with reduced survival (Ho et al., 2018). Interestingly, downregulation of JMJD4 in mouse fibroblasts resulted in decreased proliferation in cell culture, but gave contradictory results *in vivo* in mouse and drosophila where it was found to be dispensable for development (Hu et al., 2016; Shalaby et al., 2017; Yoo et al., 2016). Recently, IDH3a depletion in liver cancer cells has been shown to significantly upregulate gene expression of JMJD4 and overall, this IDH3a depletion was shown to promote hepatocellular carcinoma migration and invasion (Lui et al., 2020). Our finding that JMJD-4 is involved in germ cell to neuronal reprogramming could be related to its suggested function of mRNA translation regulation or possible unknown roles. However, the exact nature of its functions and role in reprogramming remains to be determined.

3.6 IDH3 depletion leads to altered histone methylation levels

We argued that in order to make a cell permissive for TF-mediated reprogramming, changes in cellular processes and metabolism may eventually lead to the accessibility of the chromatin for the transcription factor to initiate the reprogramming process. Our identification of decreased epigenetic marks associated with transcriptional repression (histone 3, lysine 9 [H3K9] and lysine 27 [H3K27] tri-methylation) provides a link between the metabolism change occurring upon IDH3 knockdown with chromatin changes. The conserved repressive H3K9me3 mark plays important regulatory role during development, sex determination, and tumorigenesis among others (Benevento et al., 2015; Casciello et al., 2015; Kuroki and Tachibana, 2018). Enzymes that deposit these marks have been known to repress pluripotency-related genes and H3K9me3 has been shown to be a barrier of somatic cell reprogramming into iPSCs (Epsztejn-Litman et al., 2008; Chen et al., 2013). Moreover, generation of human and mouse iPSCs is facilitated by reducing the H3K9me3 levels, achieved by interfering the activity of H3K9 methyltransferases including Setdb1; or by the activation of the respective histone demethylases such as Kdm4b and Jhdm1 (Mattout et al., 2011; Liang et al., 2012; Tran et al., 2015; Wei et al., 2017, Wang et al., 2011, Chen et al., 2012).

Similar to H3K9, H3K27me3 is a prominent repressive chromatin mark that is important during cell cycle, stem cell pluripotency and cancer (Hubaux et al., 2007; Shen et al., 2009; Bracken et al., 2003). It has been shown that a key feature that distinguishes fibroblast from iPSC epigenome is the abundance of H3K27me3 (Maherali et al., 2007). This shows that cells undergo an intensive epigenetic change in H3K27 methylation marks during the process of reprogramming.

In addition, it is possible that different chromatin changes occur at specific genomic loci that are important to unleash the cellular reprogramming potential. Yet, the overall levels of H3K4me3, which marks the active chromatin do not change. Furthermore, since these studies were carried out in *idha-1* depleted animals without the TF CHE-1 induction, it is also possible that while *idha-1* depletion leads to decrease in the repressive chromatin marks, binding of the TF CHE-1 triggers deposition of active marks on genomic sites. Together, the loss of repressive and attainment of active epigenetic marks may underlie the reprogramming process. Further experiments such as ChIP-seq for H3K4me3 and other histone modifications with and without IDHA-1 depletion are needed to address this possibility.

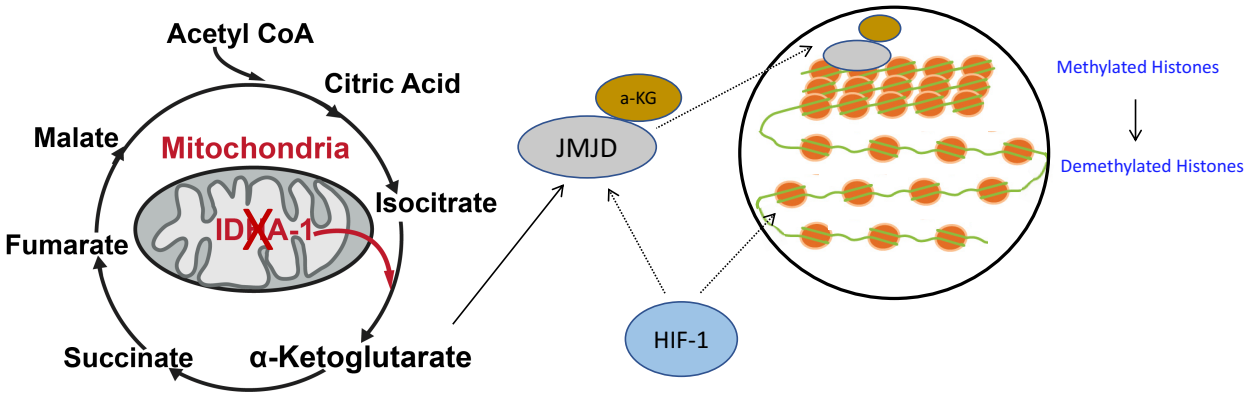

Figure 3.2 Increased chromatin accessibility upon IDH3 depletion. Jumonji proteins show increased activity upon IDH3 depletion possibly induced by HIF-1 activation. a-KG is utilized by the Jumonji proteins to mediate histone demethylation. The resulting changes in the chromatin accessibility prime the cells towards TF-mediated reprogramming.

3.7 IDH3 depletion does not result in drastic transcriptional changes

Our analysis of the transcriptome based on RNA sequencing did not reveal drastic differences in gene expression in IDH3 depleted animals (Figure 2.12.1). These results appear surprising, since a-KG dependent dioxygenases have been shown to affect cellular transcription

based on their demethylation function (Reviewed by Wu and Zhang, 2014). Furthermore, a recent study reported significant gene expression changes in IDH3a knocked down liver cancer cells including JMJD4 and HIF1a, which we also identified to be required for IDH3 depletion mediated reprogramming (Liu et al., 2020). However, it should be noted that there are two key differences in these cases: First, this study was carried out in a cancer cell line and therefore provides a different cellular context. Secondly, in mammalian systems, IDH3 mutations and the resulting a-KG changes have been shown to result in changes in DNA as well as histone demethylation and therefore gene expression. However, *C. elegans* lacks DNA methylation, and hence represents a model with a lesser degree of a-KG mediated transcriptional control (Soojin et al., 2012). In addition, the use of an *in vivo* model like *C. elegans* is intimately linked to cross tissue communication and compensatory mechanisms that possibly resulted in the observed lack of differences in a-KG levels upon IDH3 depletion. It is therefore comprehensible that such drastic gene expression changes do not occur as observed in cancer cells. It is also important to note that the RNA-seq was carried out on animals with partial *idha-1* depletion (RNAi based knock down), and the effects may therefore be different/severe upon the complete loss of the gene.

Furthermore, since IDH3 is an important metabolic enzyme, its depletion is expected to result in changes in the metabolic environment of the cell. This is also visible in our metabolite measurement experiments as well as metabolomic flux analysis (results section 2.7 & 2.9). However, increased/decreased activity of a metabolomic enzyme is not directly correlated to its rate of transcription. Many factors including the availability of substrates, co-factors, inhibitors as well as the stability of enzyme complexes themselves directly influence their activity (Nikinmaa et al., 2013). Seen in this perspective, the metabolic changes occurring upon depletion of IDH3 may be triggered by the metabolic requirements of the cells with IDH3 depletion, and can occur with limited changes in the transcriptional status of the cell.

Importantly, in order to understand the transcriptional changes that prime the cells towards reprogramming, the RNA-seq analysis was performed upon knockdown of *idha-1* only, without the induction of the fate inducing TF. The conversion of these *idha-1* depleted primed cells into neuronal fate is brought about by the induction of TF that initiates the expression of neuronal gene program distinct from the original fate. It can be thus speculated that while IDH3 depletion does not result in strong transcriptional changes, it modifies the

chromatin accessibility landscape that can then be utilized by the fate inducing TF to initiate the neuronal gene program.

Our analysis of differential transcript expression, however, revealed differential transcript expression for 25 genes. Furthermore, most of these genes showing differential transcript usage either code for proteins with enzymatic activities (such as *cka-1* coding for choline kinase) or transporter proteins. Interestingly, transporter T11G6.2 from the solute carrier family (SLC) 37 involved in transport of glucose 6 phosphate shows increased isoform expression; whereas transcript expression of an isoform of candidate C42C1.19 belonging to the same family of transporters was decreased (Table 2.2). While it remains to be determined, if and how this differential isoform transcription affects biological function of the proteins, these results nonetheless support our findings of metabolic rewiring and transport of metabolites (glucose) occurring in animals upon IDH3 depletion.

3.8 Glutamine anaplerosis as a mechanism to replenish a-KG levels upon IDH3 depletion

Based on an suppressor / enhancer RNAi screen and metabolomic studies, we identified that the cells utilize glutamine breakdown to replenish a-KG levels upon depletion of IDH3 (Results section 2.9). Such glutamine anaplerosis has been described as a hall mark for cancer with some cancer cells reported to generate up to 50% of ATP by oxidizing glutamine-derived a-KG (Reitzer et al., 1979). The activation of this glutamine breakdown pathway has been reported by multiple factors including mTOR signaling as well as proto-onco gene myc (Duvel et al., 2010; Yecies and Manning, 2011). Furthermore, in cancer, HIF-2 alpha (Homolog of HIF-1) has been shown to induce the cellular uptake of glutamine, as well as modulation of cellular metabolism towards glutamine breakdown (including activation of glutaminase GLS, homolog of GLNA-1 & GLNA-3) to generate a-KG for sustaining the TCA cycle (Li et al., 2017).

Furthermore, our results also indicate that not only is glutamine breakdown utilized to generate a-KG, but is also required for the IDH3 depletion-mediated germ cell reprogramming to occur. This raises the possibility that signaling mediated through the by-products of these glutaminolytic reactions, such as glutamate, ammonia or aspartate released during this process, may trigger changes required for this cellular conversion. Glutamine breakdown to a-KG has been shown to activate the autophagy pathway important for metabolic adaptations for cell

survival (Heiden et al., 2009). Additionally, glutaminolysis has also been reported to activate mammalian Target of Rapamycin Complex 1 (mTORC1) pathway involved in decision processes of cellular metabolism (Menon & Manning, 2008; Villar et al., 2015). Both of these pathways are shown to be upregulated in multiple cancers (Reviewed by Nguyen & Duran, 2018). Furthermore, it has been reported that epithelial cancer cells also employ such increased glutamine anaplerosis, and the additionally produced ammonia diffuses into the microenvironment and induces glutamine production in the cancer associated fibroblasts. This glutamine is then used by the cancer cells to fuel their growth (Ko et al., 2011). The effects of aspartate, which is generated during glutamine breakdown, involving citrate production and the resulting metabolic consequences are discussed in the next section. Altogether, these downstream signaling events resulting from glutamine to a-KG breakdown represent possible mechanisms that contribute to priming cells towards IDH3 depletion-mediated reprogramming, and remain to be explored for their involvement.

3.9 High intracellular citrate upon IDH3 depletion

The highest detected change upon depletion of IDH3 in our metabolomic analysis is for the TCA cycle intermediate citrate (Figure 2.7). These high citrate levels are indicative of the block in the cycle due to the depletion of its key enzyme IDH3. However, our additional results also reveal a TCA cycle that is partially active (at least in the latter half) (Results section 2.6). Together, these results suggest a model in which an ongoing TCA cycle produces citrate that cannot be utilized further due to the absence of IDH3. Under these conditions, glutamine metabolism generates a-KG to feed into the cycle and keeps it functional. This overall results in high citrate accumulation. Furthermore, aspartate produced during this glutamine anaplerosis reaction can also be converted to citrate. An alternative way of citrate production is the reductive TCA cycle which runs in the reverse direction, whereby a-KG is used to produce isocitrate by IDH2, which is then catalyzed by aconitase hydratase to form citrate and is extensively employed by cancer cells (Feng et al., 2020). However, cancer systems are associated with increased glycolysis and reduced flux through TCA cycle; the opposite of which is found true upon IDH3 depletion in our system. Therefore, since a-KG is required for the downstream TCA cycle reactions (which we found to be functional and required for reprogramming), it can be estimated that such reverse a-KG to citrate production is negligible, if occurring at all.

The highly increased citrate levels observed upon IDH3 depletion pose the question of their physiological effect and possible involvement in mediating cellular reprogramming. It has been reported that high citrate levels negatively regulate the process of glycolysis by inhibition of the enzyme phosphofructokinase 1 (PFK1); phosphofructokinase 2 (PFK2) and indirectly pyruvate kinase (PKM) (Reviewed by Lcard et al., 2012). Given that we observed decreased glycolysis flux upon depletion of IDH3, it can be assumed that these high intracellular citrate levels affect the cellular metabolism in this manner (Results section 2.9). Additionally, in the cell, citrate can be transported out of the mitochondria, converted to acetyl coenzyme A (Acetyl CoA) and utilized for protein modifications including acetylation of histones (Wellen et al., 2009). However, we did not observe any effects on reprogramming upon depletion of histone acetyltransferases (HATs) or histone deacetylases (HDACs) (Data not shown). While it cannot be excluded that aberrant histone acetylation may occur upon IDH3 depletion, these results suggest that it does not affect the reprogramming process. Furthermore, intracellular citrate levels also regulate the fatty acid synthesis by the activity of the enzyme Acetyl CoA Carboxylase which is activated by citrate binding (Berg, 2002) (Figure 3.4). Cancers including renal cell carcinoma are characterized by high intracellular fatty acid content produced due to increased citrate levels, interestingly in a HIF-1 dependent manner (Du et al., 2017). At present, it remains to be elucidated if this high citrate observed upon IDH3 depletion also results in such increased fatty acid synthesis; and if that plays a role in the reprogramming process.

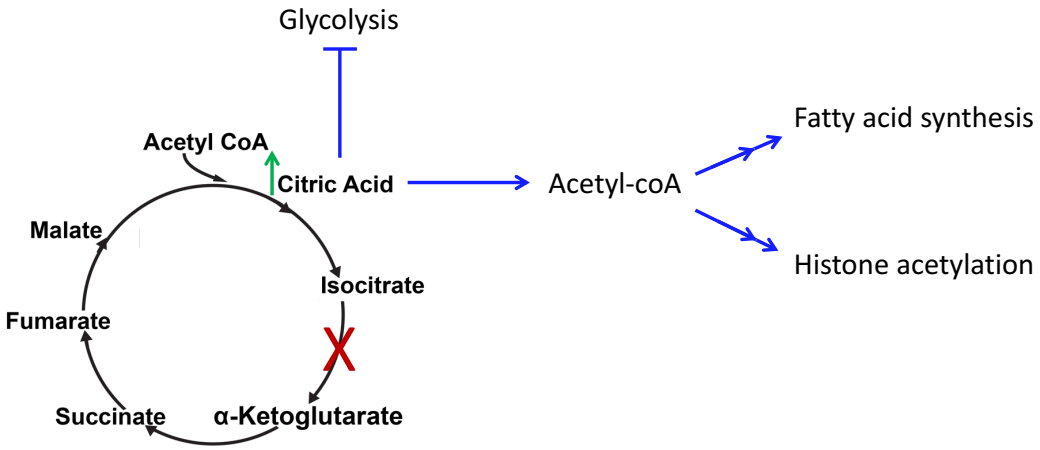

Figure 3.3 Possible high citrate induced changes upon IDHA-1 depletion. Schematic diagram showing the TCA cycle. Green arrow represents high citrate levels revealed by the GC-MS. Citrate can be exported out of the mitochondria to produce acetyl-CoA which is utilized for histone acetylation and to generate fatty acids. Furthermore, high citrate levels may also inhibit glycolysis PFK1 phosphofructokinase 1 (PFK1) and pyruvate kinase (PKM2).

3.10 IDH3 depletion results in metabolic flux changes

Our isotope labelling experiments revealed an overall decreased flux through glycolysis and slightly increased flux of the TCA cycle upon IDH3 depletion (Results section 2.9). Previous studies on isocitrate dehydrogenases in cancer systems have extensively described the correlation of IDH1/IDH2 mutations and glycolysis; and the underlying mechanism is a matter of continuous debate: one proposed mechanism is that gain-of-function mutation in IDH1 and IDH2 that results in production of 2-hydroxyglutarate underlie the metabolic reprogramming towards glycolysis. However, an alternative explanation is the loss of the isocitrate dehydrogenase activity that is responsible for this metabolic shift (Reviewed by Losman and Kaelin, 2013). Since the latter rationale relates to the enzyme activity itself, it can therefore be extended to IDH3 as well. Indeed, studies have reported the depletion of IDH3 and the resulting effect on cellular metabolism in context to cancer, but with conflicting outcomes. Depletion of IDH3 has been shown to induce a switch from oxidative phosphorylation towards glycolysis in glioma (May et al., 2019) as well as in fibroblasts where it promotes their transformation into cancer-associated fibroblasts (Zhang et al., 2015). Conversely, depletion of IDH3 in breast and lung cancer systems show significantly delayed tumor growth by suppressing the HIF-1-mediated induction towards glycolysis and angiogenesis (Zeng et al., 2014). While these studies report different outcomes on cancer progression, they highlight a direct link of IDH3 and cellular metabolism involving, but not limited to, HIF-1 activity.

We have previously identified HIF-1 to be required for IDH3 depletion mediated reprogramming. However, an established hallmark of HIF-1 is steering cellular metabolism towards glycolysis (Reviewed by Nagao et al., 2019). Keeping this in view, our results seem to be in contradiction to these established metabolic outcomes associated with HIF-1 activity. Interestingly, a recent study which describes activation of HIF-1 upon IDH2 depletion in prostate cancer shows that even upon activation of HIF-1, a number of its known targets are not increased; and includes glycolysis related enzymes (Wang et al., 2019). It is thus possible that such pseudo-hypoxic response (whereby selective activation of HIF-1 targets occurs) is activated upon depletion of IDH3 in our reprogramming system as well, and therefore no increase in glycolysis is observed.

Additionally, it cannot be ruled out that alternative mechanisms might operate upon IDH3 depletion that are responsible for the observed metabolic changes. Reflecting to the central role of IDH3 and its associated TCA cycle in cellular metabolism; and given that a

number of metabolic changes have been detected upon depletion of IDH3, it can be assumed that these changes in metabolism themself are responsible for the alterations in observed metabolic fluxes. This argument can be supported by results obtained from metabolomic analysis and RNA-seq: high intracellular citrate levels (as observed by our metabolomic analysis) have been shown to negatively regulate glycolytic enzymes (Reviewed by Lcard et al., 2012). Furthermore, our results of RNA-seq show no appreciable transcriptional changes upon depletion of *idha-1*. It can therefore be proposed that activity of metabolic enzymes (regulated by metabolite levels) rather than their expression levels results in changes of existing metabolic pathways.

Our identification of these flux changes places our reprogramming model in a distinct metabolic space than cancer systems; where increased glycolysis and decreased dependence on mitochondrial TCA cycle-based energy metabolism is considered to be a hallmark (reviewed by Derberardinis & Chandel, 2016). It is however important to note that these flux studies are preliminary, and currently ongoing. Furthermore, while we explored the roles of specific metabolites and their metabolism (for example citrate and a-KG explained in respective sections); it remains to be determined how the overall change in metabolic flux through glycolysis and TCA cycle affects the reprogramming potential of a cell. Further metabolomic and flux analysis studies, also focusing on other metabolic processes, will shed light on this question and possibly also in determination of the proposed mechanisms that underlie these changes.

3.11 Enhanced glucose transport upon IDH3 depletion

The suppressor / enhancer RNAi screen identified that putative glucose transporter F14E5.1 (GLUT1 in mammals) upon co-depletion with *idha-1* enhances the phenotype penetrance (Figure 2.9.4). This suggests that increased glucose transport exists upon IDH3 depletion and acts to stabilize cellular metabolism thereby counteracting the reprogramming process. Similar upregulation of transporters of glucose has been shown to occur in cancer systems, in order to increase glucose uptake to support cellular proliferation (Jones et al., 2009). Specifically, the expression of GLUT1 has been reported in multiple cancers including breast cancer, gastric adenocarcinoma, prostate cancer and others. Interestingly, such increase in GLUT1 expression has been suggested as a biomarker for cancer detection (Reviewed by Zambrano et al., 2019). In these systems GLUT1 expression is regulated by c-myc, the phosphatidylinositol 3-kinase/protein kinase B (PI3K/Akt) pathway as well as transcription

factors including HIF-1. (Reviewed by Zambrano et al., 2019; Semenza et al., 2012). Our results demonstrating HIF-1 activity upon IDH3 depletion suggest that HIF-1 may mediate F14E5.1 expression as a possible mechanism. However, further studies are needed to confirm this notion. Furthermore, since we did not observe activation of some known HIF-1 targets, it cannot be ruled out that a HIF-1-independent mechanism might be involved in this context.

Our work at present tested F14E5.1 as a representative glucose transporter for understanding effects on IDH3 depletion-mediated reprogramming. However, given that multiple families are involved in glucose transport, it will be interesting to study members of additional glucose transporters to test whether IDH3 depletion causes a general increase in glucose transporters, or if this effect is specific to F14E5.1. Furthermore, the mechanisms underlying the effect of this glucose transport, as well as its effect on reprogramming are needed to be studied in detail. Additionally, given that we identified cross-tissue signaling involving soma and germ line in the context of IDH3 mediating reprogramming, it is possible that this glucose transport might also occur between germ line and soma. Since our RNAi-based knock down was in whole worm, tissue-specific knock down experiments are needed to address this possibility. Results from our RNA-seq analysis also identified differential transcript expression of multiple transporter genes. While these results need to be validated, they hint towards altered transport of additional metabolites including glucose 6 phosphate, among others.

3.12 An interplay of tissues is involved in promoting IDH3 depletion-mediated germ cell conversion

Our results from RNAi mutants and tissue-specific protein degradation revealed that the germ cell to neuronal reprogramming phenotype is not tissue-autonomous (Results section 2.10). Furthermore, we identified that depletion of IDH3 in somatic gonad is required for the germ cell reprogramming to occur. Signaling between the germ line and somatic tissues has been identified in different processes in *C. elegans*. This includes germ line to intestinal signaling that affects lifespan as well as regulation of inflammatory pathways (Spanier et al., 2010; Lees et al., 2008) and neuron to germ line signaling that affects transgenerational gene silencing (Devanapally et al., 2015). Specifically, extensive signaling occurs between somatic gonad and germ line in worms. Examples of these include oocyte production in the germ line which requires $G\alpha_s$-adenylate cyclase signaling in the gonadal sheath cells as well as promotion of cell death in germ line through VAB-1/Eph receptor signaling (Govinden et al., 2009; Li et al., 2012).

Despite our attempt to identify the mechanism of cross tissue signaling between the somatic gonad and the germ line, we have not yet been able to identify the nature of this signaling event. Based on the known communication between the two tissues (mentioned above), it is possible that these known signaling pathways might also operate in the context of germ cell reprogramming. However, it is also possible that germ cell reprogramming occurs due to disruption of an existing signaling event between the germ line and soma. An interesting candidate can also be ammonia which is released during the process of glutamine metabolism (which is utilized upon IDH3 depletion), and has been shown to be transported between cells and trigger autophagy responses (Eng et al., 2010). In this context, increased glutamine transport between the two tissues to support the anaplerotic pathway for a-KG generation also serves as a possible signaling candidate. Furthermore, since we performed tissue-specific knock down studies in intestine and somatic gonad only, it cannot be ruled out that other tissues may also be involved in IDH3 depletion mediated germ line reprogramming.

Overall, the identification of cross tissue signaling highlights the importance of an *in vivo* model system such as *C. elegans* that represent complex interactions between tissues that affect processes including cell identity and reprogramming that are otherwise absent in cell culture systems.

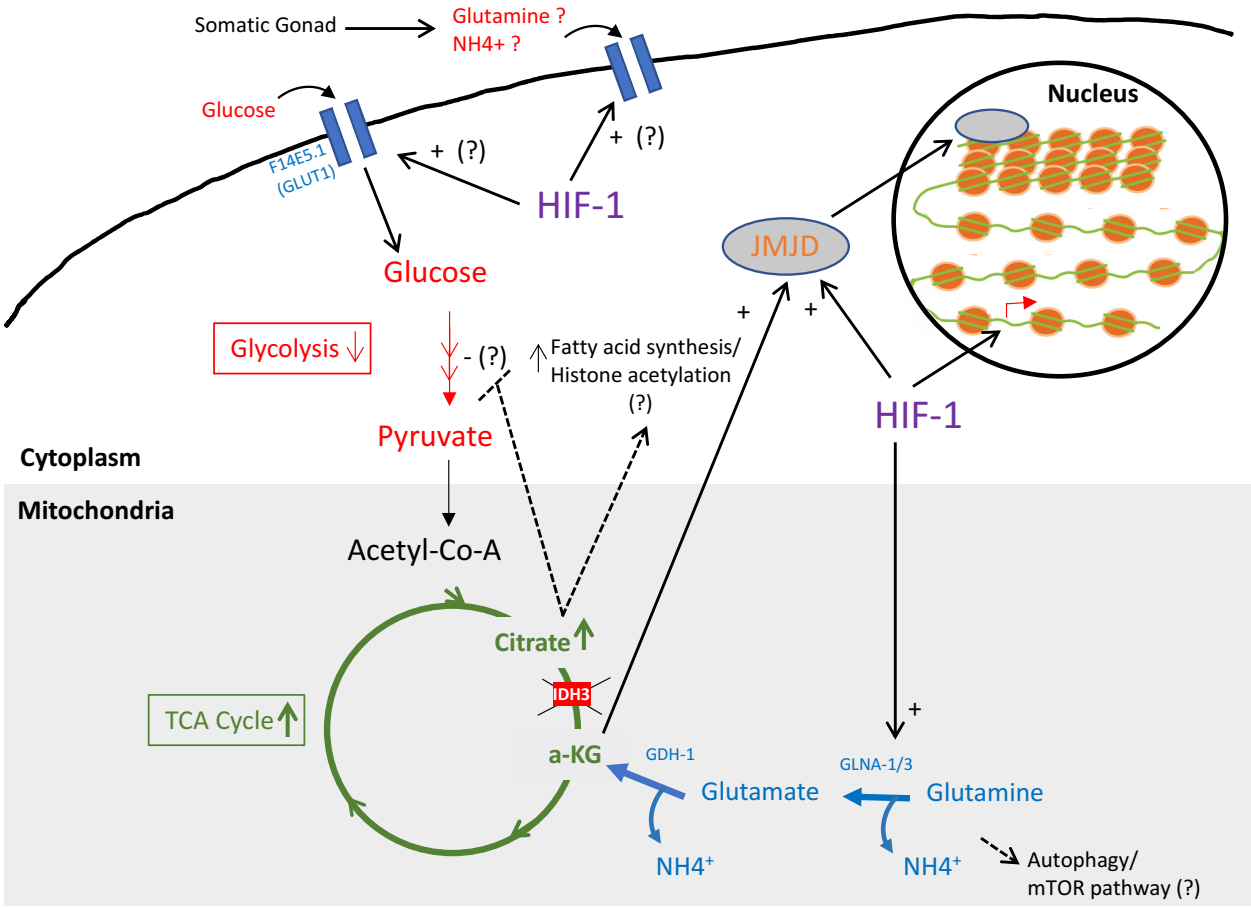

Figure 3.4. Putative cellular events upon IDH3 depletion in *C. elegans*. In *C. elegans*, depletion of mitochondrial IDH3 leads to activation of the TF HIF-1 that induces increased JMJD activity and histone demethylation. Glutamine anaplerosis (possibly induced by HIF-1) replenishes a-KG levels to keep the TCA cycle functional. Cells utilize increased glucose transport by GLUT1 homolog F14E5.1 (possibly induced by HIF-1) in order to sustain the metabolic processes, however overall glycolysis flux is reduced; in contrast to increased TCA cycle. Possible events such as increased ammonia induced autophagy and/or mTOR pathway in the cell, and increased citrate can lead to increased intracellular fatty acid production, histone acetylation and/or inhibition of glycolytic enzymes. Cross tissue communication from somatic gonad possibly involving glutamine and/or other signals also mediate cellular changes that eventually allow germ cell to neuron conversion upon ectopic CHE-1^{oe} in *C. elegans*.

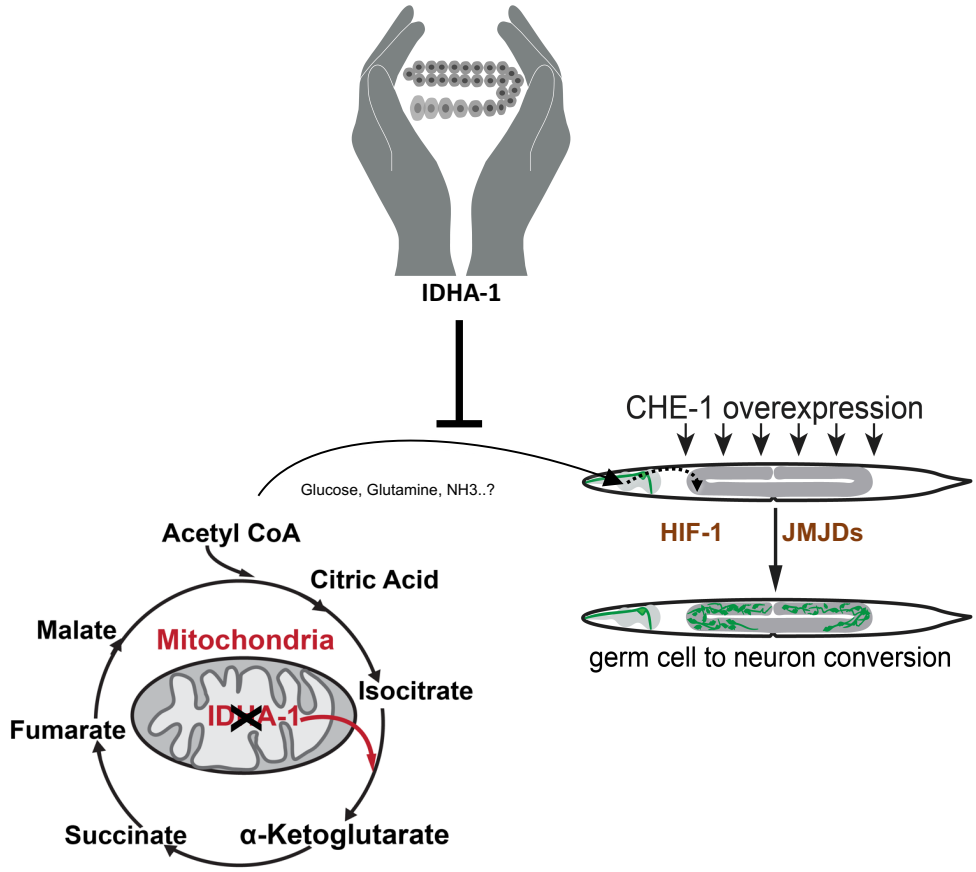

Figure 3.5. IDH3 safeguards germ cell identity in *C. elegans*. In *C. elegans*, depletion of mitochondrial IDH3 leads to cellular events involving TF HIF-1 and Jumonji proteins, as well as metabolic rewiring and transport involving glucose and possibly glutamine or ammonia. This eventually allows the TF CHE-1 mediated conversion of germ cells to neurons.

3.13 Conclusions and future directions

Mitochondrial isocitrate dehydrogenase is a key metabolic enzyme functional in the citric acid cycle. In addition to its known role in cellular metabolism, this study demonstrates that IDH3 also plays an important role in safeguarding cell fate in *C. elegans.* IDH3 is an unexpected barrier of reprogramming since it has been associated with metabolism and energy generation in the cell. Most of the recently identified reprogramming barriers are chromatin regulators, and thus directly influence the accessibility of genes, which is required for the transcription factors to achieve reprogramming (Tursun et al., 2011; Cheloufi et al., 2015; Kolundzic et al., 2018). In this context, identification of a specific mitochondrial enzyme that has important implications on the maintenance of cell fate broadens the scope of understanding how cell fate protection mechanisms work. Furthermore, understanding of cellular identity safeguarding mechanisms are also relevant in the context of cancer; since cancer development might also utilize the same pathways in order to erase the existing cellular identity.

Our identification of the TF HIF-1, Jumonji proteins, and changes in the histone methylation levels provide a possible mechanistic understanding of how IDH3 carries out its barrier function. Upon depletion of the enzyme, the overall levels of the repressive chromatin marks H3K9 and H3K27 tri-methylation are decreased, thus making the chromatin accessible for binding of the fate-inducing transcription factor. However, further characterization of the genomic loci that change in terms of their accessibility and binding of fate-inducing factors by ATAC-seq, ChIP-seq and RNA-seq will provide a deeper understanding of cell fate protection and reprogramming mechanisms. In addition, more studies are needed to understand the exact role of TF HIF-1 and its downstream gene transcription pool to decipher the mechanisms that prime the cells towards reprogramming.

Our analysis of the metabolome of worms with depleted IDHA-1 revealed a number of metabolic changes. Strikingly however, levels of most of the TCA cycle metabolites including IDH3 product a-KG were not altered. We identified that the cells use glutamine anaplerosis pathway in order to bypass the block in the TCA cycle caused by the depletion of IDH3, and thereby keep the cycle functional. However, the question of how this alternative use of energy affects the cell fate protection still remains. Glucose tracing studies identified that TCA cycle is the preferred pathway of cellular metabolism utilized upon IDH3 depletion, whereas glycolysis is reduced. Further metabolic flux studies will shed light on possible alternative

pathways that enable this rewiring of cellular metabolism; and to determine their effects in priming the cells for reprogramming in this context.

The IDH3 depletion mediated germ cell reprogramming is not cell-autonomous. We identified the somatic gonadal sheath cells as contributors to the phenotype. However, the exact nature of this communication between the two tissues remains to be explored. In addition, our identification of the glucose transporter in the reprogramming of the germ cells provides a possible candidate that could be responsible for additional signaling between tissues in order to compensate the effects of IDH3 depletion, but needs to be studied in further detail.

This identification of the non-cell autonomous nature of the IDH depletion-mediated germ cell reprogramming highlights the importance of using an *in vivo* system to study reprogramming barriers. It also serves to emphasize *C. elegans* as a powerful model organism to study biological questions and processes within the context of the dynamics displayed by multicellular organisms including complex inter-tissue communications and compensatory mechanisms.

In a broader context, the identification of a mitochondrial enzyme as a cell fate safeguarding factor provides insight into the relatively lesser-known role of mitochondria and metabolism in the fate maintenance. As shown previously for programmed cell death and RNA interference, this knowledge of mechanisms that act as roadblocks for cell identity changes studied in *C.elegans* could be translatable to human cells; and can have important implications on the perspective use of reprogramming systems for the treatment of diseases.

4. MATERIALS

The details of the chemicals, regents and kits used are given in the relevant section.

The equipment used was purchased from Bio-Rad Laboratories, Thermo Fisher Scientific and Eppendorf, unless stated otherwise.

Ultra pure water was produced using Millipore Super-Q System.

Sanger sequencing and oligonucleotide synthesis was performed by Eurofins Genomics, Ebersberg.

Repair templates for CRISPR were synthesized from Integrated DNA Technologies (IDT).

Genome-wide *C. elegans* RNAi collection (Ahringer) was purchased from Source BioScience.

4.1 *C. elegans* strains used in the study

Table 4.1 Worm strains generated by crossing

Name	Genotype
N2	*C. elegans* wildtype variant Bristol
BAT028	*otIs305 (hsp::che-1::3xHA) V; ntIs1 (gcy-5::GFP) V*
BAT326	*otIs263 [ceh-36p::tagRFP]; otIs305 [hsp::che-1::3xHA]; ntIs1 [gcy-5::GFP] V*
BAT527	*otIs355 [rab-3::NLS::TagRFP]; otIs305 [hsp-16.2p::che-1::3xHA, rol-6(su1006)] ntIs1 [gcy-5p::GFP, lin-15(+)] V.*
BAT522	*otIs305 [hsp::che-1::3xHA] ntIs1 [gcy-5::GFP] V.; otis393 [ift-20::NLS::tagRFP]*
BAT684	*juIs8 [unc-25::GFP]; barEx147 [hsp-16.2/4::unc-30]*
BAT068	*otEX4945 [hs:hlh-1, rol-6]; mgIs25 [unc-97::gfp]*
BAT770	*otIs305[hsp16-2p::che-1::3xHA::BLRP + rol-6(su1006)] ntIs1[gcy-5p::GFP + lin-15(+)] hif-1(ia4) V*
BAT1897	*jmjd-3.3(tm3104; otIs305 (hsp::che-1::3xHA) V; ntIs1 (gcy-5::GFP) V*
BAT1898	*jmjd-4(tm965); otIs305 (hsp::che-1::3xHA) V; ntIs1 (gcy-5::GFP) V*
BAT1987	*jmjd-3.3 mutant (CRISPR KO) X; otIs305 (hsp::che-1::3xHA) V; ntIs1 (gcy-5::GFP) V*
BAT1992	*jmjd-4 mutant (CRISPR KO) X; otIs305 (hsp::che-1::3xHA) V; ntIs1 (gcy-5::GFP) V*
BAT1812	*glp-4(bn4); otIs305 [hsp-16.2p::che-1::3xHA::BLRP + rol-6(su1006)]*
BAT058	*otIs305 ntIs1; rrf-1*
BAT2052	*ppw-1(pk1425) I; otIs305 (hsp::che-1::3xHA) V; ntIs1 (gcy-5::GFP) V*
BAT1994	*ieSi57 [eft-3p::TIR1::mRuby::unc-54 3'UTR + Cbr-unc-119(+)] II; otIs305 (hsp::che-1::3xHA) V; ntIs1 (gcy-5::GFP) V; barSi30 (idha-1::AID degron::3xHA I)*
BAT1995	*ieSi38 [sun-1p::TIR1::mRuby::sun-1 3'UTR + Cbr-unc-119(+)] IV. otIs305 (hsp::che-1::3xHA) V; ntIs1 (gcy-5::GFP) V; barSi30 (idha-1::AID degron::3xHA I)*

BAT1997	*ieSi61 [ges-1p::TIR1::mRuby::unc-54 3'UTR + Cbr-unc-119(+)] II; otIs305 (hsp::che-1::3xHA) V; ntIs1 (gcy-5::GFP) V; barSi30 (idha-1::AID degron::3xHA I)*
BAT2122	*barSi41[lim-7 prom::TIR-1:mRuby:unc-54 3'UTR, unc-18(+)] II rol-6, otIs305(hsp-prom-che-1::FLAG); ntIS1 (gcy-5prom::gfp), barSi30 (idha-1::AID degron::3xHA I)*
BAT483	*ogt-1(ok430) III; ntIs1 [gcy-5p::GFP, lin-15(+)] otIs305 [hsp-16.2p::che-1::3xHA, rol-6(su1006)] V.*

Table 4.2 Worm strains generated by CRISPR

Strain name	Genotype	Purpose
BAT1971	*idha-1(barSi25[idha-1::3xHA]) I*	Tagged IDHA-1
BAT1984	*barSi28 (jmjd-3.3)*	JMJD-3.3 mutant
BAT1985	*barSi29*	JMJD-4 mutant
BAT1986	*barSi30 (idha-1::AID degron::3xHA I)*	IDHA-1 tagged with Degron
BAT1944	*idhg-1(barSi24[idhg-1::3xFLAG]) III*	Tagged IDHG-1
BAT2149	*F14E5.1.1::aptamer*	Aptazyme tagged *F14E5.1.1*

4.2 Bacterial Strains used in the study

Table 4.3 Bacterial strains

Strain	Genotype	Purpose
Escherichia coli: OP50	uracil auxotroph E. coli bacteria	Food source for *C.elegans*
Escherichia coli: MACH1	F– Φ80lacZΔM15 ΔlacX74 hsdR(rK–, mK+) ΔrecA1398 endA1 tonA	Transformation
Escherichia coli: HT115(DE3)	F-, mcrA, mcrB, IN(rrnD-rrnE)1, rnc14::Tn10(DE3 lysogen: lavUV5 promoter -T7 polymerase	Transformation into RNAi bacteria (express dsRNA)
Escherichia coli: HB101	F- mcrB mrr hsdS20(rB- mB-) recA13 leuB6 ara-14 proA2 lacY1 galK2 xyl-5 mtl-1 rpsL20(SmR) glnV44 λ-	Food source for *C.elegans* (MosSCI)

4.3 Oligonucleotides

Table 4.4 List of oligos used for genotyping

Name	Sequence	Application
hif-1_F	TCGCTCTTTTTAGACACAACTC	To genotype *hif-1(ia4)* mutation
hif-1M__R	TGTCACTTACCATTACCGGC	To genotype *hif-1(ia4)* mutation

hif-1_R	TGCAAACGGAGCAGCAATAC	To genotype *hif-1(ia4)* mutation
ppw-1_M_F	CCGGTGTTTGCGTACTTTTT	To genotype *ppw-1(pk1425)* mutation
ppw-1_M_R	AAAAACCGACACCCTTGAGA	To genotype *ppw-1(pk1425)* mutation
TIR1_F	GTCTCCATGGGATGCCCAAA	To genotype TIR1
TIR1_R	CTTACGGAGGGAGTCGCATC	To genotype TIR1
jmjd-2_F	CCTCGCAGAATCCACCAACT	To genotype *jmjd-2(tm2967)* mutation
jmjd-2_R	TCGGTGCTCTCAGAGATTCAA	To genotype *jmjd-2(tm2967)* mutation
jmjd-2_M_R	ACGGAGAACCGATCTACGGA	To genotype *jmjd-2(tm2967)* mutation
jmjd-3.3_M_F	ACGTAACGTGCATCTTATTTTGC	To genotype *jmjd-3.3(tm3104)* mutation
jmjd-3.3_M_R	TGTCCAAGCCCGCGAATAAT	To genotype *jmjd-3.3(tm3104)* mutation
jmjd-4_M_F	GTCATCCACAAACCCCGACT	To genotype *jmjd-4(tm965)* mutation
jmjd-4 _R	CCGTTTCGCTCCAGGAGATT	To genotype *jmjd-4(tm965)* mutation
jmjd-4_M_R	AGAGATGCGTCAGCAAACGA	To genotype *jmjd-4(tm965)* mutation
idha-1_CRISPRMut_F	CACTTATTCGTTGGCCGGTG	To genotype *idha-1* CRISPR deletion
idha-1_CRISPRMut_R	TCTGGCTAGCTGTTTCCACG	To genotype *idha-1* CRISPR deletion
idha1_CRISPRMut_F2	TTCAAACTAACCGCGTGCAT	To genotype *idha-1* CRISPR deletion
idha-1_KI_F	AACACGCTGCTCGTATCGAA	To genotype *idha-1* CRISPR insertion
idha-1_KI_R	CAAAGTGTTTTAGTGTCTAACAGCC	To genotype *idha-1* CRISPR insertion
idhg-1_KI_F	ATCGGAACTCGTTCAATCAGTA	To genotype *idha-1* CRISPR insertion
idhg-1_KI_R	TCAGTCAACGGGGTCAAACA	To genotype *idha-1* CRISPR insertion
jmjd-3.3_CRISPRMut_F	TTGCTATGGCTGCTCTGGTC	To genotype *jmjd-3.3* CRISPR deletion
jmjd-3.3_CRISPRMut_R	GAGAGTCGAGGTGAGGGGTA	To genotype *jmjd-3.3* CRISPR deletion
jmjd-3.3_CRISPRMut_F2	CTGCTGGCGGCAAATCTTTT	To genotype *jmjd-3.3* CRISPR deletion
jmjd-4_CRISPRMut_F	GTCTTTGCCTCGGACTGTGA	To genotype *jmjd-4* CRISPR deletion
jmjd-4_CRISPRMut_F2	CCCCCAGGCAGTGAAAATCT	To genotype *jmjd-4* CRISPR deletion

jmjd-4_CRISPRMut_R	GGAAGTCGTGTGGAAGTCGT	To genotype *jmjd-4* CRISPR deletion
rde-1_CRISPRMut_F	AGTATTGCGGAGGAAACAGC	To genotype *rde-1* CRISPR deletion
rde-1_CRISPRMut_F2	GGAATGAGCCAAGATGAAGTC	To genotype *rde-1* CRISPR deletion
rde-1_CRISPRMut_R	CGAACGACATTCCAGGGTAC	To genotype *rde-1* CRISPR deletion
hif-1_KI_F	GGGGTTACCACCAGAGCTTC	To genotype *hif-1* CRISPR insertion
hif-1_KI_R	AACGGACAAACGGACACACA	To genotype *hif-1* CRISPR insertion

Table 4.5 List of oligos used for cloning

Name	Sequence	Application
Plim-7_TIR1_primer1	tgcacttataatacgactcactagtACTTGTGCCTTGATTCTC	Gibson cloning
Plim-7_TIR1_primer2	tcttttgcatTTTTTCTACCGGTACCCTC	Gibson cloning
Plim-7_TIR1_primer3	ggtagaaaaaATGCAAAAGAGAATCGCC	Gibson cloning
Plim-7_TIR1_primer4	agatatcctgcaggaattcctcgagTAAACAGTTATGTTTGGTATATTG	Gibson cloning
colony_lim-7prom_TIR1_F	AGTAGTTATTTGCCGCCGCT	Gibson cloning
colony_lim-7prom_TIR1_R	CACCAACGCTCGATCTCGTA	Gibson cloning

4.4 sgRNAs

Table 4.6 List of sgRNAs and their sequences

Targeted Gene	sgRNA name	Sequence
idha-1	gBT19	gagcattgagcatttattcg
idha-1	gBT20	gtattcgaggtctttaacac
idhg-1	gBT7	gaaattagacacggtagttg
jmjd-3.3	gBT22	gaacagtaactgaaagatta
jmjd-3.3	gBT23	gagacacacgattaacgaat
jmjd-4	gBT28	gtcgatggatcagaaattcg
jmjd-4	gBT29	gaaaattcctgggaaaaaat

4.5 Antibodies

Table 4.7 Primary antibodies used in the study

Name	Target/Type	Species	Company
PA2	Anti-FLAG	mono; mouse	Sigma – Aldrich
PA8	Anti-trimethyl-Histone H3K27	poly; rabbit	Millipore

PA9	Anti H3K27me3	mono; mouse	Dr. Hiroshi Kimura; Graduate School of Frontier Biosciences Osaka University
PA20	anti-alpha-Tubulin	mouse; mono	Sigma
PA23	anti-HA-HRP	Rat	Roche
PA24	anti-H3K9me3	poly; rabbit	Abcam
PA45	Anti-Histone H3 ab1791	poly; rabbit	Abcam
PA47	Anti-Histone H3K4me3 ab8580	poly; rabbit	Abcam
PA48	Anti-Histone H3 (acetyl K9)	poly; rabbit	Abcam
PA49	Anti-Histone H3 (acetyl K14) ab52946	mono; rabbit	Abcam
PA54	Anti-lin-53 C-term Tier 1	mono; giunea pig	Pineda
PA82	RIM-s	mono; mouse	Hybridoma Bank
PA165	anti-14-3-3 (H-8) sc-1657	mono;mouse	
PA117	α-H2A.Z #8 (HTZ-1)	poly; mouse	Bill Kelly lab
PA132	GFP antibody-NB600-308	poly; rabbit	Novus bio
PA179	Anti-HA High Affinity	rat/mono	Roche

Table 4.8 Secondary antibodies used in the study

Name	Target/Type	Species	Company
SA2	IgG-HRP	anti-mouse	Santa Cruz
SA4	IgG-HRP	anti-rabbit	Santa Cruz
SA7	AlexaFluor488	anti-mouse	Mol. Probes
SA8	AlexaFluor488	anti-rabbit	Mol. Probes
SA9	AlexaFluor568	anti-rabbit	Mol. Probes
SA10	AlexaFluor568	anti-mouse	Mol. Probes
SA11	AlexaFluor488	Anti-Guinea pig	Mol. Probes
SA12	AlexaFluor568	Anti-Guinea pig	Mol. Probes

4.6 smFISH probes

Table 4.9 smFISH probes used in the study

Probe set	Sequences	Florophore
idha-1	acttgccaagcattctgaac gtagacgacgccttttgat gctgtatctgatggattgtc ttccgtctcctggaattaaa cagaagctgaaatttccggc gcggcctcaaaaatcttctg actggagtcacatcaactgg aatacggaagactccatcgc	

	gtgcataagctcgatgcaac tcctttaagtccaactttgt aaagatctgtgtccttttcc ctcttttctcacagccaaat atggacgaacgttggcgtaa ttgtgtccttcaagggaacg gacaacatcgacattgtcgt cctctgtgttctcacgaatt tgctcaattccagagtactc tagattgaacaactcccggg tgcgagaagcagtttcagta catactcgaaggcgaagctg ggacagcagtcacaactttg aaaccgtcggattgtctcat ctcgcggcagatggacaaaa cttgatatctgggtagaggg caagcaaactgtgtcgaggt atcgtattgtgatggatcct ctccatacaagtttggcatg accagcgcacaaatcggaaa tcctttccaatatttccag gttccgtgaacggattcaaa gtcttgtccagcaatatctg agaagagcagttgggtttgc gagcatcatgacggcagata cgtgttgtggaaggttcatg tacagccttttcgatacgag acgtccatcagcaattgcat ctccgagatctccagttttg	

	tcagcggtgaatgaagagca ttcgaggtctttaacacggg gggaagtagcattgagcatt tgtctaacagcctgtttaca ggactggtgggtaatctata aaagcgattaaggacgcggg ttttgtggttcatgccaatg gttatgcgagtgaatcagag aacaaaagtctcggggtgct tgggaatcgaaagatggtgt gacgctgtaacttattgtga	
idhg-1	agaaaacgtcttggtccgtt ccagttagaggactttcaga aaagtcgccgaatatgaggc tcatctcctggagatattct gaagtgtatgaccgaggacg cttttgcacgacattcttcg tatcggagttcggtgaagtc ataacgagccagcttagttg gcaagactgtgacgttgtga ggattctctcgacatgatgg tactggagcttgaactgctg ttcagatgcatcttcctttg acaccatttctcttgatagc gtttcaatgtttcccttcaa ttcgggaaacgaagcttggg tgagttgacgacgaagttcc aaccatatcgattccagtgt aacacgaggatgtggagcat	

	tccgatttttcgcgagtaac	
	tcttccatatttctttgcga	
	cttgtgaacagcagtaacct	
	cgtctcccaacttttgaatg	
	ccaactgcatggaagcatta	
	gtttccatagagatttggca	
	cgagtccacaagcaatgttt	
	tccagaaacaagtcctggac	
	gcgtaatcttctccaatgtt	
	ttacgggttcctgtttcaaa	
	gatcttttccagcaagagtg	
	cggatgaacgcagttggatt	
	agtccgaggaaacgaagcat	
	agatcatatcggcgtgtgat	
	gcggtgtgaattctcttatc	
	gatgacttagaagttcctcc	
	tccttctcgatgaagtcgag	
	attagacacggtagttgcgg	
	aagggtaaagctagccacta	
	gtcaacggggtcaaacagag	
	agacatcaggcggaaacgtt	
	tgtgggtacagagatgagga	
	gggggagtacttaactttgt	
	agcagctctcaagtattgac	
	tagtaaactccgccttttt	
	aagtgagctagggagcattc	
	tttcctagatagtctggtga	
	accatccggtatattgaact	
	acaacgcatgttgctttcac	

	gtacaatttttctgacccga	
unc-119	ttgtagagtcttgtgctcca ttgctctgccttcatatatg cgggtgcgatcgattgttgt catctgagacgggaaggttg gttatagcctgttcggttac tgatttttcgcgagaagctc agagctagcacatcatttgg gcataggaatccttgagtga ttatagacgtttgccgatgg cgaggtcacggatttggaat gcaatttcgaagagcacgtg attctcttccgtctcatttt gatatcggacatatcttgcc aatgtgtgatcggcacatcg aagtgccgttcaatcattcg gcatttcaataaacgatcct ggcatacagaatccaaattc tgttcacagttgtttctcga gttgttgtgaaagttgtgga attattgatcatgtcgtcca aatagaagctatcggagcgg gtgcattacgagcttattct tgcatcatacgagtagtcgg ttagttttattccatcggcg gcggtaggaaaatcacatga gttttcggaatgcattttgt	
unc-10	taaatccggcatcatcgacg ttcacgttcttctgcagata ccgtgatctgtttgtctaac agatttgacagatcgcgtca caattccgtccgcaaatttg cagattgccttatttttgct gattttgactcattggctgt	

	tttgtcctttgttggttttg	
	aggcgtttgtttcatagttc	
	attctctctcattctgttgt	
	tctcggaatttccagtgtag	
	ggttgttttggttctgattc	
	ggttcaaatggtcgtcagta	
	tcgaagttgcctatgcaatc	
	cgagtttttatgatcgccat	
	atggtgacaaggacagcgat	
	ccctgttccaaaatgatcat	
	tggctgcagaattttcagtt	
	gtaatgaatgcaccgagctt	
	atgtggcattttgcagagac	
	ttgcagcgatgctatcatat	
	gaatacgccgaggatgacat	
	gatggatatgcagatggcac	
	tcagggttgggtaattgacg	
	ggctgattgtgaatgtggta	
	gatgtcgaacgattgcgtga	
	gagcaactgagagttgtcga	
	aaactggcatgagtgtctct	
	ggttcagtaaggccattata	
	tcgtaatcccagacagttag	
	gtcatttggggcaagatgat	
	tcgtcgtcgtcaatgtattc	
	atgatcagatgtgtagcctg	
	tgttggatcgtacatatcct	
	tccatcactataatatccct	
	cattgtagttggcatgctat	
	aaacttttctttcgctcctt	
	cctcagatctagcaaaaccg	
	gtgagccgatctgaagacaa	
	cttgcttcagaaagggagga	
	gcaaacttgtctgagtgagc	

	aagcacttgacgaccgacaa cttttacatagggagctgga tttggcaatgcattgtttgc ttccatacgaccgtaatcac tttgcgaaatccccatgaat cagtttataccaccctatta tttgttgccaatgctcaaga	
gcy-5	cattcggatgctccaagaac caattccaactcgaagcgtc caattggaagagttccacca tatcgcattcggtatattcc tcccactacaacatctacat tattggtatcagccaactgg tgccactcgatcaaattgga tttacagtagtcttggtcgt cttaaggttgcctcaacatc atccgcactggatatagatc cgatcttgttaatgcctcat tacgagctcgactctttaca ggaccactaattgcgcataa ccaatactcctcattgtcaa tctttcccaaacttgtttgt tggagttagtccatttgcaa ctactgtgaatgactcccaa atttctaacagcatccgcaa tgccatcccgtataagtaaa tagtaaccatttgcggcata gcggtagagattttgaccaa tcatgttaactagtgccact ccgtgacaattgcgaagacg cgtttttctttttgtggcat gtgatcttcgactatttggc actttctccggttatagttg gctatgatgtttggtggtta	

	atttctccttctcttctta ggtccatcgatagataatcc gatatcctgaagtgatcctc aaagttcataccctctgcaa ggcaagtagctgaacgtaga ctcccaatccaaaatctgtt tacgatttcctccttttttc aagtattaactccggtcgga acttgcaaatttgctcagct gttctgcaacttgttttgga tctccaattgattccacttt tgtcggtaacccagaaacac ggaaccttgaagctcttaca gcccactattaattccaatt atggatagaccaacgacacc gtatccccaaataggcaata tttccattactttccattct tgtgcagcttctgacatatg tctcctcttgaacttgtttc tgtttccattacacctttttc gattttgtgtcactgtcagt	
rab-3	caaagttctgatcgggttgt atcaggagcttgaacatgta tccaactgatgaatttccga catcacagtaacggaagagg gtagagacgaaggcagaagt cactttgaaatcgattccga tttgtctccacggaacacag ggtatcccagatttgaagtt gatagtaggcggtggtgatg cagaatgaatcccattgctc actcttcattagtgatgtca gcaccaatcctgaacactat tttcccatgagtatgtcttg	

	ccaaccaaaacaacttgagc ttcagagtccatatcacatt ccctatccatagatacaact aagttgatcagcaagttggc ggctgatgtttcgaagaatt cctttacattaatgttctcc tctccaccaacttctcaaaa tctgccatcttatcacaaat ctgtgggtccttatccaaac ttcgagcttctgtccttttg aattgcattgctgttgagca attgcgtttggaatttggga agagctacgcgcttttagaa cctagatgttgagagaggga tttacgatccatatatctgg taattaaaccaactacgccc ggggaatatgattgaacgtt gctctgggaattgtttggaa ggcgactatgattagttaga tgggaactgggaagtcacta aatcaatctttcagcgggtg cctcgaaaataatttcctcc	

4.7 Kits

Table 4.10 Kits used in the study

Name	Company
Expand Long Template PCR System	Roche
GeneJET PCR Purification Kit	GeneJET PCR Purification Kit
MinElute Gel Extraction Kit (50)	Qiagen
Zymo DNA Clean & ConcentratorTM-5	Zymo
Nextera DNA Library Preparation Kit (24 reactions)	Illumina
GeneJET RNA Cleanup and concentration MicroKit	Thermo Scientific
TruSeq RNA Sample Preparation Kit v2 Set A	Illumina
HiPure Plasmid Midiprep Kit	Invitrogen
Invisorb Spin Plasmid Mini Two	Stratec molecular
NucleoBond Xtra Midi	Macherey-Nagel
Qubit dsDNA BR Assay Kit	Life Technologies

4.8 Plasmids

Table 4.11 Plasmids used in the study

Plasmid name	Genotype
pLZ31	*pCFJ151_Peft-3^{prom}::TIR1::linker::mRuby::unc-54 3'UTR*
pGC361	*lim-7^{prom}::mCherry*
dBT825	L4440 with *idha-1* & *jmjd-3.3* target sequence
dBT827	L4440 with i*dha-1* & *jmjd-4* target sequence
dBT829	L4440 with *idha-1* & *Rluc* target sequence
dBT865	*lim-7^{prom}::TIR-1:mRuby:unc-54 3'UTR* in dBT384
pCFJ151	ttTi5605 targeting region

4.9 Repair templates for CRISPR

Table 4.12 Repair templates used in the study

Name	Sequence
IDHA-1_3xHA	actggaacttgctcttcattcaccgctgatgtttgtgcccgtgttaaagatctcgaatacccatacgacgtt ccagactatgccggctacccctatgatgtcccggactatgcaggatcttatccatatgacgtcccagatt acgcttaaatgctcaatgctacttccccttctattttcttttttcttattgtaaacagg
IDHG-1_3xFLAG	tcggaactcgttcaatcagtactcgacttcatcgagaaggagctcgaggatcgcaactaccgtgtcga ctacaaggaccacgacggagactacaaggaccacgacatcgactacaaggacgacgacgacaagt aatttctacctgataatcgaaagtttgaaacatcccacatagtggctagctt
IDHA-1_Aptazyme (k4)	tcattttcagaaccttccacaacacgctgctcgtatcgaaaaggctgtatttgatgcaattgctgatggac gtgccaaaactggagatctcggaggtactggaacttgctcttcattcacagctgatgtttgtgcccgtgtt aaagatctcgaataaatgctcaatgctacttcaaacaaacaaaggcgcgtcctggattcgtacaaaaca taccagatttcgatctggagaggtgaagaatacgaccacctgtacatccagctgatgagtcccaaata ggacgaaacgcgctcaaacaaacaaacccccttctattttcttttttcttattgtaaacaggctgttagacact aaaacactttgatgattagtaatgatttaatgacacctttttttcggttttcaattttgtatagattacccacca
IDHA-1_AID_3xHA	actggaacttgctcttcattcaccgctgatgtttgtgcccgtgttaaagatctcgaaggatccggaggtg gcgggcctaaagatccagccaaacctccggccaaggcacaagttgtgggatggccaccggtgagat cataccggaagaacgtgatggtttcctgccaaaaatcaagcggtggcccggaggcggcggcgttcg tgaagggaaagtacccatacgacgttccagactatgccggctacccctatgatgtcccggactatgca ggatcttatccatatgacgtcccagattacgcttaaatgctcaatgctacttccccttctattttcttttttcttat tgtaaacagg
HIF-1-3xHA-2xAvi	ggtccctcagatttagattttatgtacactcaacattatcaaccattccaacaagacgagacatattggca aggacagcaacagcaaaatgaacaacagcctagttcttattccccatttccaatgctctcttctggagga ggtggatcttcgggaggaggaggatcgtacccatacgacgttccagactatgccggctacccctatg atgtcccggactatgcaggatcttatccatatgacgtcccagattacgcttctggaggaggaggatccg gactcaacgacatcttcgaggcccagaagatcgagtggcacgagggtcttaatgatattttcgaagcg cagaagattgaatggcatgagtgattattttctagcccctctcaaactgttcattgttttgttttcaaaaatat actcttcattcattcaagtcacacttcttattacttaattctattgctctttttaagaataatgagtttcaagaat cctccccg

F14E5.1 _Aptazyme (k4)	attcaattccttcatttataagtatgcttatattatttcgctacttaccggaaaccaaaggacgagagattca tgatattgtgaatgaacttaaaaaaaaatgaaaacctttgaaaacgtcaaacaaacaaaggcgcgtcct ggattcgtacaaaacataccagatttcgatctggagaggtgaagaatacgaccacctgtacatccagct gatgagtcccaaataggacgaaacgcgctcaaacaaacaaatcatacggctgaaatttttacttgatcg agccaattgaacttttgttaagacttacagaaaagtgagagattttgttacaaaaaagtgagaaaaaagc gaaaatgaacaggaaaaagaagaaaaatacacc
JMJD-3.3_3xHA_2xAVI	gtgaacctaagtaatacatatgttttaaaggaaaggaagcacggtgatcatgagacacacgattaacg aattagtgacgatttacaatgagtattacccatacgacgttccagactatgccggctacccctatgatgtc ccggactatgcaggatcttatccatatgacgtcccagattacgcttctggaggaggaggatccggact caacgacatcttcgaggcccagaagatcgagtggcacgagggtcttaatgatattttcgaagcgcaga agattgaatggcatgagtaatcatttattgtttaattttgaaatttttttagattcagtgatttttaataatttattt ctgttaatctatttttttaaag
JMJD-4_3xFLAG_2xAVI	gctccacaacttttgctccaaatgctctgccttcattgagcagctcgaattttctgtcgcttctcgttttttag actacaaggaccacgacggagactacaaggaccacgacatcgactacaaggacgacgacgacaa gtctggaggaggaggatccggactcaacgacatcttcgaggcccagaagatcgagtggcacgagg gtcttaatgatattttcgaagcgcagaagattgaatggcatgagtaagtttctgctatttttttcccaggaatt ttctaatttcccgctttccagatgctctcggaggaacaattggcgactttatatg
IDHG-1_Aptazyme (k4)	tcgagaaggagctcgaggatcgcaactaccgtgtcgactacaaggaccacgacggagactacaag gaccacgacatcgactacaaggacgacgacgacaagtaatttctacctgataatccaaacaaacaaa ggcgcgtcctggattcgtacaaaacataccagatttcgatctggagaggtgaagaatacgaccacctg tacatccagctgatgagtcccaaataggacgaaacgcgctcaaacaaacaaagaaagtttgaaacat cacacatagtggctagctttacccttacgttcttttcctctgttttttttttcgattaatccatgattcgtagcata atgcgttactcattgtgctctttctctgtttgaccccgttgactga
IDHG-1_AID_3xHA	taagtacttttttaaaaatgcactacaaaactttaatttaataaattttcagtcatcggaactcgttcaatcagt actcgacttcatcgagaaggagctcgaggaccgcaactaccgtgtcggatccggaggtggcgggcc taaagatccagccaaacctccggccaaggcacaagttgtgggatggccaccggtgagatcataccg gaagaacgtgatggtttcctgccaaaaatcaagcggtggcccggaggcggcggcgttcgtgaaggg aaagtacccatacgacgttccagactatgccggctacccctatgatgtcccggactatgcaggatctta tccatatgacgtcccagattacgcttaatttctacgtgataatcgaaagtttgaaacatcccacatagtgg ctagctttacccttacgttcttttcctctgttttttttttcgattaatccatgattcgtagcataatgcgttactcatt gtgctctt

4.10 Chemicals and reagents

Table 4.13 Chemicals and reagents used in the study

Name of chemical	Company
2-Mercaptoethanol	Carl Roth GmbH + Co. KG
2-Propanol	Sigma Aldrich
Acetic acid	Carl Roth GmbH + Co. KG
Acetone	Sigma Aldrich
Agar-Agar, Kobe I Kobe I	Carl Roth GmbH + Co. KG
Agarose NEEO Ultra-Quality Roti®garose	R Carl Roth GmbH + Co. KG
Alpha ketogluterate	Sigma
Ammonium peroxydisulphate ≥98 %, p.a., ACS	Carl Roth GmbH + Co. KG
Amphotericin B (Fungizone)	USBiological

Bacto Peptone, BD Difco	A. Hartenstein GmbH
Boric acid ≥99,8 %, p.a., ACS, ISO	Carl Roth GmbH + Co. KG
Bovine Serum Albumin	Sigma Aldrich
Calcium chloride, Dihydrate	Carl Roth GmbH + Co. KG
Chloroform	Carl Roth GmbH + Co. KG
Cholesterol	Carl Roth GmbH + Co. KG
Citrate	Sigma Aldrich
Dipotassium phosphate	Carl Roth GmbH + Co. KG
DMSO	Carl Roth GmbH + Co. KG
EDTA (Ethylenediaminetetraacetic acid)	Carl Roth GmbH + Co. KG
EGTA (ethylene glycol-bis(β-aminoethyl ether)-N,N,N′,N′-tetraacetic acid	Carl Roth GmbH + Co. KG
Ethanol unvergällt 99%	MDC
Ethanol vergällt 99%	MDC
Ethidium bromide (EtBr)	Carl Roth GmbH + Co. KG
Floxuridine (5-fluorodeoxyuridine)	Abcam
Formaldehyde 37 % p.A.	Sigma Aldrich
Fumaric acid	Sigma Aldrich
Gelatin	Carl Roth GmbH + Co. KG
Gelatine 2% solution from bovine skin cell	Sigma Aldrich
Glucose	Carl Roth GmbH + Co. KG
Glycerol 98%	Carl Roth GmbH + Co. KG
Glycin PUFFERAN®	Carl Roth GmbH + Co. KG
HEPES Buffer	Applichem
Hydrochloric acid 37 %	Carl Roth GmbH + Co. KG
Hydrogen Peroxide 30 % p.A.	Carl Roth GmbH + Co. KG
Hydroxyurea 98 %	Sigma Aldrich
Indole-3-acetic acid, 98+% (Auxin)	Alfa Aesar
IPTG	Carl Roth GmbH + Co. KG
IS Mounting medium	Dianova
IS Mounting medium (DAPI)	Dianova
L- Malic acid	Th. Geyer
L-Glutamine	Fischer Scientific
LB-Agar (Luria/Miller)	Carl Roth GmbH + Co. KG
LB-Medium (Luria/Miller)	Carl Roth GmbH + Co. KG
Magnesium chloride hexahydrate	Carl Roth GmbH + Co. KG
Magnesium sulphate	Carl Roth GmbH + Co. KG
Methanol	Carl Roth GmbH + Co. KG
Polyvinylpyrrolindone	Sigma Aldrich
Potassium chloride	Carl Roth GmbH + Co.KG
RNase A	Invitrogen
RNase away	M&P Molecular Bio Products
Rotiphorese Gel 30 (37,5:1)	Carl Roth GmbH + Co. KG
Sodium acetate	Carl Roth GmbH + Co. KG
Sodium azide	Fluka-Sigma
Sodium chloride	Carl Roth GmbH + Co. KG
Sodium deoxycholate	Applichem
Sodium dodecyl sulfate	Carl Roth GmbH + Co. KG

Sodium hydroxide solution 4 N	Carl Roth GmbH + Co. KG
Sodium hypochlorite solution	Carl Roth GmbH + Co. KG
Spermidine	Sigma Aldrich
Succinic acid	Sigma Aldrich
TEMED 99%	Carl Roth GmbH + Co. KG
TRIS PUFFERAN®	Carl Roth GmbH + Co. KG
Triton® X-100	Sigma Aldrich
Trizol® Reagent	life technologies
Tween20	Sigma Aldrich

5. METHODS

5.1 Nematode specific methods

5.1.1 Maintenance:

C. elegans strains were maintained on plates with Nematode Growth Medium (NGM) agar (3 g NaCl, 20 g Agar, 2,5 g Peptone for 1L ddH_2O, supplemented with 5µg/mL Cholesterol, 1 mM $MgSO_4$, 1 mM $CaCl_2$, 25 mM K_2PO_4, 2.5 µg/mL Amphotericin B) and OP50 bacteria for food at 15 degrees as described before (Brenner, 1974). Temperature sensitive (ts) and strains containing heat shock promoter were kept exclusively at 15°C. Worms were transferred on fresh plate for maintenance every two weeks. Males occur in the population at a low frequency of 0.1%. In order to maintain males, hermaphrodites were cross fertilized with males of the same genotype every week.

C. elegans strains used and generated in the study are listed in the table 4.1 and 4.2.

5.1.2 Animal synchronization:

Animals were synchronized by bleach treatment. Gravid adult worms were exposed to the bleaching solution containing 4% NaClO, 2M NaOH in ddH_2O. Since worms are sensitive to the bleach, they burst open thereby releasing eggs. Eggs survive the bleach treatment due to the eggshell which protects the larvae. The egg pellet was obtained by centrifugation and was washed three times with M9 buffer (22 mM KH_2PO_4, 42 mM Na_2HPO_4, 86 mM NaCl, 1 mM $MgSO_4$ in ddH_2O) and the eggs were then place on fresh NGM plates seeded with OP50 bacteria to hatch.

5.1.3 Transgenic crossing

C. elegans strains can be crossed together to obtain animals with genetic compositions of different strains together. For mating, 11 males and 3 hermaphrodites were places on a plate containing a drop of OP50 overnight. This restricts the animals to the limited space containing food and increase the probability of mating. Single hermaphrodites were then transferred to fresh plates and allowed to lay progeny. SuccessfµLmating was identified by occurrence of 50 % male population in the F1 progeny. This heterozygous cross progeny was then singled and

the homozygous F2 progeny worms were identified by reported expression, roller phenotype or genotyping as described by Fay (2013).

5.1.4 Lysis

For genotyping, 1-10 worms were places into 20 µL of lysis buffer (50 mM KCl, 10 mM Tris pH 8.3, 2,5 mM $MgCl_2$, 0,45% Tween20 (v/v), 0,01% Gelatin (v/v) in ddH_2O) containing 1 mg/mL of proteinase K. Worms were then freeze cracked by placing at -80°C for an hour in order to break the cuticle. The tubes containing the worms were then placed in the thermocycler for 1 hour at 65 degrees followed by an inactivation of the proteinase K for 30 min at 95°C. The lysate thus obtained was stored at -20°C until further used, or 1-2 µL was used for PCR for genotyping purposes.

5.1.5 Genotyping

In order to identify the presence of a mutation or transgenic sequence after crossing, CRISPR injection or transgenesis, genotyping of the worms was performed. 1-2 µL of the worm lysate was used as a template in the PCR reaction using Mango Taq (Bioline), Expand long template (Roche) or Taq Polymerase (NEB). Deletions and insertions were detected by the difference in size of the PCR band compared to the wildtype control. Sequences of insertions and point mutations were confirmed by Sanger sequencing. N2 worms were used as the wild type control for CRISPR and transgenic genotyping.

Details of the primers used for genotyping are given in table 4.4.

5.1.6 RNAi treatment

For RNAi knockdown of genes, animals were grown on NGM agar plates containing 1mM IPTG and 50 µg/mL Carbenicilin. These plates were seeded with RNAi bacteria grown overnight at 37 degrees from Ahringer library (Source Bioscience) (Kamath et al., 2003). For negative control, RNAi against *Renilla luciferase* (Rluc) was used.

For P0 experiments, worms were bleached and eggs were placed onto the RNAi plates and grown at 15 °C until most of the P0 animals reached L4 stage. At this stage, the plates were

heat shocked 37°C for 30 min followed by an overnight incubation at 25°C as described before (Seelk et al., 2016). The following day, animals were screened for ectopic GFP under a dissecting scope.

For F1 RNAi treatment, worms were synchronized by bleaching and allowed to hatch and reach L4 stage at normal food. They were then transferred to the RNAi plates and gown at 15°C until most of the F1 progeny reached L4 stage. The plates were then heat shocked at 37°C for 30 minutes and transferred to 25°C incubator overnight as described above. Animals were then screened for ectopic GFP under a dissection scope the following day. Unless stated otherwise, all reprogramming experiments were carried out with F1 RNAi.

For double RNAi, bacterial cultures were grown overnight and OD_{600} was measured to ensure that the bacteria were mixed in 1:1 ratio. These cultures were then seeded onto the RNAi plates. For double RNAi experiments, mixed cultures of Rluc and the gene of interest were used as a control.

5.1.7 Metabolite and Auxin Feeding

For the metabolite and Auxin feeding, 400mM stock solution was prepared and diluted into the NGM agar. PH of the MGM media was adjusted to 6 as described by Chin et al., (2014) and Edwards et al., (2015). The plates were then seeded with RNAi bacteria and the worms were subjected to the F1 RNAi as described.

5.1.8 Generation of CRISPR alleles

Mutants and tagged versions of genes listed in table 4.2 were generated by CRISPR. For this, a mixture of the sgRNAs, Cas9 protein, DNA sequence with homology arms to the site of insertion, and plasmid containing a florescent marker (*myo-2:RFP)* was injected in the animals as described by Dokshin et al, (2018). F1 progeny was then screened for the RFP in the pharynx and genotyped for the presence of mutation as described before (Arribere et al., 2014). Positive animals were homozygoused by singling and the sequence of the inserted sequence was confirmed by Sanger sequencing.

5.1.9 Dissection of *C. elegans* gonads

To perform gonad specific ATAC-seq, gonads of adult worms were dissected. Animals were washed off from the plates and washed three times with M9 to get rid of the bacteria. The worms were then placed on a glass coverslip in a drop of gonad buffer (118 mM NaCl, 48 mM KCl, 2 mM $CaCl_2$, 2 mM $MgCl_2$, 10 mM HEPES in ddH_2O, pH 7.3) supplemented with 0.1% Tween20 and 0.25 mM levamisole and the gonad dissection was carried out as described before (Memar et al., 2017). The heads of the worms were cut off near the pharynx using two 26 G hypodermic needles (Sterican). This resulted in the extrusion of the gonad arms. The gonads were then transferred to a 1.5 ml tube and processed.

5.1.10 Freezing worms for long-term storage

Worms can be stored for long term by freezing L1 larvae at -80°C as described by Brenner et al., (1974). For freezing the worms for long term storage, worms were grown on NGM plates until a lot of L1 larvae were found. The worms were the washed off the plates with M9 and washed three times with the M9 buffer to remove the bacteria. After the washing, the worms were then resuspended in 1 ml M9 and freezing solution (100 mM NaCl; 20 mM KH_2PO_4 (pH 6); 4 % glycerol (v/v) and 300 mM $MgSO_4$) was added in 1:1 ratio. The solution containing worms were then transferred to CryoTubes and frozen at -80°C in Styrofoam boxes to freeze slowly. One tube of the frozen stock was thawed and tested for the worm survival after 2 weeks.

5.2 Biochemical methods

5.2.1 DNA isolation

Invisorb plasmid mini kit (Stratec) was used according to manufacturer's instructions to isolate DNA for molecular cloning and other applications. In order to obtain high quality DNA for injections of transgenes into the animals, HiPure Plasmid Midiprep Kit (Invitrogen) was used according to manufacturer's instructions.

5.2.2 RNA isolation

Whole transcriptome sequencing was carried out on the worms to analyze changes in the gene expression. For this, a pellet of 100 µL of F1 generation of worms grown on RNAi was collected at the L4 stage. Guanidinium thiocyanate-phenol-chloroform extraction method was used to isolate the RNA (Chomczynski and Sacchi, 1987). Addition of chloroform in the worm sample suspended in TRIzol® (Life Technologies) results in the separation of phases consisting of an aqueous phase containing RNA, an inter phase and an organic phase containing DNA and proteins. RNA is extracted from the aqueous phase by isopropanol.

In brief, worms were harvested into the 1.5 ml tubes. The collected worms were washed three times with M9 to remove bacteria and TRIzol® was added in the washed worm pellet to make the volume of 500 µL in total. The sample was then frozen in the liquid nitrogen for 15 minutes to crack the cuticle followed by incubation for 15 minutes at 65°C to inactivate nucleases. The sample containing tubes were then incubated for 5 minutes at room temperature and chloroform was added followed by vortexing and centrifugation for 15 minutes at 13.000 g at 4°C. This resulted in the separation of the phases. The aqueous phase containing the RNA was separated and isopropanol was added to precipitate it. The sample was incubated for 10 minutes at -20 degrees, and centrifuged for sixty minutes at 13.000 g at 4 degrees to pellet the RNA. The RNA was washed with 1ml of ice cold 75 % ethanol and centrifuged again for 10 minutes at 13.000 g at 4 degrees. The dry RNA pellet was dissolved in nuclease-free ddH_2O. The sample was treated with DNAses for 30 minutes to remove any DNA contamination, and GeneJET RNA Cleanup and Concentration Micro Kit (ThermoFisher Scientific) was used according to the manufacturers protocol to purify the RNA. Agilent 2100 Bioanalyzer (Agilent) was used to measure the final RNA concentration.

5.2.3 cDNA synthesis

GoScript Reverse Transcriptase (Promega) was used according to the manufacturers instructions to synthesize the cDNA using the oligo dT primers that bind to the poly-A-tail of RNA. Briefly, 1 µg of RNA, 1 µL of oligo dT primer and 2 µL of random hexamer primer were added together to make a final volume of 5 ul. The tube containing the mixture was incubated for 5 minutes at 70°C and 5 minutes at 4°C to remove the secondary structures in the RNA. This was followed by the addition of 1 µL of 0.5 mM dNTps, 1 µL of GoScript Reverse Transcriptase, 4 µL of 5x GoScript reaction buffer and 1.5 µL of 1.74 mM $MgCl_2$. The mixture was incubated for 10 minutes at 25°C for annealing and 60 minutes at 42°C for extension. This was followed by an incubation at 70°C for 15 minutes to denature the reverse transcriptase.

The cDNA synthesis was performed by Mr. Sergej Herzog.

5.2.4 Worm protein lysates

Whole cell protein extraction was done on the animal samples for analysis by western blotting. For this, animals were treated with RNAi and F1 generation was collected at L4 stage by washing off with M9. The worm pellet was washed with M9 three times to remove bacteria and 5XSDS sample buffer (10% w/v SDS, 10 mM dithiothreitol (DTT), 20% v/v glycerol, 0,2 M Tris-HCl pH 6.8, 0,05% w/v bromophenolblue) was added to the worms. This treatment with SDS leads to a denaturation of proteins, disables protein-protein-interactions and confers a negative charge. The samples were then incubated at 96°C for 10 minutes and stored at -20 degrees.

5.2.5 SDS polyacrylamide gel electrophoresis

The protein lysate samples were separated by SDS polyacrylamide gel electrophoresis (SDS-PAGE). The samples were loaded in 4–20% Mini-PROTEAN Precast Protein Gels (BioRad) and the separation was carried out in a vertical Mini-PROTEAN Tetra Electrophoresis system (BioRad) containing using 1x SDS Running buffer (24,8 mM Tris-HCl, 192 mM Glycin, 0,01 % SDS (w/v)). 10 mA current was applied per gel until the samples ran from stacking gel to the separating gel and was increased to 20 mA per gel afterwards. PageRuler Plus Prestained protein ladder (Thermo Scientific) was used as a marker.

5.2.6 Western Blot

The proteins separated by the SDS-PAGE were transferred to the nitrocellulose membrane for immunological detection by antibodies. For this, wet blotting chambers were used containing the Tankblot transfer buffer (25 mM Tris, 192 mM glycine pH 8.3, 20% MeOH) at 100 V constant for 60 minutes.

The nitrocellulose membrane was then blocked in 3% BSA in 1xTBST (25 mM Tris pH 7.5, 150 mM NaCl, 0.1% v/v Tween20) for 1 hour at room temperature with gentle shaking. After blocking, the membrane was incubated with primary antibodies for 4 hours at room temperature or overnight at 4°C. The membrane was washed three times for 15 minutes with the washing buffer (1xTBST). This was followed by the incubation with the secondary antibody linked to HRP for 1 hour at room temperature. The antibody-antigen complexes were detected using the Lumi-Light Western Blotting substrate (Roche Applied Science) according to the manufacturers instruction. The detection was done at the Luminescent Image Analyzer (GE Heathcare) with the ImageQuant LAS4000 software. Primary antibodies coupled to peroxidase-coupled were washed 3x for 10 min in wash buffer and immediately detected as described above.

Antibodies used in this study are listed in table 4.7 and 4.8.

5.2.7 Antibody staining

For detection of FLAG and UNC-10 in whole worms, animals were fixed and permeabilized according the method described by Bettinger et al., (1996). Briefly, animals were washed off with M9 and resuspended in RFB (160 mM KCl, 40 mM NaCl, 20 mM EGTA, 10 mM Spermidine) supplemented with 2% formaldehyde followed by three freeze-thaw cycles. The samples were then incubated for 30 minutes at 25°C and washed with TTE (100 mM Tris pH 7.4, 1 % Triton, 1mM EDTA). This was followed by incubation in TTE supplemented with 1% beta-Mercaptoethanol for 4 hours at 37 °C. The samples were then washed with BO3 buffer (10 mM H_3BO_3, 10 mM NaOH, 2 % Triton) and incubated with BO3 buffer supplemented with 10 mM DTT for 15 minutes at 37°C. This was followed by another was with the BO3 buffer after which the samples were added with BO3 buffer supplemented with 0.3 % H_2O_2 and incubated for 15 minutes at 25°C. The sample was then washed again

with BO3 and blocked with 0.2 % gelatin + 0.25 % Triton in PBS for one hour and stained with antibodies.

Worms were incubated with primary antibodies (diluted in PBS with 0,25 % Triton + 0,2 % gelatin) overnight at 4°C with gentle shaking. This was followed by washing for five times with PBS + 0.25 % Triton and addition of secondary antibodies (Alexa Fluor dyes at 1:1500 dilution) in PBS with 0,25 % Triton + 0,2 % gelatin and incubation overnight at 4°C with gentle shaking. Samples were washed five times with PBS + 0.25 % Triton and mounted on glass slides with DAPI-containing mounting medium (Dianove, #CR-3448).

For HA, anti-H3K4me3, anti-H3K9me3 and anti-H3K27me3 stainings, worms were sheared by slide crack and processed as described before (Jones et al., 1996). Briefly, Glass slides were placed on metal tray on dry ice. Drop of worms suspended in M9 were pipetted onto the slide and another slide was placed on top of it. The two slides were then split apart placed in 4% paraformaldehyde (Methanol for HA) solution for 10 minutes for fixation. This was followed by washing with PBST (0.1% Tween20 in 1xPBS) 3 times. The samples were then blocked with 0.2% gelatin in PBST for 1 hour and stained with primary and secondary antibodies as described above.

Antibodies used in this study are listed in table 4.7 and 4.8.

5.2.8 Single molecule florescence in situ hybridization (smFISH):

smFISH was performed using Custom Stellaris FISH probes, purchased from Biosearch Technologies and the staining was done according to the manufacturers protocol. Briefly, worms were treated with *idha-1* and control RNAi and washed off the plates with M9. This was followed by five washing steps with nuclease free water. The animals were then fixed in 4% PFA for 45 minutes. After fixation, the worms were washed with 1xPBS treated with DEPc twice and permeabilized by rotating in 70% EtOH overnight at 4°C. The worms were then washed with Wash buffer (2 mL deionized formamide, 2 mL 20x SSC (RNase-free), 100 µLTriton X-100, 16 mL DEPC-treated nuclease-free H_2O) and resuspended in Hybridization buffer containing the probe (125 µLof 20% dextran sulfate, , 25 µLdeionized formamide, 37.5 µLEthylene Carbonate, H_2O up to 50 uL) and incubated in the dark at 37°C for 16 hours. After incubation, the worms were washed with Wash buffer in the dark at 37°C for 30 minutes. This was followed by a 30 min incubation with DAPI to counterstain the nuclei. After

counterstaining, worms were resuspended in a small drop of Vectashield Mounting Medium and mounted on glass slides.

Sequences of all the smFISH probes used are listed in table 4.9.

5.2.9 Fluorescent microscopy

Worms were imaged with using Zeiss Axio Imager 2 fluorescent microscope connected to a digital camera (Sensicam, PCO) and Fluorescent Microscope DM6B (Leica). Animals were mounted on 2 % agarose pads on glass slides in M9 containing 20 mM tetramisole to anesthetize.

5.2.10 Metabolomic analysis of the worms

The analysis of the metabolome was carried out in collaboration with the Kempa laboratory at the BIMSB. Jenny Grobe supported the sample preparation and carried out the measurement at the GC-MS and Tobias Opialla performed the analysis.

Gas-chromatography coupled to mass spectrometry (GC-MS) was used for the metabolomic analysis. Ident-mixes for the identification were added to the samples during processing. Quant mixes were added in the dilution of 1:1, 1:2, 1:5, 1:10, 1:20, 1:50, 1:100, 1:200 for the quantification of the identified compounds (Pietzke et al., 2014).

5.2.10.1 Sample preparation for metabolomics

Worm strains with the endogenously tagged *idha-1* with 3xHA were subjected to F1 and P0 RNAi, and 15 mM fumarate feeding. Animals were collected at L4 stage and washed 3 times with M9 to remove the bacteria. After this, the worm pellet was weighed and flash frozen in liquid nitrogen. For the analysis, worm pellet of up to 50 mg was used.

Sample extraction was performed by adding methanol:chloroform:water (5:2:1, MCW) of 1 mL per 50 mg of sample. The worm sample was then transferred to a new tube containing silica beads and was lysed mechanically by tissue lyser. at 6.500 m/s, 2x20 sec ON, 5 sec OFF for three times. This was followed by sonication for 10 min in an ultrasound bath. After sonication, the supernatant was taken off and the left over MCW (x – 500 µL) was added,

vortexed and shortly incubated on dry ice. The samples were then shaken for 15 minutes, centrifuged for 1400 rpm at 4°C and 0.5 volume of water was added for phase separation. After this, the samples were vortexed and shaken for 15 min, at 1400 rpm at 4 °C. Vortexing was repeated and the sample was centrifuged at 20,000 g, 4°C for 10 min to ensure phase separation. The polar phase at the top was collected and dried in speed vacuum overnight. This was followed by derivatization and the Kempa lab used a slightly modified protocol from Roessner-Tunali et al., (2003) as indicated in Kempa et al. (2009). Briefly, 10 µL of 40 mg/mL methoxyamine hydrochloride (MeOx) solution in pyridine is added and incubated for 90 min at 30 °C with shaking. 30 µL N-Methyl-N-(trimethylsilyl) trifluoroacetamide (MSTFA) spiked with alkanes as retention index markers is then added to the sample and incubated 60 min at 37 °C. The samples were then centrifuged for 10 minutes at room temperature at 20,000 g and transferred to the glass vials for the GC-MS analysis.

The GC-MS measurement was carried out by Jenny Grobe and Tobias Opialla using a standard procedure established in the Kempa laboratory (Pietzke et al., 2014). The data analysis was carried out by Tobias Opialla using Maui-SILVIA (Kuich et al., 2014).

5.3 Molecular biology methods

5.3.1 Molecular Cloning

In order to make plasmids for RNAi against two genes simultaneously (Stitched RNAi), the sequence of the gene was amplified from an existing RNAi plasmid using PCR. To remove unwanted nucleotides, salts and primers from the PCR product, GeneJET PCR purification kit (Thermo Scientific) was used to purify it. This gene sequence was then cloned into the RNAi plasmid containing the other gene using Gibson Assembly (Gibson et al., 2009). The correctly cloned plasmid was identified by Sanger sequencing. This plasmid was then transformed in competent HT115 E. coli bacterial strain.

Details of the bacterial strain are described in detail in table 4.3.

To generate the strain containing TIR1 expressed under the somatic gonad specific promoter (*lim-7*^{prom}::TIR1::mRuby), the promoter sequence of *lim-7* was amplified from the plasmid pGC361 (from Hubbard Lab) and TIR1::mRuby::*unc-54* 3'UTR sequence was amplified from pLZ31 (from Addgene). The two fragments were cloned into the plasmid pCFJ151 (restricted with Spe1/Xho1) for MosSCI (single copy) integration. The correct plasmid was identified by Sanger sequencing and transformed into competent Mach1 cells and allowed to from colonies. The plasmid was purified from the bacteria using NucleoBond Xtra MidiPrep Kit (Macherey-Nagel) and was then injected into worm strain EG8079 for single copy insertion by MosSCI (Frokjaer-Jensen et al., 2008).

Details of the primers used for cloning are given in table 4.5.

5.3.2 Whole Transcriptome Sequencing (RNA-seq)

RNA for transcriptome analysis was isolated from wildtype and *glp-4 (bn2)* animals treated with control and *idha-1* P0 RNAi as described above.

The library preparation was done using the TruSeq RNA Library Prep Kit v2 (Illumina) according to the manufacturer's instructions. The protocol consisted of fragmentation, end-repair, phosphorylation of the 5' ends and A-tailing of the 3' ends to facilitate adapter ligation. Briefly, total RNA was extracted and purified and polyA selection was done using RNA-purification beads. The RNA was then eluted in a step that involved priming for adapter ligation and fragmentation of RNA to pieces in 200-300 bp to make them suited for the range of the

read-length of the sequencer. This was followed by reverse transcription of the RNA into cDNA using SuperScriptII reverse transcriptase (Invitrogen). The cDNA fragments were made blunt and phosphorylated at the 5' by incubation with an End Repair Mix (Illumina) at 30°C for 30 minutes. Free 3' adenine was added to the cDNA to facilitate the ligation of adapters. These adapters provide the unique sequence for the later identification of the reads belonging to the same library in a pooled sample. This was followed by the amplification and purification of the libraries and was done according to the manufacturer's instructions. Libraries were sequenced on a HiSeq4000 machine (Illumina) using single end sequencing length of a 75 nucleotides.

5.4 Computational Analysis

5.4.1 Statistics

Student's t-test or one-way ANOVA was used for data analysis unless indicated otherwise.

5.4.2 RNA-seq Analysis

Analysis of the RNAseq data was done using the PiGx RNAseq pipeline version 0.0.10 with the mapping part of the star aligner adjusted to account for a higher number of collapsed junctions and increased buffers size ("--limitOutSJcollapsed 20000000 --limitIObufferSize=600000000") using genome assembly and transcript annotation data from Ensembl (Ricardo et al., 2018) (WBcel235, Release 97).

The analysis was performed by Mr. Alexander Blume.

6. REFERENCES

1. Almada, A. E., & Wagers, A. J. (2016). Molecular circuitry of stem cell fate in skeletal muscle regeneration, ageing and disease. *Nature reviews Molecular cell biology*, *17*(5), 267.
2. Alvarado, A. S., & Yamanaka, S. (2014). Rethinking differentiation: stem cells, regeneration, and plasticity. *Cell*, *157*(1), 110-119.
3. Alvarez-Dolado, M. (2007). Cell fusion: biological perspectives and potential for regenerative medicine. *Front Biosci*, *12*, 1-12.
4. Ariyachet, C., Tovaglieri, A., Xiang, G., Lu, J., Shah, M. S., Richmond, C. A., ... & Shivdasani, R. A. (2016). Reprogrammed stomach tissue as a renewable source of functional β cells for blood glucose regulation. *Cell stem cell*, *18*(3), 410-421.
5. Arribere, J. A., Bell, R. T., Fu, B. X., Artiles, K. L., Hartman, P. S., & Fire, A. Z. (2014). Efficient marker-free recovery of custom genetic modifications with CRISPR/Cas9 in Caenorhabditis elegans. *Genetics*, *198*(3), 837-846.
6. Banga, A., Akinci, E., Greder, L. V., Dutton, J. R., & Slack, J. M. (2012). *In vivo* reprogramming of Sox9+ cells in the liver to insulin-secreting ducts. *Proceedings of the National Academy of Sciences*, *109*(38), 15336-15341.
7. Banito, A., Rashid, S. T., Acosta, J. C., Li, S., Pereira, C. F., Geti, I., ... & Vallier, L. (2009). Senescence impairs successful reprogramming to pluripotent stem cells. *Genes & development*, *23*(18), 2134-2139.
8. Baumeister, R., & Ge, L. (2002). The worm in us–Caenorhabditis elegans as a model of human disease. *Trends in biotechnology*, *20*(4), 147-148.
9. Berg JM, Tymoczko JL, Stryer L. Biochemistry. 5th edition. New York: W H Freeman; 2002. Available from: https://www.ncbi.nlm.nih.gov/books/NBK21154/
10. Bertholet, A. M., Delerue, T., Millet, A. M., Moulis, M. F., David, C., Daloyau, M., ... & Rojo, M. (2016). Mitochondrial fusion/fission dynamics in neurodegeneration and neuronal plasticity. *Neurobiology of disease*, *90*, 3-19.
11. Bettinger, J. C., Lee, K., & Rougvie, A. E. (1996). Stage-specific accumulation of the terminal differentiation factor LIN-29 during Caenorhabditis elegans development. *Development*, *122*(8), 2517-2527.
12. Beyer, S., Kristensen, M. M., Jensen, K. S., Johansen, J. V., & Staller, P. (2008). The histone demethylases JMJD1A and JMJD2B are transcriptional targets of hypoxia-inducible factor HIF. *Journal of Biological Chemistry*, *283*(52), 36542-36552.
13. Bird, Adrian. "DNA methylation patterns and epigenetic memory." *Genes & development* 16, no. 1 (2002): 6-21.
14. Blau, H. M., & Baltimore, D. (1991). Differentiation requires continuous regulation. *The Journal of cell biology*, *112*(5), 781-783.
15. Boland, M. L., Chourasia, A. H., & Macleod, K. F. (2013). Mitochondrial dysfunction in cancer. *Frontiers in oncology*, *3*, 292.
16. Borkent, M., Bennett, B. D., Lackford, B., Bar-Nur, O., Brumbaugh, J., Wang, L., ... & Maherali, N. (2016). A serial shRNA screen for roadblocks to reprogramming identifies the protein modifier SUMO2. *Stem cell reports*, *6*(5), 704-716.
17. Boulin, T., Etchberger, J. F., & Hobert, O. (2006). Reporter gene fusions. In *WormBook: The Online Review of C. elegans Biology [Internet]*. WormBook.
18. Brenner, S. (1974). The genetics of Caenorhabditis elegans. *Genetics*, *77*(1), 71-94.
19. Brumbaugh, J., Di Stefano, B., & Hochedlinger, K. (2019). Reprogramming: identifying the mechanisms that safeguard cell identity. *Development*, *146*(23).

20. Buckley, S. M., Aranda-Orgilles, B., Strikoudis, A., Apostolou, E., Loizou, E., Moran-Crusio, K., ... & Stadtfeld, M. (2012). Regulation of pluripotency and cellular reprogramming by the ubiquitin-proteasome system. *Cell stem cell*, *11*(6), 783-798.
21. Buenrostro, J. D., Giresi, P. G., Zaba, L. C., Chang, H. Y., & Greenleaf, W. J. (2013). Transposition of native chromatin for fast and sensitive epigenomic profiling of open chromatin, DNA-binding proteins and nucleosome position. *Nature methods*, *10*(12), 1213.
22. Burchfield, J. S., Li, Q., Wang, H. Y., & Wang, R. F. (2015). JMJD3 as an epigenetic regulator in development and disease. *The international journal of biochemistry & cell biology*, *67*, 148-157.
23. Calvert, A. E., Chalastanis, A., Wu, Y., Hurley, L. A., Kouri, F. M., Bi, Y., ... & Stegh, A. H. (2017). Cancer-associated IDH1 promotes growth and resistance to targeted therapies in the absence of mutation. *Cell reports*, *19*(9), 1858-1873.
24. Campbell, K. H., Loi, P., Otaegui, P. J., & Wilmut, I. (1996). Cell cycle co-ordination in embryo cloning by nuclear transfer. *Reviews of reproduction*, *1*(1), 40-46.
25. Carey, B. W., Finley, L. W., Cross, J. R., Allis, C. D., & Thompson, C. B. (2015). Intracellular α-ketoglutarate maintains the pluripotency of embryonic stem cells. *Nature*, *518*(7539), 413-416.
26. Chalfie, M., Tu, Y., Euskirchen, G., Ward, W. W., & Prasher, D. C. (1994). Green fluorescent protein as a marker for gene expression. *Science*, *263*(5148), 802-805.
27. Chan, D. C. (2012). Fusion and fission: interlinked processes critical for mitochondrial health. *Annual review of genetics*, *46*.
28. Cheloufi, S., Elling, U., Hopfgartner, B., Jung, Y. L., Murn, J., Ninova, M., ... & Wesche, D. J. (2015). The histone chaperone CAF-1 safeguards somatic cell identity. *Nature*, *528*(7581), 218-224.
29. Chin, R. M., Fu, X., Pai, M. Y., Vergnes, L., Hwang, H., Deng, G., ... & Hu, E. (2014). The metabolite α-ketoglutarate extends lifespan by inhibiting ATP synthase and TOR. *Nature*, *510*(7505), 397-401.
30. Choi, H. W., Kim, J. H., Chung, M. K., Hong, Y. J., Jang, H. S., Seo, B. J., ... & Han, S. G. (2015). Mitochondrial and metabolic remodeling during reprogramming and differentiation of the reprogrammed cells. *Stem cells and development*, *24*(11), 1366-1373.
31. Choi, P. S., Van Riggelen, J., Gentles, A. J., Bachireddy, P., Rakhra, K., Adam, S. J., ... & Felsher, D. W. (2011). Lymphomas that recur after MYC suppression continue to exhibit oncogene addiction. *Proceedings of the National Academy of Sciences*, *108*(42), 17432-17437.
32. Chomczynski, P., & Sacchi, N. (1987). Single step method of RNA isolation by acid guanidinium thiocyanate-phenol-chloroform extraction Anal Biochem 162: 156–159. *Find this article online*.
33. Chung, S., Dzeja, P. P., Faustino, R. S., Perez-Terzic, C., Behfar, A., & Terzic, A. (2007). Mitochondrial oxidative metabolism is required for the cardiac differentiation of stem cells. *Nature clinical practice Cardiovascular medicine*, *4*(1), S60-S67.
34. Cliff, T. S., & Dalton, S. (2017). Metabolic switching and cell fate decisions: implications for pluripotency, reprogramming and development. *Current opinion in genetics & development*, *46*, 44-49.
35. Cloonan, S. M., & Choi, A. M. (2013). Mitochondria: sensors and mediators of innate immune receptor signaling. *Current opinion in microbiology*, *16*(3), 327-338.
36. Corsi, A. K., Wightman, B., & Chalfie, M. (2015). A transparent window into biology: a primer on Caenorhabditis elegans. *Genetics*, *200*(2), 387-407.

37. Dang, L., Yen, K., & Attar, E. C. (2016). IDH mutations in cancer and progress toward development of targeted therapeutics. *Annals of Oncology*, *27*(4), 599-608.
38. Davis, R. L., Weintraub, H., & Lassar, A. B. (1987). Expression of a single transfected cDNA converts fibroblasts to myoblasts. *Cell*, *51*(6), 987-1000.
39. De Craene, B., & Berx, G. (2013). Regulatory networks defining EMT during cancer initiation and progression. *Nature Reviews Cancer*, *13*(2), 97-110.
40. DeBerardinis, R. J., & Chandel, N. S. (2016). Fundamentals of cancer metabolism. *Science advances*, *2*(5), e1600200.
41. DeBerardinis, R. J., Mancuso, A., Daikhin, E., Nissim, I., Yudkoff, M., Wehrli, S., & Thompson, C. B. (2007). Beyond aerobic glycolysis: transformed cells can engage in glutamine metabolism that exceeds the requirement for protein and nucleotide synthesis. *Proceedings of the National Academy of Sciences*, *104*(49), 19345-19350.
42. Devanapally, S., Ravikumar, S., & Jose, A. M. (2015). Double-stranded RNA made in C. elegans neurons can enter the germ line and cause transgenerational gene silencing. *Proceedings of the National Academy of Sciences*, *112*(7), 2133-2138.
43. Dillon, J., Franks, C. J., Murray, C., Edwards, R. J., Calahorro, F., Ishihara, T., ... & O'Connor, V. (2015). Metabotropic Glutamate Receptors MODULATORS OF CONTEXT-DEPENDENT FEEDING BEHAVIOUR IN C. ELEGANS. *Journal of Biological Chemistry*, *290*(24), 15052-15065.
44. Dokshin, G. A., Ghanta, K. S., Piscopo, K. M., & Mello, C. C. (2018). Robust genome editing with short single-stranded and long, partially single-stranded DNA donors in Caenorhabditis elegans. *Genetics*, *210*(3), 781-787.
45. Du, B., Li, X., & Li, Y. (2018). Effect of IDH3α on glucose uptake in lung adenocarcinoma. *Journal of Nuclear Medicine*, *59*(supplement 1), 1265-1265.
46. Du, W., Zhang, L., Brett-Morris, A., Aguila, B., Kerner, J., Hoppel, C. L., ... & Campbell, S. (2017). HIF drives lipid deposition and cancer in ccRCC via repression of fatty acid metabolism. *Nature communications*, *8*(1), 1-12.
47. Du, Z., & Lovly, C. M. (2018). Mechanisms of receptor tyrosine kinase activation in cancer. *Molecular cancer*, *17*(1), 58.
48. Edwards, C., Canfield, J., Copes, N., Brito, A., Rehan, M., Lipps, D., ... & Bradshaw, P. C. (2015). Mechanisms of amino acid-mediated lifespan extension in Caenorhabditis elegans. *BMC genetics*, *16*(1), 8.
49. Eng, C. H., Yu, K., Lucas, J., White, E., & Abraham, R. T. (2010). Ammonia derived from glutaminolysis is a diffusible regulator of autophagy. *Science signaling*, *3*(119), ra31-ra31.
50. Erpf, A. C., Memar, N., Schnabel, R., & Mikeladze-Dvali, T. (2017, January). t3421, a mutation in a novel protein required for centrosome matrix assembly in the one-cell stage C. elegans embryo. In *MOLECULAR BIOLOGY OF THE CELL*(Vol. 28). 8120 WOODMONT AVE, STE 750, BETHESDA, MD 20814-2755 USA: AMER SOC CELL BIOLOGY.
51. Etchberger, J. F., Lorch, A., Sleumer, M. C., Zapf, R., Jones, S. J., Marra, M. A., ... & Hobert, O. (2007). The molecular signature and cis-regulatory architecture of a C. elegans gustatory neuron. *Genes & development*, *21*(13), 1653-1674.
52. Fay, D. S. (2013). Classical genetic methods. *WormBook: the online review of C. elegans biology*, 1.
53. Feng, X., Zhang, L., Xu, S., & Shen, A. Z. (2020). ATP-citrate lyase (ACLY) in lipid metabolism and atherosclerosis: An updated review. *Progress in lipid research*, *77*, 101006.
54. Flippo, K. H., & Strack, S. (2017). Mitochondrial dynamics in neuronal injury, development and plasticity. *Journal of cell science*, *130*(4), 671-681.

55. Flores, A., Schell, J., Krall, A. S., Jelinek, D., Miranda, M., Grigorian, M., ... & Graeber, T. (2017). Lactate dehydrogenase activity drives hair follicle stem cell activation. *Nature cell biology*, *19*(9), 1017-1026.
56. Folmes, C. D., Dzeja, P. P., Nelson, T. J., & Terzic, A. (2012). Metabolic plasticity in stem cell homeostasis and differentiation. *Cell stem cell*, *11*(5), 596-606.
57. Folmes, C. D., Nelson, T. J., Martinez-Fernandez, A., Arrell, D. K., Lindor, J. Z., Dzeja, P. P., ... & Terzic, A. (2011). Somatic oxidative bioenergetics transitions into pluripotency-dependent glycolysis to facilitate nuclear reprogramming. *Cell metabolism*, *14*(2), 264-271.
58. Foshay, K. M., Looney, T. J., Chari, S., Mao, F. F., Lee, J. H., Zhang, L., ... & Di, C. G. (2012). Embryonic stem cells induce pluripotency in somatic cell fusion through biphasic reprogramming. *Molecular cell*, *46*(2), 159-170.
59. Foster, K. J., Cheesman, H. K., Liu, P., Peterson, N. D., Anderson, S. M., & Pukkila-Worley, R. (2020). Innate Immunity in the C. elegans Intestine Is Programmed by a Neuronal Regulator of AWC Olfactory Neuron Development. *Cell reports*, *31*(1), 107478.
60. Frøkjær-Jensen, C., Davis, M. W., Hopkins, C. E., Newman, B. J., Thummel, J. M., Olesen, S. P., ... & Jorgensen, E. M. (2008). Single-copy insertion of transgenes in Caenorhabditis elegans. *Nature genetics*, *40*(11), 1375.
61. Fu, W., Liu, Y., & Yin, H. (2019). Mitochondrial dynamics: biogenesis, fission, fusion, and mitophagy in the regulation of stem cell behaviors. *Stem cells international*, *2019*.
62. Fukushige, T., & Krause, M. (2005). The myogenic potency of HLH-1 reveals wide-spread developmental plasticity in early C. elegans embryos. *Development*, *132*(8), 1795-1805.
63. Fukushige, T., Hawkins, M. G., & McGhee, J. D. (1998). The GATA-factor elt-2 is essential for formation of the Caenorhabditis elegans intestine. *Developmental biology*, *198*(2), 286-302.
64. Gascón, S., Murenu, E., Masserdotti, G., Ortega, F., Russo, G. L., Petrik, D., ... & Schroeder, T. (2016). Identification and successful negotiation of a metabolic checkpoint in direct neuronal reprogramming. *Cell stem cell*, *18*(3), 396-409.
65. Gehring, W. (1966). Cell heredity and changes of determination in cultures of imaginal discs in Drosophila melanogaster. *Journal of embryology and experimental morphology*, *15*(1), 77-111.
66. Gehring, W. (1966). Übertragung und Änderung der Determinations qualitäten in Antennenscheiben-Kulturen von Drosophila melanogaster. *Development*, *15*(1), 77-111.
67. Gibson, D. G., Young, L., Chuang, R. Y., Venter, J. C., Hutchison, C. A., & Smith, H. O. (2009). Enzymatic assembly of DNA molecules up to several hundred kilobases. *Nature methods*, *6*(5), 343-345.
68. Golden, J. W., & Riddle, D. L. (1984). The Caenorhabditis elegans dauer larva: developmental effects of pheromone, food, and temperature. *Developmental biology*, *102*(2), 368-378.
69. Govindan, J. A., Nadarajan, S., Kim, S., Starich, T. A., & Greenstein, D. (2009). Somatic cAMP signaling regulates MSP-dependent oocyte growth and meiotic maturation in C. elegans. *Development*, *136*(13), 2211-2221.
70. Graf, T. (2011). Historical origins of transdifferentiation and reprogramming. *Cell stem cell*, *9*(6), 504-516.
71. Guo, Z., Zhang, L., Wu, Z., Chen, Y., Wang, F., & Chen, G. (2014). *In vivo* direct reprogramming of reactive glial cells into functional neurons after brain injury and in an Alzheimer's disease model. *Cell stem cell*, *14*(2), 188-202.

72. Gurdon, J. B., Elsdale, T. R., & Fischberg, M. (1958). Sexually mature individuals of Xenopus laevis from the transplantation of single somatic nuclei. *Nature*, *182*(4627), 64-65.
73. Hadorn, E. (1963). Differenzierungsleistungen wiederholt fragmentierter Teilstücke männlicher Genitalscheiben von Drosophila melanogaster nach Kultur *in vivo*. *Developmental Biology*, *7*, 617-629.
74. Hajduskova, M., Baytek, G., Kolundzic, E., Gosdschan, A., Kazmierczak, M., Ofenbauer, A., ... & Seelk-Müthel, S. (2019). MRG-1/MRG15 is a barrier for germ cell to neuron reprogramming in Caenorhabditis elegans. *Genetics*, *211*(1), 121-139.
75. Haniuda, K., Fukao, S., & Kitamura, D. (2020). Metabolic Reprogramming Induces Germinal Center B Cell Differentiation through Bcl6 Locus Remodeling. *Cell Reports*, *33*(5), 108333.
76. Hansson, J., Rafiee, M. R., Reiland, S., Polo, J. M., Gehring, J., Okawa, S., ... & Krijgsveld, J. (2012). Highly coordinated proteome dynamics during reprogramming of somatic cells to pluripotency. *Cell reports*, *2*(6), 1579-1592.
77. Harvey, A. J. (2019). Mitochondria in early development: linking the microenvironment, metabolism and the epigenome. *Reproduction*, *157*(5), R159-R179.
78. Harvey, A. J., Rathjen, J., & Gardner, D. K. (2016). Metaboloepigenetic regulation of pluripotent stem cells. *Stem Cells International*, *2016*.
79. Hino, S., Sakamoto, A., Nagaoka, K., Anan, K., Wang, Y., Mimasu, S., ... & Nakao, M. (2012). FAD-dependent lysine-specific demethylase-1 regulates cellular energy expenditure. *Nature communications*, *3*(1), 1-12.
80. Hochedlinger, K., & Jaenisch, R. (2006). Nuclear reprogramming and pluripotency. *Nature*, *441*(7097), 1061-1067.
81. Hom, J. R., Quintanilla, R. A., Hoffman, D. L., de Mesy Bentley, K. L., Molkentin, J. D., Sheu, S. S., & Porter Jr, G. A. (2011). The permeability transition pore controls cardiac mitochondrial maturation and myocyte differentiation. *Developmental cell*, *21*(3), 469-478.
82. Horner, M. A., Quintin, S., Domeier, M. E., Kimble, J., Labouesse, M., & Mango, S. E. (1998). pha-4, anHNF-3 homolog, specifies pharyngeal organ identity in Caenorhabditis elegans. *Genes & development*, *12*(13), 1947-1952.
83. Hsu, Y. C., Wu, Y. T., Yu, T. H., & Wei, Y. H. (2016, April). Mitochondria in mesenchymal stem cell biology and cell therapy: from cellular differentiation to mitochondrial transfer. In *Seminars in cell & developmental biology* (Vol. 52, pp. 119-131). Academic Press.
84. Hu, J., Jing, H., & Lin, H. (2014). Sirtuin inhibitors as anticancer agents. *Future medicinal chemistry*, *6*(8), 945-966.
85. Hwang, S. M. (2008). *U.S. Patent No. 7,422,736*. Washington, DC: U.S. Patent and Trademark Office.
86. Icard, P., Poulain, L., & Lincet, H. (2012). Understanding the central role of citrate in the metabolism of cancer cells. *Biochimica et Biophysica Acta (BBA)-Reviews on Cancer*, *1825*(1), 111-116.
87. Ieda, M., Fu, J. D., Delgado-Olguin, P., Vedantham, V., Hayashi, Y., Bruneau, B. G., & Srivastava, D. (2010). Direct reprogramming of fibroblasts into functional cardiomyocytes by defined factors. *Cell*, *142*(3), 375-386.
88. Imai, S. I., & Guarente, L. (2014). NAD+ and sirtuins in aging and disease. *Trends in cell biology*, *24*(8), 464-471.
89. Inagawa, K., Miyamoto, K., Yamakawa, H., Muraoka, N., Sadahiro, T., Umei, T., ... & Kurihara, C. (2012). Induction of cardiomyocyte-like cells in infarct hearts by gene transfer of Gata4, Mef2c, and Tbx5. *Circulation research*, *111*(9), 1147-1156.

90. Ito, K., & Suda, T. (2014). Metabolic requirements for the maintenance of self-renewing stem cells. *Nature reviews Molecular cell biology*, *15*(4), 243-256.
91. Ito, K., Carracedo, A., Weiss, D., Arai, F., Ala, U., Avigan, D. E., ... & Pandolfi, P. P. (2012). A PML–PPAR-δ pathway for fatty acid oxidation regulates hematopoietic stem cell maintenance. *Nature medicine*, *18*(9), 1350.
92. Jacobson, J., & Duchen, M. R. (2004). Interplay between mitochondria and cellular calcium signalling. *Molecular and cellular biochemistry*, *256*(1-2), 209-218.
93. Jaenisch, R., & Young, R. (2008). Stem cells, the molecular circuitry of pluripotency and nuclear reprogramming. *Cell*, *132*(4), 567-582.
94. Jarriault, S., Schwab, Y., & Greenwald, I. (2008). A Caenorhabditis elegans model for epithelial–neuronal transdifferentiation. *Proceedings of the National Academy of Sciences*, *105*(10), 3790-3795.
95. Jin, Y., Hoskins, R., & Horvitz, H. R. (1994). Control of type-D GABAergic neuron differentiation by C. elegans UNC-30 homeodomain protein. *Nature*, *372*(6508), 780-783.
96. John, J. C. S., Jokhi, R. P., & Barratt, C. L. (2005). The impact of mitochondrial genetics on male infertility. *International Journal of Andrology*, *28*(2), 65-73.
97. Jones, A. R., Francis, R., & Schedl, T. (1996). GLD-1, a Cytoplasmic Protein Essential for Oocyte Differentiation, Shows Stage-and Sex-Specific Expression duringCaenorhabditis elegansGerm line Development. *Developmental biology*, *180*(1), 165-183.
98. Jun, Y. J., Jang, S. M., Han, H. L., Lee, K. H., Jang, K. S., & Paik, S. S. (2011). Clinicopathologic significance of GLUT1 expression and its correlation with Apaf-1 in colorectal adenocarcinomas. *World Journal of Gastroenterology: WJG*, *17*(14), 1866.
99. Kaelin Jr, W. G., & McKnight, S. L. (2013). Influence of metabolism on epigenetics and disease. *Cell*, *153*(1), 56-69.
100. Kaelin, W.G., and Ratcliffe, P.J. (2008). Oxygen sensing by metazoans: the central role of the HIF hydroxylase pathway. Mol. Cell *30*, 393–402.
101. Kagias, K., Ahier, A., Fischer, N., & Jarriault, S. (2012). Members of the NODE (Nanog and Oct4-associated deacetylase) complex and SOX-2 promote the initiation of a natural cellular reprogramming event *in vivo*. *Proceedings of the National Academy of Sciences*, *109*(17), 6596-6601.
102. Kamath, R. S., Fraser, A. G., Dong, Y., Poulin, G., Durbin, R., Gotta, M., ... & Welchman, D. P. (2003). Systematic functional analysis of the Caenorhabditis elegans genome using RNAi. *Nature*, *421*(6920), 231-237.
103. Kaminska, B., Czapski, B., Guzik, R., Król, S. K., & Gielniewski, B. (2019). Consequences of IDH1/2 mutations in gliomas and an assessment of inhibitors targeting mutated IDH proteins. *Molecules*, *24*(5), 968.
104. Kang, K., Park, S., Kim, Y. S., Lee, S., & Back, K. (2009). Biosynthesis and biotechnological production of serotonin derivatives. *Applied microbiology and biotechnology*, *83*(1), 27-34.
105. Kelly, R. D., Sumer, H., McKenzie, M., Facucho-Oliveira, J., Trounce, I. A., Verma, P. J., & John, J. C. S. (2013). The effects of nuclear reprogramming on mitochondrial DNA replication. *Stem cell reviews and reports*, *9*(1), 1-15.
106. Kempa, S., Hummel, J., Schwemmer, T., Pietzke, M., Strehmel, N., Wienkoop, S., ... & Weckwerth, W. (2009). An automated GCxGC-TOF-MS protocol for batch-wise extraction and alignment of mass isotopomer matrixes from differential 13C-labelling experiments: a case study for photoautotrophic-mixotrophic grown Chlamydomonas reinhardtii cells. *Journal of basic microbiology*, *49*(1), 82-91.

107. Kilic-Eren, M., Boylu, T., & Tabor, V. (2013). Targeting PI3K/Akt represses Hypoxia inducible factor-1α activation and sensitizes Rhabdomyosarcoma and Ewing's sarcoma cells for apoptosis. *Cancer cell international*, *13*(1), 36.
108. Kimble, J., & Hirsh, D. (1979). The postembryonic cell lineages of the hermaphrodite and male gonads in Caenorhabditis elegans. *Developmental biology*, *70*(2), 396-417.
109. Klimova, T., and Chandel, N.S. (2008). Mitochondrial complex III regulates hypoxic activation of HIF. Cell Death Differ. *15*, 660–666.
110. Ko, Y. H., Lin, Z., Flomenberg, N., Pestell, R. G., Howell, A., Sotgia, F., ... & Martinez-Outschoorn, U. E. (2011). Glutamine fuels a vicious cycle of autophagy in the tumor stroma and oxidative mitochondrial metabolism in epithelial cancer cells: implications for preventing chemotherapy resistance. *Cancer biology & therapy*, *12*(12), 1085-1097.
111. Kochat, V., Equbal, Z., Baligar, P., Kumar, V., Srivastava, M., & Mukhopadhyay, A. (2017). JMJD3 aids in reprogramming of bone marrow progenitor cells to hepatic phenotype through epigenetic activation of hepatic transcription factors. *PloS one*, *12*(3), e0173977.
112. Kolundzic, E., Ofenbauer, A., Bulut, S. I., Uyar, B., Baytek, G., Sommermeier, A., ... & Akalin, A. (2018). FACT sets a barrier for cell fate reprogramming in Caenorhabditis elegans and human cells. *Developmental cell*, *46*(5), 611-626.
113. Kouzarides, T. (2002). Histone methylation in transcriptional control. *Current opinion in genetics & development*, *12*(2), 198-209.
114. Krell, D., Assoku, M., Galloway, M., Mulholland, P., Tomlinson, I., & Bardella, C. (2011). Screen for IDH1, IDH2, IDH3, D2HGDH and L2HGDH mutations in glioblastoma. *PloS one*, *6*(5), e19868.
115. Krell, J., Frampton, A. E., Mirnezami, R., Harding, V., De Giorgio, A., Alonso, L. R., ... & Castellano, L. (2014). Growth arrest-specific transcript 5 associated snoRNA levels are related to p53 expression and DNA damage in colorectal cancer. *PloS one*, *9*(6), e98561.
116. Kuich, P. H. J. L., Hoffmann, N., & Kempa, S. (2015). Maui-VIA: a user-friendly software for visual identification, alignment, correction, and quantification of gas chromatography–mass spectrometry data. *Frontiers in bioengineering and biotechnology*, *2*, 84.
117. Kulessa, H., Frampton, J., & Graf, T. (1995). GATA-1 reprograms avian myelomonocytic cell lines into eosinophils, thromboblasts, and erythroblasts. *Genes & development*, *9*(10), 1250-1262.
118. Kumsta, C., & Hansen, M. (2012). C. elegans rrf-1 mutations maintain RNAi efficiency in the soma in addition to the germ line. *PloS one*, *7*(5), e35428.
119. Kutscher, L. M., & Shaham, S. (2014). Forward and reverse mutagenesis in C. elegans. *WormBook: the online review of C. elegans biology*, 1.
120. Kuzmichev, A., Nishioka, K., Erdjument-Bromage, H., Tempst, P., & Reinberg, D. (2002). Histone methyltransferase activity associated with a human multiprotein complex containing the Enhancer of Zeste protein. *Genes & development*, *16*(22), 2893-2905.
121. Ladewig, J., Koch, P., & Brüstle, O. (2013). Leveling Waddington: the emergence of direct programming and the loss of cell fate hierarchies. *Nature reviews Molecular cell biology*, *14*(4), 225-236.
122. Lee, C., Kim, S. J., Jeong, D. G., Lee, S. M., & Ryu, S. E. (2003). Structure of human FIH-1 reveals a unique active site pocket and interaction sites for HIF-1 and von Hippel-Lindau. *Journal of Biological Chemistry*, *278*(9), 7558-7563.

123. Lee, P. Y., Chien, Y., Chiou, G. Y., Lin, C. H., Chiou, C. H., & Tarng, D. C. (2012). Induced pluripotent stem cells without c-Myc attenuate acute kidney injury via downregulating the signaling of oxidative stress and inflammation in ischemia–reperfusion rats. *Cell transplantation*, *21*(12), 2569-2585.
124. Li, H., Collado, M., Villasante, A., Strati, K., Ortega, S., Cañamero, M., ... & Serrano, M. (2009). The Ink4/Arf locus is a barrier for iPS cell reprogramming. *Nature*, *460*(7259), 1136-1139.
125. Li, R., Liang, J., Ni, S., Zhou, T., Qing, X., Li, H., ... & Qin, B. (2010). A mesenchymal-to-epithelial transition initiates and is required for the nuclear reprogramming of mouse fibroblasts. *Cell stem cell*, *7*(1), 51-63.
126. Li, W., Chen, C., Zhao, X., Ye, H., Zhao, Y., Fu, Z., ... & Li, Z. (2017). HIF-2α regulates non-canonical glutamine metabolism via activation of PI 3K/mTORC 2 pathway in human pancreatic ductal adenocarcinoma. *Journal of cellular and molecular medicine*, *21*(11), 2896-2908.
127. Lin, S. J., Ford, E., Haigis, M., Liszt, G., & Guarente, L. (2004). Calorie restriction extends yeast life span by lowering the level of NADH. *Genes & development*, *18*(1), 12-16.
128. Liu, S., Cadoux-Hudson, T., & Schofield, C. J. (2020). Isocitrate dehydrogenase variants in cancer—Cellular consequences and therapeutic opportunities. *Current Opinion in Chemical Biology*, *57*, 122-134.
129. Liu, X., Qiao, Y., Ting, X., & Si, W. (2020). Isocitrate dehydrogenase 3A, a rate-limiting enzyme of the TCA cycle, promotes hepatocellular carcinoma migration and invasion through regulation of MTA1, a core component of the NuRD complex. *American Journal of Cancer Research*, *10*(10), 3212.
130. Liu, Y., Miao, Q., Yuan, J., Zhang, P., Li, S., Rao, Z., ... & Cheng, L. (2015). Ascl1 converts dorsal midbrain astrocytes into functional neurons *in vivo*. *Journal of Neuroscience*, *35*(25), 9336-9355.
131. Loi, M., Müller, A., Steinbach, K., Niven, J., da Silva, R. B., Paul, P., ... & Annaheim, N. (2016). Macroautophagy proteins control MHC class I levels on dendritic cells and shape anti-viral CD8+ T cell responses. *Cell reports*, *15*(5), 1076-1087.
132. Losman, J. A., & Kaelin, W. G. (2013). What a difference a hydroxyl makes: mutant IDH,(R)-2-hydroxyglutarate, and cancer. *Genes & development*, *27*(8), 836-852.
133. Lunt, S. Y., & Vander Heiden, M. G. (2011). Aerobic glycolysis: meeting the metabolic requirements of cell proliferation. *Annual review of cell and developmental biology*, *27*, 441-464.
134. Ly, C. H., Lynch, G. S., & Ryall, J. G. (2020). A Metabolic Roadmap for Somatic Stem Cell Fate. *Cell Metabolism*.
135. Ma, T., Peng, Y., Huang, W., Liu, Y., & Ding, J. (2017). The β and γ subunits play distinct functional roles in the α 2 βγ heterotetramer of human NAD-dependent isocitrate dehydrogenase. *Scientific reports*, *7*(1), 1-12.
136. Madala, H. R., Punganuru, S. R., Arutla, V., Misra, S., Thomas, T. J., & Srivenugopal, K. S. (2018). Beyond Brooding on Oncometabolic Havoc in IDH-Mutant Gliomas and AML: Current and Future Therapeutic Strategies. *Cancers*, *10*(2), 49.
137. Mandal, S., Lindgren, A. G., Srivastava, A. S., Clark, A. T., & Banerjee, U. (2011). Mitochondrial function controls proliferation and early differentiation potential of embryonic stem cells. *Stem cells*, *29*(3), 486-495.
138. Mango, S. E., Lambie, E. J., & Kimble, J. (1994). The pha-4 gene is required to generate the pharyngeal primordium of Caenorhabditis elegans. *Development*, *120*(10), 3019-3031.

139. Markolovic, S., Leissing, T. M., Chowdhury, R., Wilkins, S. E., Lu, X., & Schofield, C. J. (2016). Structure–function relationships of human JmjC oxygenases—demethylases versus hydroxylases. *Current opinion in structural biology*, *41*, 62-72.
140. Matoba, S., & Zhang, Y. (2018). Somatic cell nuclear transfer reprogramming: mechanisms and applications. *Cell Stem Cell*, *23*(4), 471-485.
141. Matsumura, H., Tada, M., Otsuji, T., Yasuchika, K., Nakatsuji, N., Surani, A., & Tada, T. (2007). Targeted chromosome elimination from ES-somatic hybrid cells. *Nature methods*, *4*(1), 23-25.
142. Mattout, A., Biran, A., & Meshorer, E. (2011). Global epigenetic changes during somatic cell reprogramming to iPS cells. *Journal of molecular cell biology*, *3*(6), 341-350.
143. May, J. L., Kouri, F. M., Hurley, L. A., Liu, J., Tommasini-Ghelfi, S., Ji, Y., ... & Stegh, A. H. (2019). IDH3α regulates one-carbon metabolism in glioblastoma. *Science advances*, *5*(1), eaat0456.
144. Melton, C., Judson, R. L., & Blelloch, R. (2010). Opposing microRNA families regulate self-renewal in mouse embryonic stem cells. *Nature*, *463*(7281), 621-626.
145. Menon, S., & Manning, B. D. (2008). Common corruption of the mTOR signaling network in human tumors. *Oncogene*, *27*(2), S43-S51.
146. Mihaylova, M. M., & Shaw, R. J. (2011). The AMPK signalling pathway coordinates cell growth, autophagy and metabolism. *Nature cell biology*, *13*(9), 1016-1023.
147. Mikkelsen, T. S., Hanna, J., Zhang, X., Ku, M., Wernig, M., Schorderet, P., ... & Meissner, A. (2008). Dissecting direct reprogramming through integrative genomic analysis. *Nature*, *454*(7200), 49-55.
148. Miles, D. C., de Vries, N. A., Gisler, S., Lieftink, C., Akhtar, W., Gogola, E., ... & Beijersbergen, R. L. (2017). TRIM28 is an epigenetic barrier to induced pluripotent stem cell reprogramming. *Stem Cells*, *35*(1), 147-157.
149. Milne, T. A., Briggs, S. D., Brock, H. W., Martin, M. E., Gibbs, D., Allis, C. D., & Hess, J. L. (2002). MLL targets SET domain methyltransferase activity to Hox gene promoters. *Molecular cell*, *10*(5), 1107-1117.
150. Molenaar, R. J., Botman, D., Smits, M. A., Hira, V. V., van Lith, S. A., Stap, J., ... & van Noorden, C. J. (2015). Radioprotection of IDH1-mutated cancer cells by the IDH1-mutant inhibitor AGI-5198. *Cancer research*, *75*(22), 4790-4802.
151. Molenaar, R., Sanikommu, S. R., Patel, B. J., Przychodzen, B., van Noorden, C. J., Radivoyevitch, T., ... & Maciejewski, J. P. (2015). Whole-exome sequencing identifies germ line IDH2 and IDH3 mutations that predispose to myeloid neoplasms.
152. Moussaieff, A., Rouleau, M., Kitsberg, D., Cohen, M., Levy, G., Barasch, D., ... & Bomze, D. (2015). Glycolysis-mediated changes in acetyl-CoA and histone acetylation control the early differentiation of embryonic stem cells. *Cell metabolism*, *21*(3), 392-402.
153. Müller, J., Hart, C. M., Francis, N. J., Vargas, M. L., Sengupta, A., Wild, B., ... & Simon, J. A. (2002). Histone methyltransferase activity of a Drosophila Polycomb group repressor complex. *Cell*, *111*(2), 197-208.
154. Nagao, A., Kobayashi, M., Koyasu, S., Chow, C. C., & Harada, H. (2019). HIF-1-dependent reprogramming of glucose metabolic pathway of cancer cells and its therapeutic significance. *International journal of molecular sciences*, *20*(2), 238.
155. Nagaraj, R., Sharpley, M. S., Chi, F., Braas, D., Zhou, Y., Kim, R., ... & Banerjee, U. (2017). Nuclear localization of mitochondrial TCA cycle enzymes as a critical step in mammalian zygotic genome activation. *Cell*, *168*(1-2), 210-223.
156. Nakamura, T., Mori, T., Tada, S., Krajewski, W., Rozovskaia, T., Wassell, R., ... & Canaani, E. (2002). ALL-1 is a histone methyltransferase that assembles a

supercomplex of proteins involved in transcriptional regulation. *Molecular cell*, *10*(5), 1119-1128.
157. Nguyen, T. L., & Durán, R. V. (2018). Glutamine metabolism in cancer therapy. *Cancer Drug Resist*, *1*, 126-38.
158. Nikinmaa, M., McCairns, R. J., Nikinmaa, M. W., Vuori, K. A., Kanerva, M., Leinonen, T., Primmer, C. R., Merilä, J., & Leder, E. H. (2013). Transcription and redox enzyme activities: comparison of equilibrium and disequilibrium levels in the three-spined stickleback. *Proceedings. Biological sciences*, *280*(1755), 20122974.
159. Ogura, A., Inoue, K., & Wakayama, T. (2013). Recent advancements in cloning by somatic cell nuclear transfer. *Philosophical Transactions of the Royal Society B: Biological Sciences*, *368*(1609), 20110329.
160. Okita, K., Ichisaka, T., & Yamanaka, S. (2007). Generation of germ line-competent induced pluripotent stem cells. *nature*, *448*(7151), 313-317.
161. Onder, T. T., Kara, N., Cherry, A., Sinha, A. U., Zhu, N., Bernt, K. M., ... & Lander, E. S. (2012). Chromatin-modifying enzymes as modulators of reprogramming. *Nature*, *483*(7391), 598-602.
162. Orlando, V. (2003). Polycomb, epigenomes, and control of cell identity. *Cell*, *112*(5), 599-606.
163. Otera, H., Ishihara, N., & Mihara, K. (2013). New insights into the function and regulation of mitochondrial fission. *Biochimica et Biophysica Acta (BBA)-Molecular Cell Research*, *1833*(5), 1256-1268.
164. Pang, Y., Zheng, B., Kimberly, S. L., Cai, Z., Rhodes, P. G., & Lin, R. C. (2012). Neuron-oligodendrocyte myelination co-culture derived from embryonic rat spinal cord and cerebral cortex. *Brain and behavior*, *2*(1), 53-67.
165. Parsons, D. W., Jones, S., Zhang, X., Lin, J. C. H., Leary, R. J., Angenendt, P., ... & Kinzler, K. W. (2008). An integrated genomic analysis of human glioblastoma multiforme. *science*, *321*(5897), 1807-1812.
166. Patel, T., & Hobert, O. (2017). Coordinated control of terminal differentiation and restriction of cellular plasticity. *Elife*, *6*, e24100.
167. Patel, T., Tursun, B., Rahe, D. P., & Hobert, O. (2012). Removal of Polycomb repressive complex 2 makes C. elegans germ cells susceptible to direct conversion into specific somatic cell types. *Cell reports*, *2*(5), 1178-1186.
168. Pereira, M., Birtele, M., Shrigley, S., Benitez, J. A., Hedlund, E., Parmar, M., & Ottosson, D. R. (2017). Direct reprogramming of resident NG2 glia into neurons with properties of fast-spiking parvalbumin-containing interneurons. *Stem cell reports*, *9*(3), 742-751.
169. Pereira, S. L., Grãos, M., Rodrigues, A. S., Anjo, S. I., Carvalho, R. A., Oliveira, P. J., ... & Ramalho-Santos, J. (2013). Inhibition of mitochondrial complex III blocks neuronal differentiation and maintains embryonic stem cell pluripotency. *PloS one*, *8*(12), e82095.
170. Pietzke, M., Zasada, C., Mudrich, S., & Kempa, S. (2014). Decoding the dynamics of cellular metabolism and the action of 3-bromopyruvate and 2-deoxyglucose using pulsed stable isotope-resolved metabolomics. *Cancer & metabolism*, *2*(1), 9.
171. Pires, C. F., F Rosa, F., Kurochkin, I., & Pereira, C. F. (2019). Understanding and modulating immunity with cell reprogramming. *Frontiers in Immunology*, *10*, 2809.
172. Pollard, P. J., Loenarz, C., Mole, D. R., McDonough, M. A., Gleadle, J. M., Schofield, C. J., & Ratcliffe, P. J. (2008). Regulation of Jumonji-domain-containing histone demethylases by hypoxia-inducible factor (HIF)-1α. *Biochemical Journal*, *416*(3), 387-394.

173. Polo, J. M., Liu, S., Figueroa, M. E., Kulalert, W., Eminli, S., Tan, K. Y., ... & Natesan, S. (2010). Cell type of origin influences the molecular and functional properties of mouse induced pluripotent stem cells. *Nature biotechnology*, *28*(8), 848-855.
174. Prieto, J., León, M., Ponsoda, X., Sendra, R., Bort, R., Ferrer-Lorente, R., ... & Torres, J. (2016). Early ERK1/2 activation promotes DRP1-dependent mitochondrial fission necessary for cell reprogramming. *Nature communications*, *7*(1), 1-13.
175. Prigione, A., & Adjaye, J. (2010). Modulation of mitochondrial biogenesis and bioenergetic metabolism upon in vitro and *in vivo* differentiation of human ES and iPS cells. *International Journal of Developmental Biology*, *54*(11-12), 1729-1741.
176. Qian, L., Huang, Y., Spencer, C. I., Foley, A., Vedantham, V., Liu, L., ... & Srivastava, D. (2012). *In vivo* reprogramming of murine cardiac fibroblasts into induced cardiomyocytes. *Nature*, *485*(7400), 593-598.
177. Qian, W., Choi, S., Gibson, G. A., Watkins, S. C., Bakkenist, C. J., & Van Houten, B. (2012). Mitochondrial hyperfusion induced by loss of the fission protein Drp1 causes ATM-dependent G2/M arrest and aneuploidy through DNA replication stress. *Journal of cell science*, *125*(23), 5745-5757.
178. Qin, H., Diaz, A., Blouin, L., Lebbink, R. J., Patena, W., Tanbun, P., ... & Ramalho-Santos, M. (2014). Systematic identification of barriers to human iPSC generation. *Cell*, *158*(2), 449-461.
179. Raizen, D. M., Zimmerman, J. E., Maycock, M. H., Ta, U. D., You, Y. J., Sundaram, M. V., & Pack, A. I. (2008). Lethargus is a Caenorhabditis elegans sleep-like state. *Nature*, *451*(7178), 569-572.
180. Reitzer, L. J., Wice, B. M., & Kennell, D. (1979). Evidence that glutamine, not sugar, is the major energy source for cultured HeLa cells. *Journal of Biological Chemistry*, *254*(8), 2669-2676.
181. Richard, J. P., Zuryn, S., Fischer, N., Pavet, V., Vaucamps, N., & Jarriault, S. (2011). Direct *in vivo* cellular reprogramming involves transition through discrete, non-pluripotent steps. *Development*, *138*(8), 1483-1492.
182. Roessner-Tunali, U., Hegemann, B., Lytovchenko, A., Carrari, F., Bruedigam, C., Granot, D., & Fernie, A. R. (2003). Metabolic profiling of transgenic tomato plants overexpressing hexokinase reveals that the influence of hexose phosphorylation diminishes during fruit development. *Plant Physiology*, *133*(1), 84-99.
183. Ryall, J. G., Cliff, T., Dalton, S., & Sartorelli, V. (2015). Metabolic reprogramming of stem cell epigenetics. *Cell stem cell*, *17*(6), 651-662.
184. Sabari, B. R., Tang, Z., Huang, H., Yong-Gonzalez, V., Molina, H., Kong, H. E., ... & Roeder, R. G. (2015). Intracellular crotonyl-CoA stimulates transcription through p300-catalyzed histone crotonylation. *Molecular cell*, *58*(2), 203-215.
185. Samavarchi-Tehrani, P., Golipour, A., David, L., Sung, H. K., Beyer, T. A., Datti, A., ... & Wrana, J. L. (2010). Functional genomics reveals a BMP-driven mesenchymal-to-epithelial transition in the initiation of somatic cell reprogramming. *Cell stem cell*, *7*(1), 64-77.
186. Sandoval, I. T., Delacruz, R. G. C., Miller, B. N., Hill, S., Olson, K. A., Gabriel, A. E., ... & Jones, D. A. (2017). A metabolic switch controls intestinal differentiation downstream of Adenomatous polyposis coli (APC). *Elife*, *6*, e22706.
187. Schell, J. C., Wisidagama, D. R., Bensard, C., Zhao, H., Wei, P., Tanner, J., ... & Olson, K. A. (2017). Control of intestinal stem cell function and proliferation by mitochondrial pyruvate metabolism. *Nature cell biology*, *19*(9), 1027-1036.
188. Schläpfer, T. (1963). Der Einfluß des adulten Wirtsmilieus auf die Entwicklung von larvalen Augenantennen-Imaginalscheiben vonDrosophila melanogaster. *Wilhelm Roux'Archiv für Entwicklungsmechanik der Organismen*, *154*(4), 378-404.

189. Seelk, S., Adrian-Kalchhauser, I., Hargitai, B., Hajduskova, M., Gutnik, S., Tursun, B., & Ciosk, R. (2016). Increasing Notch signaling antagonizes PRC2-mediated silencing to promote reprograming of germ cells into neurons. *Elife*, *5*, e15477.
190. Serocki, M., Bartoszewska, S., Janaszak-Jasiecka, A., Ochocka, R. J., Collawn, J. F., & Bartoszewski, R. (2018). miRNAs regulate the HIF switch during hypoxia: a novel therapeutic target. *Angiogenesis*, *21*(2), 183-202.
191. Shahbazian, M. D., & Grunstein, M. (2007). Functions of site-specific histone acetylation and deacetylation. *Annual review of biochemistry*, *76*.
192. Shi, Yujiang, et al. "Histone demethylation mediated by the nuclear amine oxidase homolog LSD1." *Cell* 119.7 (2004): 941-953.
193. Shyh-Chang, N., & Ng, H. H. (2017). The metabolic programming of stem cells. *Genes & development*, *31*(4), 336-346.
194. Shyh-Chang, N., Daley, G. Q., & Cantley, L. C. (2013). Stem cell metabolism in tissue development and aging. *Development*, *140*(12), 2535-2547.
195. Simsek, T., Kocabas, F., Zheng, J., DeBerardinis, R. J., Mahmoud, A. I., Olson, E. N., ... & Sadek, H. A. (2010). The distinct metabolic profile of hematopoietic stem cells reflects their location in a hypoxic niche. *Cell stem cell*, *7*(3), 380-390.
196. Smirnova, E., Griparic, L., Shurland, D. L., & Van Der Bliek, A. M. (2001). Dynamin-related protein Drp1 is required for mitochondrial division in mammalian cells. *Molecular biology of the cell*, *12*(8), 2245-2256.
197. Smith, S. S., Kan, J. L. C., Baker, D. J., Kaplan, B. E., & Dembek, P. (1991). Recognition of unusual DNA structures by human DNA (cytosine-5) methyltransferase. *Journal of molecular biology*, *217*(1), 39-51.
198. Smith, Z. D., Sindhu, C., & Meissner, A. (2016). Molecular features of cellular reprogramming and development. *Nature Reviews Molecular Cell Biology*, *17*(3), 139-154.
199. Sonnhammer, E. L., & Durbin, R. (1997). Analysis of Protein Domain Families inCaenorhabditis elegans. *Genomics*, *46*(2), 200-216.
200. Soojin, V. Y. (2012). Birds do it, bees do it, worms and ciliates do it too: DNA methylation from unexpected corners of the tree of life. *Genome biology*, *13*(10), 174.
201. Spanier, B., Rubio-Aliaga, I., Hu, H., & Daniel, H. (2010). Altered signalling from germ line to intestine pushes daf-2; pept-1 Caenorhabditis elegans into extreme longevity. *Aging cell*, *9*(4), 636-646.
202. Srivastava, D., & DeWitt, N. (2016). *In vivo* cellular reprogramming: the next generation. *Cell*, *166*(6), 1386-1396.
203. St. John, J. C., Ramalho-Santos, J., Gray, H. L., Petrosko, P., Rawe, V. Y., Navara, C. S., ... & Schatten, G. P. (2005). The expression of mitochondrial DNA transcription factors during early cardiomyocyte in vitro differentiation from human embryonic stem cells. *Cloning and stem cells*, *7*(3), 141-153.
204. Stadtfeld, M., Maherali, N., Breault, D. T., & Hochedlinger, K. (2008). Defining molecular cornerstones during fibroblast to iPS cell reprogramming in mouse. *Cell stem cell*, *2*(3), 230-240.
205. Stegh, A. (2017). CSIG-21. IDH3 promotes glioblastoma growth through regulation of one carbon metabolism. *Neuro-oncology*, *19*(Suppl 6), vi54.
206. Stehling, O., Wilbrecht, C., & Lill, R. (2014). Mitochondrial iron–sulfur protein biogenesis and human disease. *Biochimie*, *100*, 61-77.
207. Stewart, M. D., Zelin, E., Dhall, A., Walsh, T., Upadhyay, E., Corn, J. E., ... & Klevit, R. E. (2018). BARD1 is necessary for ubiquitylation of nucleosomal histone H2A and for transcriptional regulation of estrogen metabolism genes. *Proceedings of the National Academy of Sciences*, *115*(6), 1316-1321.

208. Suda, T., Takubo, K., & Semenza, G. L. (2011). Metabolic regulation of hematopoietic stem cells in the hypoxic niche. *Cell stem cell*, *9*(4), 298-310.
209. Suhr, S. T., Chang, E. A., Tjong, J., Alcasid, N., Perkins, G. A., Goissis, M. D., ... & Cibelli, J. B. (2010). Mitochondrial rejuvenation after induced pluripotency. *PloS one*, *5*(11), e14095.
210. Sulston, J. E. (1983, January). Neuronal cell lineages in the nematode Caenorhabditis elegans. In *Cold Spring Harbor symposia on quantitative biology* (Vol. 48, pp. 443-452). Cold Spring Harbor Laboratory Press.
211. Sulston, J. E., & Horvitz, H. R. (1977). Post-embryonic cell lineages of the nematode, Caenorhabditis elegans. *Developmental biology*, *56*(1), 110-156.
212. Taguchi, N., Ishihara, N., Jofuku, A., Oka, T., & Mihara, K. (2007). Mitotic phosphorylation of dynamin-related GTPase Drp1 participates in mitochondrial fission. *Journal of Biological Chemistry*, *282*(15), 11521-11529.
213. Tait, S. W., & Green, D. R. (2010). Mitochondria and cell death: outer membrane permeabilization and beyond. *Nature reviews Molecular cell biology*, *11*(9), 621-632.
214. Takahashi, K., Tanabe, K., Ohnuki, M., Narita, M., Ichisaka, T., Tomoda, K., & Yamanaka, S. (2007). Induction of pluripotent stem cells from adult human fibroblasts by defined factors. *cell*, *131*(5), 861-872.
215. Takubo, K., Goda, N., Yamada, W., Iriuchishima, H., Ikeda, E., Kubota, Y., ... & Suda, T. (2010). Regulation of the HIF-1α level is essential for hematopoietic stem cells. *Cell stem cell*, *7*(3), 391-402.
216. Tatapudy, S., Aloisio, F., Barber, D., & Nystul, T. (2017). Cell fate decisions: emerging roles for metabolic signals and cell morphology. *EMBO reports*, *18*(12), 2105-2118.
217. TeSlaa, T., Chaikovsky, A. C., Lipchina, I., Escobar, S. L., Hochedlinger, K., Huang, J., ... & Teitell, M. A. (2016). α-Ketoglutarate accelerates the initial differentiation of primed human pluripotent stem cells. *Cell metabolism*, *24*(3), 485-493.
218. TeSlaa, T., Setoguchi, K., & Teitell, M. A. (2016, April). Mitochondria in human pluripotent stem cell apoptosis. In *Seminars in cell & developmental biology* (Vol. 52, pp. 76-83). Academic Press.
219. Theret, M., Gsaier, L., Schaffer, B., Juban, G., Ben Larbi, S., Weiss-Gayet, M., ... & Sanz, P. (2017). AMPK α1-LDH pathway regulates muscle stem cell self-renewal by controlling metabolic homeostasis. *The EMBO journal*, *36*(13), 1946-1962.
220. Tormos, K. V., Anso, E., Hamanaka, R. B., Eisenbart, J., Joseph, J., Kalyanaraman, B., & Chandel, N. S. (2011). Mitochondrial complex III ROS regulate adipocyte differentiation. *Cell metabolism*, *14*(4), 537-544.
221. Tran, K. A., Pietrzak, S. J., Zaidan, N. Z., Siahpirani, A. F., McCalla, S. G., Zhou, A. S., ... & Sridharan, R. (2019). Defining reprogramming checkpoints from single-cell analyses of induced pluripotency. *Cell reports*, *27*(6), 1726-1741.
222. Tsukada, Y. I., Fang, J., Erdjument-Bromage, H., Warren, M. E., Borchers, C. H., Tempst, P., & Zhang, Y. (2006). Histone demethylation by a family of JmjC domain-containing proteins. *Nature*, *439*(7078), 811-816.
223. Tursun B. (2012). Cellular reprogramming processes in Drosophila and C. elegans. *Current opinion in genetics & development*, *22*(5), 475–484.
224. Tursun, B., Patel, T., Kratsios, P., & Hobert, O. (2011). Direct conversion of C. elegans germ cells into specific neuron types. *Science*, *331*(6015), 304-308.
225. Uchida, O., Nakano, H., Koga, M., & Ohshima, Y. (2003). The C. elegans che-1 gene encodes a zinc finger transcription factor required for specification of the ASE chemosensory neurons. *Development*, *130*(7), 1215-1224.

226. Utikal, J., Polo, J. M., Stadtfeld, M., Maherali, N., Kulalert, W., Walsh, R. M., ... & Hochedlinger, K. (2009). Immortalization eliminates a roadblock during cellular reprogramming into iPS cells. *Nature*, *460*(7259), 1145-1148.
227. Van Blerkom, J. (2008). Mitochondria as regulatory forces in oocytes, preimplantation embryos and stem cells. *Reproductive biomedicine online*, *16*(4), 553-569.
228. Van Blerkom, J. (2009, May). Mitochondria in early mammalian development. In *Seminars in cell & developmental biology* (Vol. 20, No. 3, pp. 354-364). Academic Press.
229. Vander Heiden, M. G., Cantley, L. C., & Thompson, C. B. (2009). Understanding the Warburg effect: the metabolic requirements of cell proliferation. *science*, *324*(5930), 1029-1033.
230. Vannini, N., Girotra, M., Naveiras, O., Nikitin, G., Campos, V., Giger, S., ... & Lutolf, M. P. (2016). Specification of haematopoietic stem cell fate via modulation of mitochondrial activity. *Nature communications*, *7*(1), 1-9.
231. Vierbuchen, T., & Wernig, M. (2012). Molecular roadblocks for cellular reprogramming. *Molecular cell*, *47*(6), 827-838.
232. Vierbuchen, T., Ostermeier, A., Pang, Z. P., Kokubu, Y., Südhof, T. C., & Wernig, M. (2010). Direct conversion of fibroblasts to functional neurons by defined factors. *Nature*, *463*(7284), 1035-1041.
233. Villar, V. H., Merhi, F., Djavaheri-Mergny, M., & Durán, R. V. (2015). Glutaminolysis and autophagy in cancer. *Autophagy*, *11*(8), 1198-1208.
234. Waddington, C. H. (1957). The Strategy of the Genes. Allen.
235. Walport, L. J., Hopkinson, R. J., Chowdhury, R., Schiller, R., Ge, W., Kawamura, A., & Schofield, C. J. (2016). Arginine demethylation is catalysed by a subset of JmjC histone lysine demethylases. *Nature communications*, *7*(1), 1-12.
236. Wang, R., Dillon, C. P., Shi, L. Z., Milasta, S., Carter, R., Finkelstein, D., ... & Green, D. R. (2011). The transcription factor Myc controls metabolic reprogramming upon T lymphocyte activation. *Immunity*, *35*(6), 871-882.
237. Wang, W., Yang, J., Liu, H., Lu, D., Chen, X., Zenonos, Z., ... & Bradley, A. (2011). Rapid and efficient reprogramming of somatic cells to induced pluripotent stem cells by retinoic acid receptor gamma and liver receptor homolog 1. *Proceedings of the National Academy of Sciences*, *108*(45), 18283-18288.
238. Wang, Y., Agarwal, E., Bertolini, I., Ghosh, J. C., Seo, J. H., & Altieri, D. C. (2019). IDH2 reprograms mitochondrial dynamics in cancer through a HIF-1α-regulated pseudohypoxic state. *The FASEB Journal*, *33*(12), 13398-13411.
239. Wangkheimayum Madal, D., & Saikia, L. P. (2018). Multiple Object Detection using Deep Neural Networks.
240. Weintraub, H., Tapscott, S. J., Davis, R. L., Thayer, M. J., Adam, M. A., Lassar, A. B., & Miller, A. D. (1989). Activation of muscle-specific genes in pigment, nerve, fat, liver, and fibroblast cell lines by forced expression of MyoD. *Proceedings of the National Academy of Sciences*, *86*(14), 5434-5438.
241. Wellen, K. E., Hatzivassiliou, G., Sachdeva, U. M., Bui, T. V., Cross, J. R., & Thompson, C. B. (2009). ATP-citrate lyase links cellular metabolism to histone acetylation. *Science*, *324*(5930), 1076-1080.
242. Wernig, M., Meissner, A., Foreman, R., Brambrink, T., Ku, M., Hochedlinger, K., ... & Jaenisch, R. (2007). In vitro reprogramming of fibroblasts into a pluripotent ES-cell-like state. *nature*, *448*(7151), 318-324.
243. White, J. G., Southgate, E., Thomson, J. N., & Brenner, S. (1986). The structure of the nervous system of the nematode Caenorhabditis elegans. *Philos Trans R Soc Lond B Biol Sci*, *314*(1165), 1-340.

244. Wilson, F. H., Hariri, A., Farhi, A., Zhao, H., Petersen, K. F., Toka, H. R., ... & Scheinman, S. J. (2004). A cluster of metabolic defects caused by mutation in a mitochondrial tRNA. *Science*, *306*(5699), 1190-1194.
245. Worringer, K. A., Rand, T. A., Hayashi, Y., Sami, S., Takahashi, K., Tanabe, K., ... & Yamanaka, S. (2014). The let-7/LIN-41 pathway regulates reprogramming to human induced pluripotent stem cells by controlling expression of prodifferentiation genes. *Cell stem cell*, *14*(1), 40-52.
246. Wurmus, R., Uyar, B., Osberg, B., Franke, V., Gosdschan, A., Wreczycka, K., ... & Akalin, A. (2018). PiGx: reproducible genomics analysis pipelines with GNU Guix. *Gigascience*, *7*(12), giy123.
247. Xia, X., Lemieux, M. E., Li, W., Carroll, J. S., Brown, M., Liu, X. S., & Kung, A. L. (2009). Integrative analysis of HIF binding and transactivation reveals its role in maintaining histone methylation homeostasis. *Proceedings of the National Academy of Sciences*, *106*(11), 4260-4265.
248. Xie, H., Ye, M., Feng, R., & Graf, T. (2004). Stepwise reprogramming of B cells into macrophages. *Cell*, *117*(5), 663-676.
249. Yamanaka, S., & Blau, H. M. (2010). Nuclear reprogramming to a pluripotent state by three approaches. *Nature*, *465*(7299), 704-712.
250. Yan, H., Parsons, D. W., Jin, G., McLendon, R., Rasheed, B. A., Yuan, W., ... & Bigner, D. D. (2009). IDH1 and IDH2 mutations in gliomas. *New England journal of medicine*, *360*(8), 765-773.
251. Yu, S., Avery, L., Baude, E., and Garbers, D.L. (1997). Guanylyl cyclase expression in specific sensory neurons: a new family of chemosensory receptors. Proc. Natl. Acad. Sci. U.S.a. *94*, 3384–3387.
252. Yuzyuk, T., Fakhouri, T. H. I., Kiefer, J., & Mango, S. E. (2009). The polycomb complex protein mes-2/E (z) promotes the transition from developmental plasticity to differentiation in C. elegans embryos. *Developmental cell*, *16*(5), 699-710.
253. Zambrano, A., Molt, M., Uribe, E., & Salas, M. (2019). Glut 1 in cancer cells and the inhibitory action of resveratrol as a potential therapeutic strategy. *International Journal of Molecular Sciences*, *20*(13), 3374.
254. Zeng, L., Morinibu, A., Kobayashi, M., Zhu, Y., Wang, X., Goto, Y., ... & Itasaka, S. (2015). Aberrant IDH3α expression promotes malignant tumor growth by inducing HIF-1-mediated metabolic reprogramming and angiogenesis. *Oncogene*, *34*(36), 4758-4766.
255. Zeng, S. S., Yamashita, T., Kondo, M., Nio, K., Hayashi, T., Hara, Y., ... & Kaneko, S. (2014). The transcription factor SALL4 regulates stemness of EpCAM-positive hepatocellular carcinoma. *Journal of hepatology*, *60*(1), 127-134.
256. Zhang, D., Wang, Y., Shi, Z., Liu, J., Sun, P., Hou, X., ... & Mi, J. (2015). Metabolic reprogramming of cancer-associated fibroblasts by IDH3α downregulation. *Cell reports*, *10*(8), 1335-1348.
257. Zhang, Y., & Reinberg, D. (2001). Transcription regulation by histone methylation: interplay between different covalent modifications of the core histone tails. *Genes & development*, *15*(18), 2343-2360.
258. Zhao, S., Lin, Y., Xu, W., Jiang, W., Zha, Z., Wang, P., Yu, W., Li, Z., Gong, L., Peng, Y., et al. (2009). Glioma-derived mutations in IDH1 dominantly inhibit IDH1 catalytic activity and induce HIF-1. Science *324*, 261–265.
259. Zhou, Q., Brown, J., Kanarek, A., Rajagopal, J., & Melton, D. A. (2008). *In vivo* reprogramming of adult pancreatic exocrine cells to β-cells. *nature*, *455*(7213), 627-632.

260. Zhou, W., Choi, M., Margineantu, D., Margaretha, L., Hesson, J., Cavanaugh, C., ... & Ruohola-Baker, H. (2012). HIF1α induced switch from bivalent to exclusively glycolytic metabolism during ESC-to-EpiSC/hESC transition. *The EMBO journal*, *31*(9), 2103-2116.
261. Zhou, Yang, et al. "Bmi1 is a key epigenetic barrier to direct cardiac reprogramming." *Cell stem cell* 18.3 (2016): 382-395.
262. Zhu, J., Fukushige, T., McGhee, J. D., & Rothman, J. H. (1998). Reprogramming of early embryonic blastomeres into endodermal progenitors by a Caenorhabditis elegans GATA factor. *Genes & development*, *12*(24), 3809-3814.
263. Zhu, X., Enomoto, K., Zhao, L., Zhu, Y. J., Willingham, M. C., Meltzer, P., ... & Cheng, S. Y. (2017). Bromodomain and extraterminal protein inhibitor JQ1 suppresses thyroid tumor growth in a mouse model. *Clinical Cancer Research*, *23*(2), 430-440.
264. Zuryn, S., Ahier, A., Portoso, M., White, E. R., Morin, M. C., Margueron, R., & Jarriault, S. (2014). Sequential histone-modifying activities determine the robustness of transdifferentiation. *Science*, *345*(6198), 826-829.

LIST OF FIGURES

LIST OF TABLES

LIST OF ABBREVIATIONS

°C	**D**egree **C**elsius
aa	**a**mino **a**cid
Amp	**Amp**icillin
ASE	**A**mphid neurons (**s**ingle ciliated **e**ndings)
Bovine serum albumin	**B**ovine **s**erum **a**lbumin
bp	**b**ase **p**airs
C. elegans	*Caenorhabditis elegans*
CGC	**C**aenorhabditis **G**enetics **C**enter
D. melanogaster	*Drosophila melanogaster*
DNA	**D**eoxyribo**n**ucleic acid
DNase	**D**eoxyribo**n**ucle**ase**
dNTPs	**d**eoxyribo**n**ucleotide **t**ri**p**hosphate
Doxy	**Doxy**cycline
DTT	**Di**thi**t**hreitol
DTT	**Di**thi**t**hreitol
EDTA	**E**thylene**d**iamine**t**etraacetic **a**cid
ESC	**E**mbryonic **s**tem **c**ell
GFP	**G**reen **F**luorescent **P**rotein
H3	**H**istone **3**
H3K4	**H**istone **3** Lysine (**K**) **4**
H3K27	**H**istone **3** Lysine (**K**) **27**
H3K9me3/ac	**H**istone **3** Lysine (**K**) **9 trime**thylation/**ac**etylation
H3K4me3	**H**istone **3** Lysine (**K**) **4 tri**methylation
kDa	**k**ilo**d**alton
LB	**L**uria-**B**ertani
MEF	**M**ouse **E**mbryonic **F**ibroblast
min	**m**inute
mL	**m**ili**l**iters
mM	**m**ili **M**olar
MosSCI	**Mos**1-mediated **S**ingle **C**opy **I**nsertion

mRNA	**m**essenger **RNA**
ng	**n**ano**g**rams
NGM	**N**ematode **G**rowth **M**edium
nM	**n**ano **M**olar
OXPHOS	**Ox**idative **Phos**phorylation
PBS	**P**hosphate **b**uffered **s**aline
PCR	**P**olymerase **c**hain **r**eaction
PFA	**P**ara**f**orm**a**ldehyde
Rluc	**R**enilla **luc**iferase
RNA	**r**ibo**n**ucleic **a**cid
RNAi	**RNA i**ntereference
rpm	**r**evolutions **p**er **m**inute
RT	**R**oom **T**emperature
s	**s**econds
SCNT	**S**omatic **c**ell **n**uclear **t**ransfer
SDS-PAGE	**SDS-p**oly**a**crylamide **g**el **e**lectrophoresis
SEM	**S**tandard **e**rror of the **m**ean
smFISH	**s**ingle **m**olecule **f**luorescent **i**n **s**itu **h**ybridization
STD	**St**andard **d**eviation
TAE	**T**ris **A**cetat **E**DTA
TBST	**T**ris-**B**uffered **S**aline-**T**ween 20
Tet	**Tet**racycline
TF	**T**ranscription **F**actor
V	**V**olts
WB	**W**estern **B**lot
WT	**w**ild **t**ype
µg	**m**icro**g**ram
µM	**m**icro **M**olar
µm	**m**icro**m**eter

ACKNOWLEDGEMENTS

First, I would like to thank Dr. Baris Tursun for giving me the opportunity to work in his lab, for being a great mentor, for his guidance and support throughout the years. It was a privilege to work with him.

I would also like to thank my committee members Prof. Dr. Thomas Sommer, Dr. Sevinc Ercan, Dr. Andrew Plested, and Prof. Dr. Andreas Hermann. Special thanks to Dr. Stephan Kempa for his helpful comments and involvement in the project.

I'm thankful to Anna for being an amazing teacher and friend. To Mei with whom I started this journey and to Selman who helped me bring it to an end. I'm truly thankful to my students Tim, Amanda and Amin. To all my lab fellows especially Andreas, Ismail, Marlon, Iris, Clara and Margaux for being so much support and fun throughout the time. I'm also grateful to Alex and Tobias for their helpful discussions and contributions to the project.

To all my friends especially Rabia and Miriam for sharing this journey with me and cheering me through it.

Finally, I'm extremely thankful to Mama and Baba Jan who have always loved and supported me and pushed me forward. To Yousaf, Rida and Ahmad for being amazing siblings and cheerleaders. To Faraz for listening to my endless rants and standing by my side. To all my family for their love, support and encouragement. I couldn't have done it without you.

This Ph.D. has been a remarkable journey. I'm so grateful to have experienced it. Alhamdulillah.